JAERI-M
84-129

JAERI TANDEM

ANNUAL REPORT

1 9 8 3

April 1, 1983 - March 31, 1984

July 1984

Department of Physics

日 本 原 子 力 研 究 所
Japan Atomic Energy Research Institute

JAERI-M レポートは，日本原子力研究所が不定期に公刊している研究報告書です。

入手の問合わせは，日本原子力研究所技術情報部情報資料課（〒319—11 茨城県那珂郡東海村）あて，お申しこしください。なお，このほかに財団法人原子力弘済会資料センター（〒319—11 茨城県那珂郡東海村日本原子力研究所内）で複写による実費頒布をおこなっております。

JAERI-M reports are issued irregularly.

Inquiries about availability of the reports should be addressed to Information Section, Division of Technical Information, Japan Atomic Energy Research Institute, Tokai-mura, Naka-gun, Ibaraki-ken 319—11, Japan.

編集兼発行　日本原子力研究所
印　　刷　日立高速印刷株式会社

JAERI-M 84-129

JAERI TANDEM
Annual Report
1983

April 1, 1983 - March 31, 1984

Department of Physics
Tokai Research Establishment, JAERI
(Received June 27, 1984)

This annual report describes research activities which have been performed with JAERI tandem accelerator from April 1, 1983 to March 31, 1984. Summary reports of 32 papers, publications, personnel and a list of co-operative reserches with universities are contained.

Keywords: JAERI TANDEM, Materials Science, Nuclear Chemistry, Nuclear Physics, Fast Neutron Physics, Annual Report

---

Editors Kichinosuke Harada
Michio Maruyama
Hiroshi Okashita
Kunio Ozawa
Naomoto Shikazono
Shigeya Tanaka

JAERI－M 84－129

原研タンデム58年度年次報告

日本原子力研究所東海研究所
物　理　部

（1984年6月27日受理）

本年次報告は，原研タンデム加速器で1983年4月1日から1984年3月31日までの間に行われた研究活動をとりまとめたものである。

32篇の小論文，公表された文献，関与した職員及び大学との協力研究のリストを収録している。

（編集者）　原田吉之助・鹿園　直基・丸山　倫夫・岡下　　宏
小沢　国夫・田中　茂也

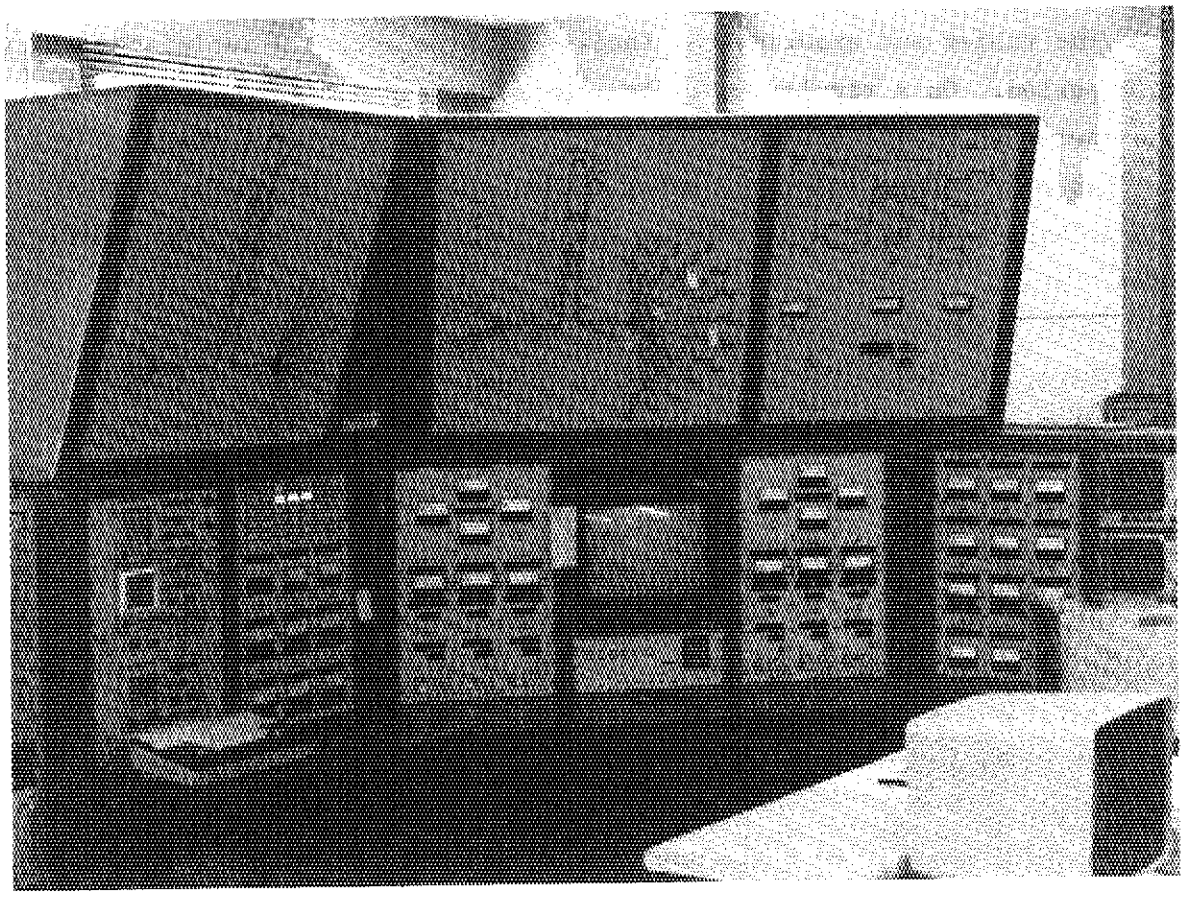

PREFACE

This is the second annual report on research activities which have been carried out with JAERI tandem during the period from April 1, 1983 to March 31, 1984.

The tandem and experimental facilities have operated satisfactorily in this period. On a regular schedule, the tandem operates in accordance with the operation cycle which is composed of about 3 months for research studies and the machine development and then 1 month for the maintenance. The machine time is rather crowded and is allocated by the program advisory committee.

Main subjects of our research activities are following five:

1) Atomic and solid state physics
2) Radiation effects in materials
3) Nuclear chemistry
4) Nuclear physics
5) Fast neutron physics

In the period, more than 60 staff members in JAERI have been working in the five fields of researches, and about 40 colleagues of universities and institutions outside JAERI have joined and collaborated in these studies. The tandem provided various kinds of heavy ions for these purposes.

A joint seminar on heavy ion nuclear physics and nuclear chemistry was held at Tokai Research Establishment of JAERI, January, 1984, and several experimental results described in this annual report were presented in the seminar. The report of the seminar is published in JAERI-M 84-085.

Kichinosuke Harada

Kichinosuke Harada
Director,
Department of Physics

CONTENTS

I ACCELERATOR OPERATION AND DEVELOPMENT

1.1 Tandem Accelerator Operation

Tandem Accelerator Group

Accelerators Division, Department of Physics,
Japan Atomic Energy Research Institute

Accelerator operation

The scheduled operation for experiments was performed through the fiscal year containing four short periods for the scheduled maintainance. The following are summary of the operation from April 1, 1983 to March 31, 1984.

1) Time distribution by terminal voltage

17-18 MV	1 days	0.6 %	11-12 MV	4 days	2.5 %
16-17	22	14.0	10-11	11	7.0
15-16	21	13.4	9-10	15	9.6
14-15	51	32.5	8- 9	2	1.3
13-14	24	15.3	7- 8	1	0.6
12-13	5	3.2			

2) Time distribution by projectile

H	2 days	1.3 %	Cl	52 days	33.1 %
D	14	8.9	Ni	8	5.1
B	1	0.6	Cu	1	0.6
C	38	24.2	Br	3	1.9
O	21	13.4	In	1	0.6
F	2	1.3	I	1	0.6
Si	1	0.6	Others (N,P,Kr,Xe etc. for test)	7	4.5
S	5	3.2			

3) Time distribution by activity

Operation for research		160 days	44 %
Atomic and solid state physics	20.5		
Radiation effects in materials	19		
Nuclear chemistry	27		
nuclear physics	64.5		
Fast neutron physics	13		
Accelerator development	16		
Voltage conditioning		38	10
Scheduled maintainance(4 tank openings)		85	23
Unschduled repairs (2 tank openings)		13	4
Holidays and vacation		70	19

The negative ions were produced by Hiconex sputter cone source, Heinicke-

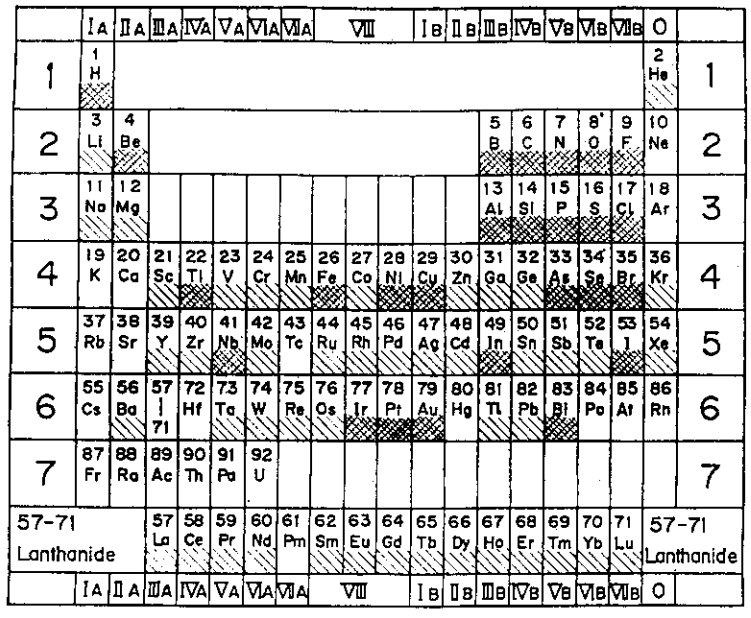

Fig.1. Periodic table showing the extracted (hatched) and accelerated(doubly hatched) ions.

Penning source and a direct extraction duoplasmatron source. Practical amounts of negative ions of 72 elements have been extracted from the ion sources and 26 kinds of ions of them were already tried to accelerate to date. They are now usable for experiments. In the periodic table of fig.1, the extracted and accelerated ions are shown.

Tank openings

The accelerator was opened four times for the scheduled maintainance and two times for the unexpected repairs in the period. Since August, 1983, no opening during the machine time periods has happened.

1) April 15-May 12, 1983

Scheduled maintainance.

2) June 28-July 1, 1983

Unscheduled repair. Replacement of timing drive belt of 10 KVA terminal generator.

3) July 5-7, 1983

Unschduled repair. Repair of mechanical joint between rotating shaft and 15 KVA terminal generator.

4) July 22-29, 1983

Legal inspection of service platforms.

5) September 5-20, 1983

Scheduled maintainance.

6) January 5-25, 1984

Scheduled maintainance.

1.2 Production and Acceleration of Various Heavy Ions at the JAERI Tandem Accelerator

Eisuke Minehara, Shinichi Abe, Susumu Hanashima, Masumi Ohoshima, Tadashi Yoshida, Chiaki Kobayashi, Yutaka Sato and Mamoru Kanda

Accelerators Division, Department of Physics, Japan Atomic Energy Research Institute

Ions of ^{9}Be, ^{14}N, ^{31}P, ^{75}As, ^{80}Se, $^{191,193}Ir$ and ^{209}Bi have been successfully accelerated by the JAERI tandem accelerator. Negatively-charged atomic and molecular ions of these elements were obtained from a negative ion sputter source (NISS as an abbreviation) by using the cesium surface ionization gun developed in our laboratory. Details of the ion source and the gun were already reported in the previous paper[1),2)].

Several tens of cones and several kinds of gases were tested to know how much current we could get from them, and how stable and how long they worked. After this test, 13 cones of Be, BeO, BN, GaAs, Se, ZnSe, CdSe, Ir, Bi and Bi_2O_3, and NH_3, PH_3, SeH_2, and AsH_3 gases were selected and applied to accelerate Be, N, P, As, Se, Ir and Bi.

Table 1 Typical parameters of the ion sources, negative ion currents and ion source materials.

Ion Source	NISS	NISS	NISS	NISS
Beam Species	Se^-	Se^-	CAs^-	Ir^-
Negative Ion Current	3900nA*	761nA*	635nA	530nA*
Ion Source Materials	ZnSe	C+SeH_2	C+AsH_3	Ir
Gas Spray	/	0.53torr·l/s	0.27torr·l/s	/
Extraction Voltage	24KV	24KV	24KV	24KV
Current	0.7mA	2.1mA	1.3mA	1.5mA
Focus Voltage	13.3KV	12.6KV	12.8KV	13KV
Einzel Voltage	20.1KV	17.8KV	18.1KV	19.4KV
Ionizer Voltage	6.0V	5.8V	5.9V	5.5V
Current	21A	29A	29A	27A
Oven Current	0.15A	0.16A	0.18A	0.17A

*:This indicates the summed current of ion beams which we could not resolve into their isotope currents.

Typical results of the test are shown in table 1. This table contains typical parameters of the ion sources, negative ion currents and ion source materials.

Table 2 Beam currents and operational parameters of the tandem accelerator. IS and AM mean the ion source and the analyzing magnet, respectively.

Element	Be	N	P	As	Se	Ir	Bi
Atomic Number	4	7	15	33	34	77	83
Mass Number	9	14	31	75	80	191,193	209
Ion Source Materials	Be	$C+NH_3$	$C+PH_3$	$C+AsH_3$	ZnSe	Ir	Bi_2O_3
Negative Ion	BeH^-	CN^-	CP^-	CAs^-	Se^-	Ir^-	BiO_2^-
Charge State	3+	5+	10+	10+	10+	10+	10+
Beam Current (after IS)	100nA	3400nA	850nA	635nA	5000nA*	530nA*	2000nA
Beam Current (after AM)	1.0pnA	60pnA	11pnA	21pnA	50pnA	1.1pnA	2.0pnA
Final Energy	52MeV	38MeV	143MeV	145MeV	146MeV	146MeV	145MeV

*:This indicates the summed current of ion beams which we could not resolve into their isotope currents.

Thirty elements including these 7 elements tested here have been accelerated and used for experiments. Forty nine elements other than the 30 elements have been extracted from the ion sources. Typical beam current, final energy, charge state and so on are summarized in table 2. The beam current were measured by electron-suppressed Faraday cups arranged along the beam lines.

References

1) E.Minehara, S.Abe, C.Kobayashi and S.Kikuchi., Proc. 4th Symp. on Ion Sources and Ion Application Technology, Tokyo, June 24th-26th, 1981, p261.

2) S.Abe, E.Minehara, C.Kobayashi and S.Kikuchi., Proc.6th Symp. on Ion Sources and Ion-Assisted Technology, Tokyo, June 7th-9th, 1982, p185.

1.3 KrF^- and XeF^- Ion Beams for the Tandem Electrostatic Accelerator

Eisuke Minehara, Tadashi Yoshida, Shinichi Abe and Susumu Hanashima

Accelerators Division, Department of Physics, Japan Atomic Energy Research Institute

Negative atomic ions of inert gas elements heavier than helium are unstable and their electron affinities have been observed to be negative. The inert gases have been thought to be so inactive that they could not react with others to make any compound having positive electron affinities. Therefore, it had not been tried to obtain any negatively-charged ion beam of the inert gases and their compounds before our work. In the previous work(1,2), we first confirmed the formation and extraction of KrF^- and XeF^- ions from a Penning ion source with radial extraction by measuring their mass fragmentation patterns. There is a large possibility that we can accelerate Kr and Xe ion beams in tandem electrostatic accelerators by utilizing them.

Krypton and xenon difluorides were prepared by using a cryo-quenched electric discharge apparatus(3). The apparatus is illustrated in fig.1. They are so unstable that they have to be stored

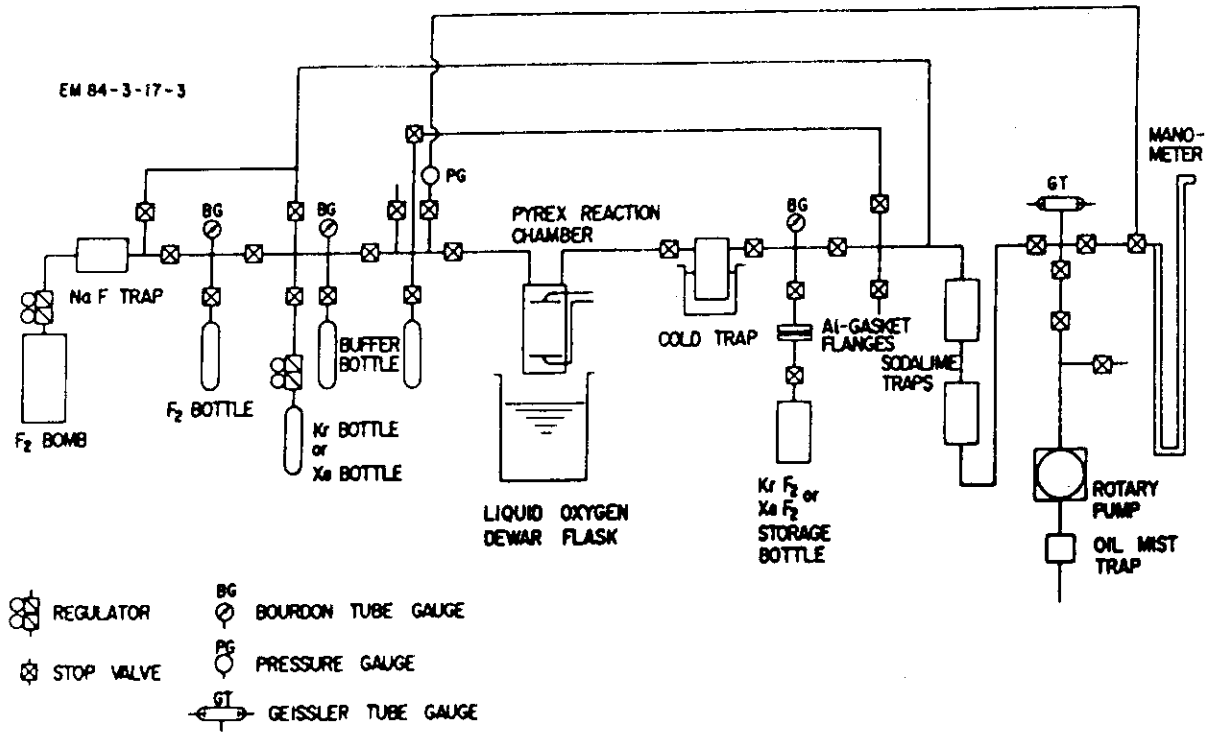

Fig.1. A cryo-quenched electric discharge apparatus.

in a stainless steel bottle at 77°K to avoid the thermal disintegration. An evaporation and gas feed system shown in fig.2 was reported in detail in the previous work. The system was designed for keeping the

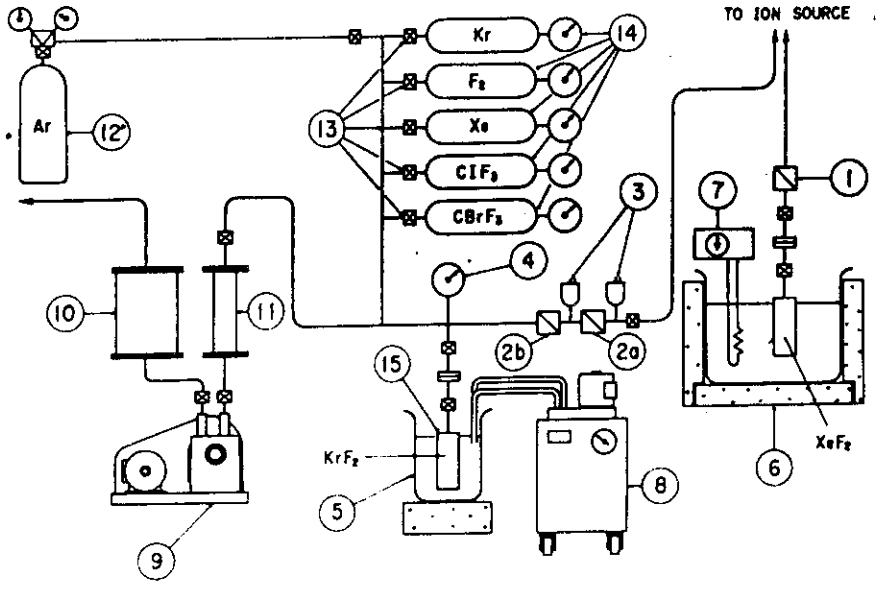

Fig.2. An evaporation and gas feed system.
1,2. metering valve, 3. pirani gauges, 4. negative and positive pressure Bourdon tube gauge, 5. cold bath, 6. warm bath, 7. heater, 8. refrigerator and coolant circulation pump, 9. rotary pump, 10. oil trap, 11. soda-lime trap, 12. argon bomb and regulator, 13. manifold valves, 14. gas bottle and Bourdon tube gauge, and 15. gas container.

temperature and vapour pressure of the difluorides constant. The system was repeatedly prefluorinated with F_2 gas before use. During their feeding to the ion source from the system, we often have to cool the system intermittently in order to eliminate intruder peaks of impurities in the mass spectra. By using the system, we could confirm the formation of the KrF^- and XeF^- ions.

A streamlined version of the system shown in fig.3 was specially designed for feeding the difluorides constantly and minimizing their condensation and thermal disintegration during the transfer. In order to avoid their condensation and thermal disintegration and to maximize their feeding to the ion source, we removed a pair of pirani gauges, one of the metering valves and gas bottles for mass-magnetic field calibration and long teflon and stainless steel piping lines.

The system was prefluorinated for a few days with 1 kg/cm^2 F_2 gas before use. The negative ion injector of the JAERI tandem

accelerator(4) was used as a test apparatus to increase the KrF^- and XeF^- intensities. We could have the negative ion currents one order of magnitude larger than the currents reported previously. Typical

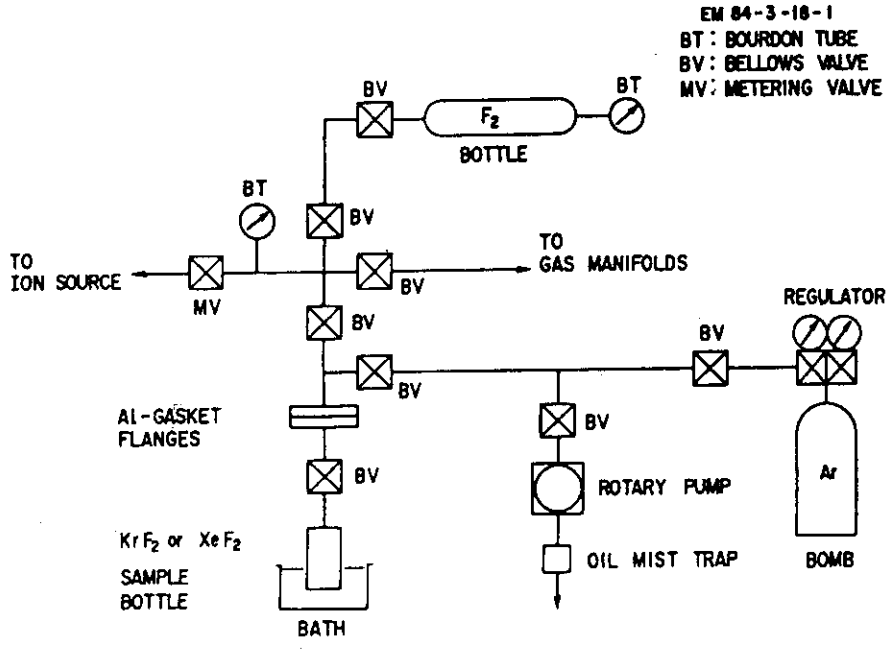

Fig.3. A streamlined version of the gas feed system.

intensities for KrF^- and XeF^- were 100nA and 50nA, and the maximum ones 320nA and 150nA, respectively.

The trial to accelerate them by the tandem accelerator is now in progress. This technique will be applicable to several interesting fields, for examples, nuclear physics using high energy Kr and Xe ion beams, measurements on solar neutrino flux and monitoring of ^{85}Kr exhausted from nuclear fuel reprocessing plants.

We would like to express our gratitude to Dr.T.Sakurai of Physical Chemistry Laboratory, Division of Chemistry, JAERI, for his help in synthesis and supply of the krypton and xenon difluorides.

References

(1) E.Minehara and S.Abe.,Nucl.Instr. and Meth. 190(1981)215.
(2) E.Minehara and S.Abe.,Nucl.Instr. and Meth. 212(1982)533.
(3) V.N.Prusakov and V.B.Sokolov, Soviet At. Energy, 31(1971)990.
(4) M.Maruyama, "The JAERI Tandem Accelerator Facility", Proceedings of the Third International Conference on Electrostatic Accelerator Technology, Oak Ridge, Tennessee, April 13-16, 1981.

1.4 Development of Technics for Automated Accelerator Control

Susumu Hanashima, Eisuke Minehara, Isao Ohuchi, Katsuzo Horie, Susumu Kanda and Yoshihiro Tsukihashi

Department of Physics, Japan Atomic Energy Research Institute

1. Improvement of a computer system for JAERI tandem

We went on with works to switch a system program to new one for JAERI tandem. The new system program is intended to enable easy addition of high level control features to the accelerator control system, while the old is not. The new system consists of a commercially available multi-tasking operating system(OS/32), a basic CAMAC communication system and application programs. The basic CAMAC communication system provides communication between control consoles and the accelerator. It also provides interfaces between operating parameters of the accelerator and the application programs. These interfaces enable us to write the application programs for accelerator control without any knowledge for internal data structures of the communication system. In the system, addition or deletion of some feature for high level control is done with only starting or stopping such a task having the feature without stopping accelerator control.

Hardware and software of the computer system for the control system have been expanded for that purpose. There are 1 M bytes of main memory and about 170 M bytes of disc storages under 2 CPU(a main system and a backup system). The multi-tasking operating system(OS/32) and Pascal compiler were installed and have been used for program development. Till the 1st quarter of 1984, design and coding of CAMAC handler and basic design of the system were completed.

2. Tests of feasibility of computer aided parameter setting for the tandem

There are many parameters for beam transport of the tandem. Thus it is one of the most important subject to develop technics for automated setting of beam optical parameters. In the tandem, all optical parameters are controlled through a computer system and they lie on a main memory of the computer. It gives us the first basis for thinking about computer aided beam tansportation.

For the purpose, we tested reproducibility of beam-optical conditions

of the tandem, at first. In the test, some ion beam was extracted from a negative ion source of the tandem and manually transported through the accelerator to a Faraday cup behind an analyzer of the final energy. All the setting value for control of the tandem were stored to a disc file for later use. After that, the parameters of the tandem were changed to accelerate other beams. Next, the stored parameter set was recalled to reproduce the old beam condition. Current settings for three bending magnets in the system were manually tuned to reproduce the old readings of the magnetic fields. Current in the Faraday cup was compared to the old current reading and over all reproducibility was tested. In this way, ^{12}C, ^{16}O, ^{19}F and ^{35}Cl ion beams were accelerated and their current readings in the Faraday cup showed no degradation in the beam transportation in a day or even after a few months.

The second experiment was performed to examine an algolithm to set parameters for a specific beam. In the method, a set of parameters that provides enough transportation for some beam is used as a reference. The new set of parameters are calculated to give the same optical effect to the beam as the reference. A computer program is used to set the parameters(about 40 parameters including steerers). In the program, ratio between pre-acceleration voltage and the terminal voltage of the tandem is selected to be same as the reference's one. In the way, $^{12}C^{5+}$ at Vt=15.0 MV, $^{12}C^{5+}$ at Vt=14.1 MV, $^{19}F^{6+}$ at Vt=15.0 MV, $^{19}F^{8+}$ at Vt=14.1 MV and $^{35}Cl^{9+}$ at Vt=14.1 MV were successfully transported using a single set of parameters for $^{12}C^{6+}$ at Vt=15.0 MV as the reference.

In the present work, capability of the automated beam trasportation was demonstrated to some extent. On the other hand, problems have appeared. One of them is how to keep the reference data stable through months, maintenances, etc. Another is how to tune ion sources to match with the acceptance of the tandem which is realized by the above method. For the first problem, we will improve accuracy of the devices(high voltage power supplies, current power supplies, etc.) to remove the problem. For the second, we consider a feedback tuning method from a beam monitor is effective.

II ATOMIC AND SOLID STATE PHYSICS

2.1 Transmission Sputterings of Titanium and Silicon Carbide by Heavy Ions

Teikichi A.Sasaki*, Yuji Baba*, Kiichi Hojou* and Takeo Aruga**

*Department of Chemistry and **Department of Fuels and Materials Research, Japan Atomic Energy Research Institute.

Transmission sputtering has been confirmed to provide very useful information about the spatial distribution of deposited energy in solid. However, it has not been popular because of experimental difficulty in preparing the thin target appropriate for the ion bombardment. To date, the most experiments have been performed using heavy ions whose energies are less than 1 MeV.[1] Energetic heavy ions make it possible to study the transmission sputtering of the thick target without being worried with physical and chemical heterogeneities charactreristic to the thin target. In this communication, we present results of the transmission sputtering for bombardments with 114 MeV F^{7+} and 140 MeV Cl^{9+} ions.

Target foils of high-purity Ti with various thickness were placed on Ag catcher foils. In the case of CVD-SiC target a wedge-shaped specimen was prepared by means of automatic polishing over 4 days using a diamond paste of 1/4 micron. A shiny Pt foil was used as catcher of the sputtered Si and C atoms. Heavy ions from tandem accelerator of JAERI impinged at normal incidence and the beam currents were monitored with two removable Faraday cups. About 6 mmΦ around the beam center was kept to be uniform intensity using an ion-beam scanner. Information about the sputtering yield was obtained with AES by the use of 5 keV electrons.

Relative yield of the sputtering for various target thickness is shown in Fig.1 together with deposited-energy distribution of the incident ion. For comparison, a blow-up for the region of the target thickness where the sputtering has been observed is made. A good agreement between the experimental data and calculated deposited-energy distribution implies that the AES is one of useful techniques for the determinations of energy deposition in the solid. The sputtering yield Y is estimated as follows,

$$Y = \frac{C(Ti)\cdot n_{\ell}}{N(F)} \qquad (1)$$

where N(F) and C(Ti) are total fluence of F^{7+} ions and concentration of the

Ti atoms in the mono-atomic layer respectively, and n_ℓ the number of the Ag atomic layer where the Ti atoms are trapped. Although C(Ti)x n_ℓ depends upon energy spectrum of the sputtered atoms, it is evident that the peak position of the experimental curve in Fig.1 is from a number of the sputtered atoms implanted in the layer of ∿10 A from the surface. Since signal-height ratio h(Ti)/h(Ag) determined from the AES measurements is correlated with C(Ti) and sensitivity factors S of the Auger electrons as

$$\frac{h(Ti)}{h(Ag)} = \frac{S(Ti_{LMM})}{S(Ag_{MNN})} \frac{C(Ti)}{C(Ag)} , \qquad (2)$$

eq.(1) can be written as

$$Y = \frac{C(Ag)}{N(F)} \frac{h(Ti)}{h(Ag)} \frac{S(Ag_{MNN})}{S(Ti_{LMM})} \cdot n_\ell \quad . \qquad (3)$$

Replacing with the known experimental parameters, we obtain $Y \fallingdotseq 4.8\ n_\ell$. Because the value of n_ℓ is considered to be 3-5 at the maximum position in Fig.1, Y is of the order of 14-24.

In Fig.2 the result of the transmission sputtering for the CVD-SiC is presented. Since the specimen used is somewhat porous, the discrepancy between the expeimental data and calculated deposited-energy distribution is considered to be due to density effect.

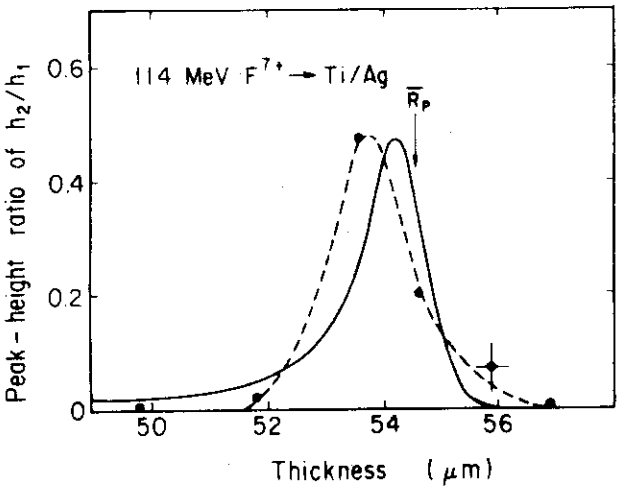

Fig.1 Ti/Ag ratio on Ag foil irradiated with 1.8×10^{14} ions/cm^2 of 114 MeV F^{7+}. ———: deposited-energy distribution, -----: experimental.

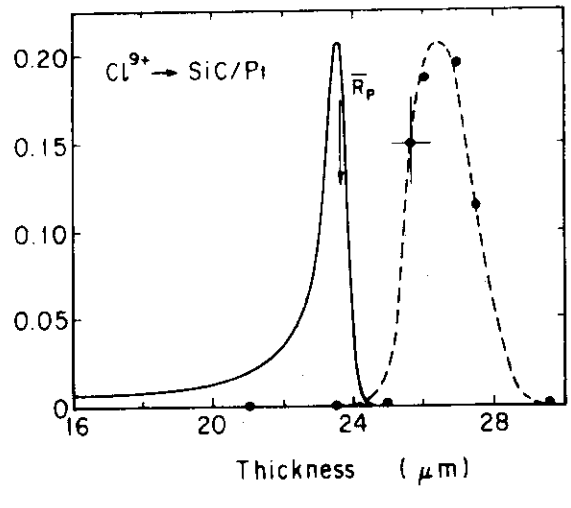

Fig.2 Si/Pt ratio on Pt foil irradiated with 1.2×10^{15} ions/cm^2 of 140 MeV Cl^{9+}. ———: deposited-energy distribution, -----: experimental.

Reference

1) G.Ayrault et al.: J.Appl.Phys. 53(1982)6968, and references therein.

2.2 Beam-Foil Interaction of Highly Ionized Chlorine Ions in High Energy Region

Hidenori Yamaguchi, Kunio Ozawa, Kiyoshi Kawatsura, Masao Sataka
Tetsuo Kitahara*, Akira Kikuchi**, Ken-ichiro Komaki***,
Akio Ootuka*** and Fuminori Fujimoto***

Department of Physics, Japan Atomic Energy Research Institute,
*Yamanashi Medical University, **Faculty of Engineering, Ibaraki University and ***College of General Education, University of Tokyo

In the previous report[1], we have shown the first results on the measurements of the distribution of charge states and the multiple scattering widths of angular distributions of highly charged chlorine ions passing through thin carbon foils (2.5-180 $\mu g/cm^2$). The results suggested that the multiple scattering process of high energy ions scattered by the thin foils has a correlation with the charge exchange process and that the above two processes are not in equilibrium for the foils thinner than about 10 $\mu g/cm^2$.

To get further information on the correlation between the multiple scattering and charge state as a function of foil thicknesses, a series of measurements has been performed for 150 MeV incident $^{37}Cl^{10+}$ ions with the experimental arrangement using a two-dimensional position sensitive detector (2D-PSD) instead of one-dimensional PSD. The foil thicknesses were measured by an energy loss technique and by the yield counting of the elastic scattering of high energy chlorine ions passing through the foils. The 2D-PSD (24×24 mm^2) purchased from Hamamatsu Photonics was used to obtain simultaneously two kinds of spectra corresponding to charge state and angular distributions. The charge

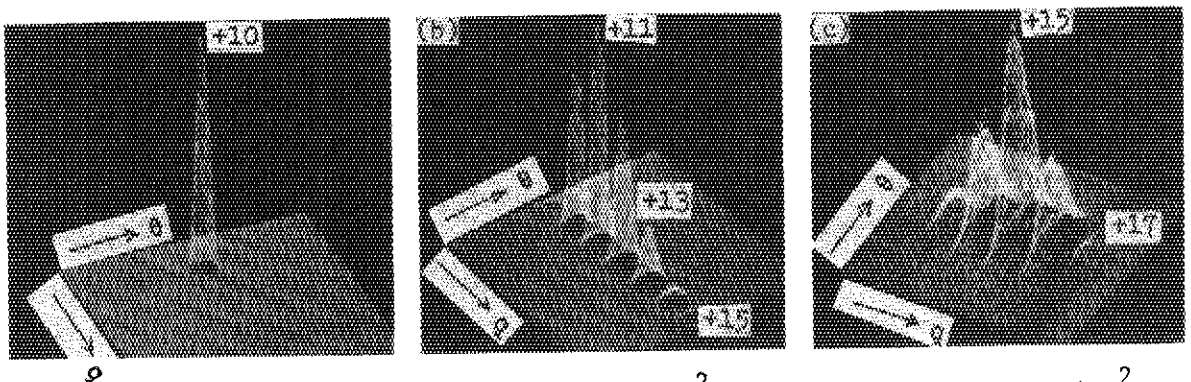

no foil 2.5 $\mu g/cm^2$ 52.7 $\mu g/cm^2$

Fig. 1. Charge state and angular distributions, measured with 2D-PSD, emerging from carbon foils of various thicknesses after impact of 150 MeV $^{37}Cl^{10+}$ ions.

state and angular distributions of highly charged chlorine ions in the foil-exited beams are measured in the parallel and perpendicular directions to the electric field between the electrostatic deflectors, respectively.

The data were accumulated in the list mode and analyzed by a PDP 11/45 computer. The foil-exited 2-parameter spectra for the faint beams (∿100 cps on the target foil) of 150 MeV $^{37}Cl^{10+}$ ions are shown in Fig. 1 (a), (b) and (c) for the cases of no foil, after traversing 2.5 and 52.7 μg/cm^2 carbon foils, respectively. A remarkable target-thickness dependence of both the charge state and angular distributions in the foil-exited beams is observed.

Figure 2 shows the charge state distributions integrated over the scattering angle of Cl ions emerging from 2.5 to 180 μg/cm^2 carbon foils following impact of 150 MeV $^{37}Cl^{10+}$ ions. The result shows that the distribution for the foils of 2.5 and 8.5 μg/cm^2 in thickness displays characteristic nonequilibrium behavior. The mean charge states increase to the higher ones with increasing the foil thicknesses and are about the equilibrium value of q=15 for the foils thicker than 50 μg/cm^2, which reflects importance of the multiple scattering. The shape of each distribution is a simple Gaussian for the lower charges but the populations for the charges of q=16 and 17 deviate from the Gaussian distribution due to the greater binding energy of the K-shell electrons.

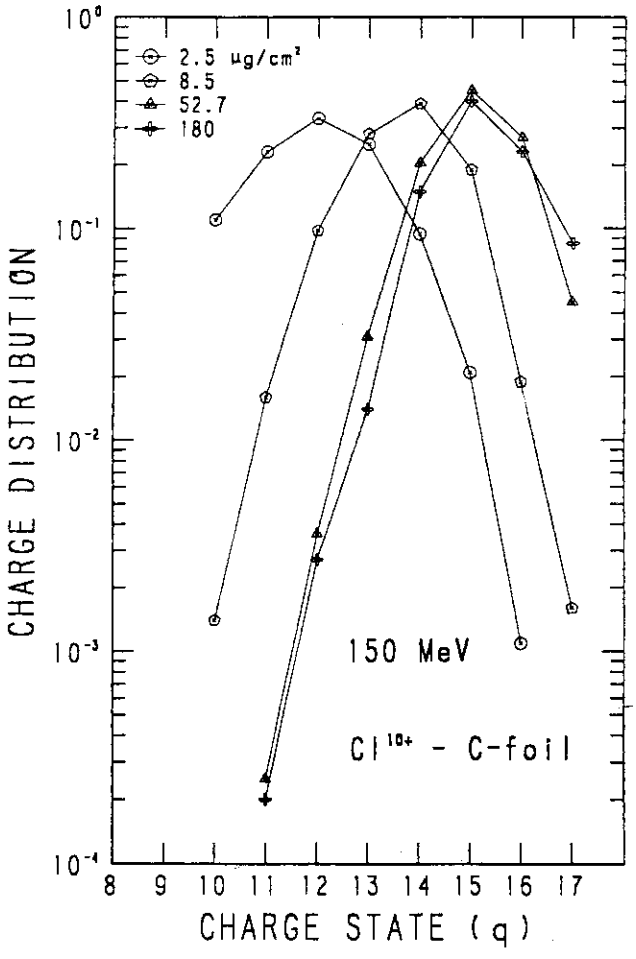

Fig. 2. Charge state distributions of 150 MeV ^{37}Cl ions with initial charge of 10+ impinging on the carbon foils of various thicknesses.

In Fig. 3 is represented the charge state dependence of the half angle of scattering ($\theta_{1/2}$), i.e. full width at half maximum (FWHM) of the angular distribution, for the various thicknesses of foils as parameters.

The widths of the angular distributions for the emerging ions show a tendency to increase with the increasing charge state of projectiles emerging from the foils. Furthermore, a significant enhancement in the widths above charge state of q=15 becomes readily evident, reflecting the greater binding energy of K-shell electrons compared with L-shell ones, which is consistent with the experimental findings as shown in Fig. 2 for the post-foil charge state distributions. A most striking feature is the remarkable broadening of $^{37}Cl^{16+}$ ions exiting from the thinnest foil of 2.5 $\mu g/cm^2$. Present results are similar to those obtained by Kanter[2] on the multiple scattering width for 1-4 MeV N^+ projectiles in thin carbon foils. The dependence of $\theta_{1/2}$ on q represents that the ions of higher charge states (Cl^{16+} and Cl^{17+}) experience hard collisions with small impact parameters in the foil.

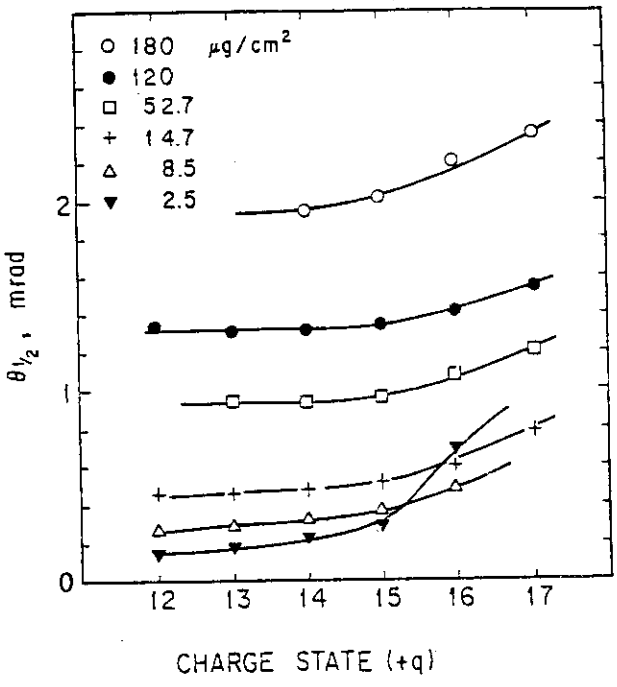

Fig. 3 Charge state dependence of half angle of scattering as a function of foil thickness for 150 MeV $^{37}Cl^{10+}$ ions.

More detailed analyses are in progress especially on the impact parameter dependence of charge states.

References

1) H. Yamaguchi et al: "JAERI TANDEM Annual Report 1982", JAERI-M 83-095 (1983) 15.

2) E.P. Kanter: Phys. Rev. A28 (1983) 1401.

2.3 Beam-Foil Spectra of Chlorine Ions in High Energy Region (I)

Masao Sataka, Kunio Ozawa, Kiyoshi Kawatsura, Keishi Ishii*, Akio Ootuka**, Ken-ichiro Komaki**, Fuminori Fujimoto**, Akira Kikuchi*** and Tetsuo Kitahara****

Department of Physics, Japan Atomic Energy Research Institute, *Department of Engineering Science, Kyoto University, **College of General Education, University of Tokyo, ***Faculty of Engineering, Ibaraki University and ****Yamanashi Medical University

A beam-foil investigation of multi-charged ions has started. The experimental apparatus is shown in Fig. 1. The ion beam enters a target chamber in which the ion beam is excited by foils. The foils can be moved 30 cm parallel to the beam so that the lifetime measurement can be made. The photon spectra emitted from foil-excited ions are measured by a 2.2 m grazing incidence spectrometer mounted at 90° to the beam direction. The photons are detected with a channel electron multiplier. The wavelength range from 50 to 2000 Å is covered with use of three interchangeable gratings. The ion beam is measured by a biased Faraday cup behind the foil. Data aquisition system is standard one making use

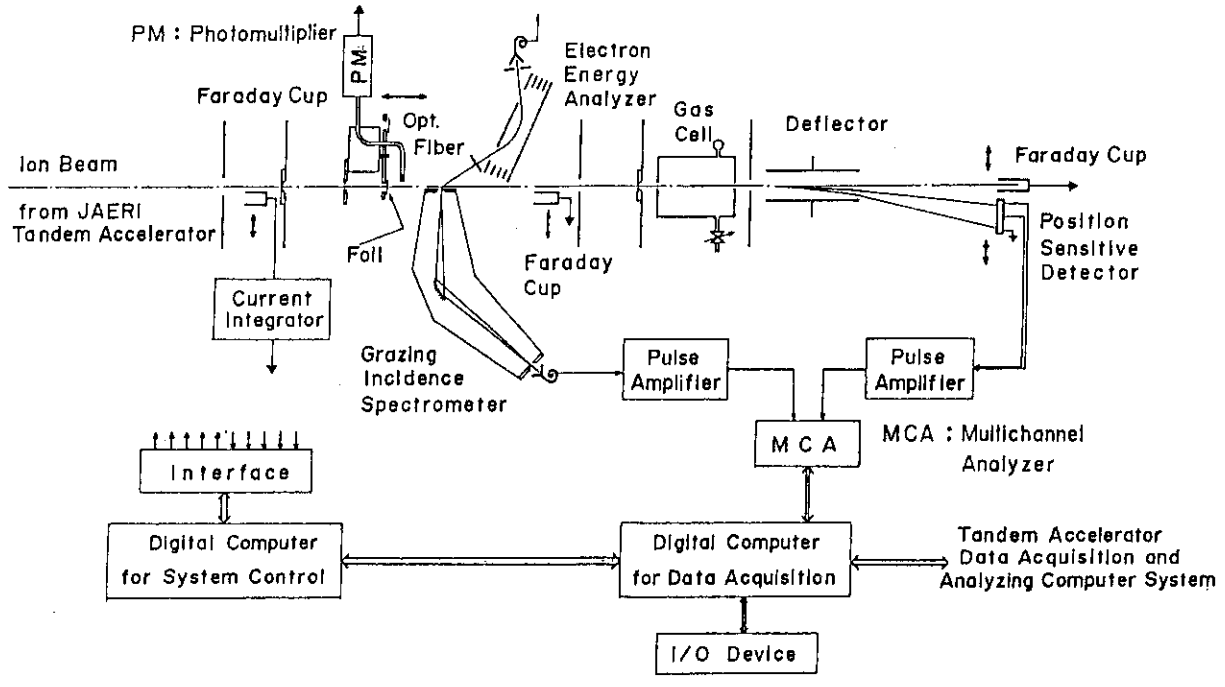

Fig. 1. Schematic diagram of the apparatus.

of the multi-scaler portion of multichannel analyzer. The ion current is monitored by a current integrator. A trigger pulse from the integrator advances the channel address and scans the spectrometer.

The preliminary result of chlorine spectrum in the wavelength region 370-470 Å is shown in Fig. 2. The lines attributed to $\Delta n=0$ transitions belonging to Cl XIV-Cl XV mainly appear. Incident ion was $^{35}Cl^{7+}$ at beam energy 80 MeV. The current of the beam passed through the foil was about 50 nA. The entrance and exit slits of the spectrometer were vertical and the grating used was one of 600 grooves/mm. The spectrum was taken at 2 mm downstream from the foil whose thickness was 30 μg/cm^2. Wavelength scale for the spectrum was fixed at the 384 Å peak (Cl XV 2s $^2S_{1/2}$ - 2p $^2P_{3/2}$). Three strong lines identified in the spectrum are tabulated in Table 1. These measured wavelengths are in good agreement with experimental results measured by Ishii et al.[1] and Forester et al.[2] The origin of weak lines can not be identified at present.

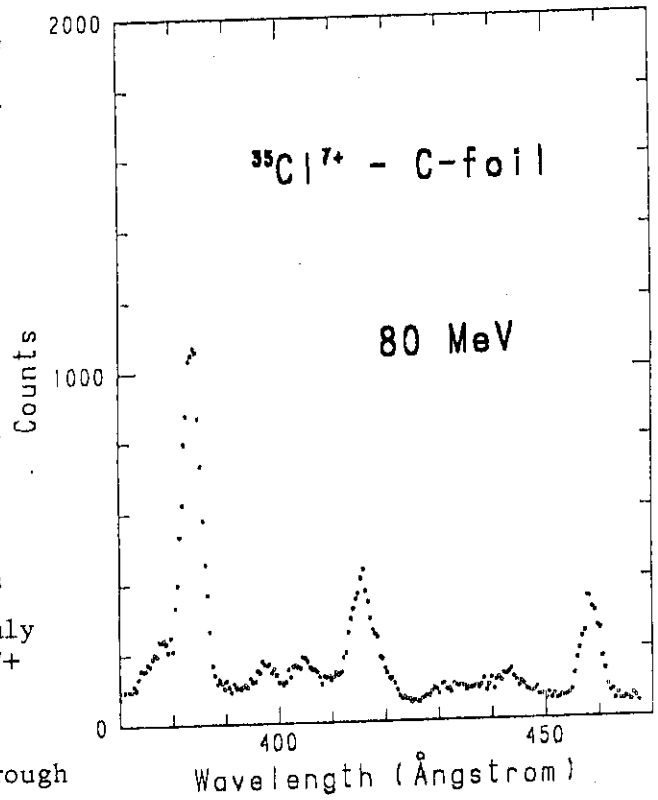

Fig. 2. The measured spectrum of 80 MeV chlorine ions.

Table 1.

Spectrum	Wavelength(Å)	Transition
XV	384.0	2s $^2S_{1/2}$ - 2p $^2P_{3/2}$
XV	415.7	2s $^2S_{1/2}$ - 2p $^2P_{1/2}$
XIV	458.3	2s2p $^1P_1$ - 2p^2 $^1D_2$

References

1) K.Ishii et al.: Physica Scripta, 18 (1978) 57.

2) J.P.Forester et al.: Phys. Rev. A18 (1978) 1476.

2.4 Defect Production Cross Sections of Aluminum for Energetic Heavy Ion Irradiations

Akihiro Iwase*, Shigemi Sasaki*, Tadao Iwata* and Takeshi Nihira**

*Department of Physics, Japan Atomic Energy Research Institute and
**Faculty of Engineering, Ibaraki University.

Defect production in metals by energetic heavy ion irradiation has been of great interest recently because high energy cascade damage by energetic heavy ions simulates the damage structure for fission and fusion reactor irradiations. Moreover, defect production in metals by energetic heavy ions has an advantage that the damage rate by heavy ions is very large and that, in only a few hours, heavy ions produce radiation damage which is expected for reactor irradiations in several years.

Defect production cross section is the number of displaced atoms for unit fluence of incident particles, and is one of the most important parameters in radiation damage studies. The number of displaced atoms are commonly calculated by the modified Kinchin-Pease model which is based on the damage calculation code MARLOWE.[1] But the discrepancy between the calculated values and the experimental ones has been reported recently in a case of heavy ion and neutron irradiations.[2-4]

In this experiment, we measured the defect production cross sections of aluminum for several ion-irradiations by means of electrical resistivity measurements at liquid helium temperatures. The defect production cross section σ_d is related to the irradiation induced electrical resistivity increment $\Delta\rho$ by the following equation.[5]

$$\sigma_d = \frac{1}{\rho_f} \frac{d(\Delta\rho)}{d\Phi} \quad , \qquad (1)$$

where ρ_f is the Frenkel pair resistivity and $d(\Delta\rho)/d\Phi$ is the change of the electrical resistivity per incident ion/cm^2. A value of $\rho_f = 3.9\times10^{-4}$ Ωcm was used in the present work.[6]

The specimens were thin Al foils with thicknesses of 0.2-0.5 μm which were grown onto Al_2O_3 substrates by vapor deposition at a pressure below 3×10^{-7} Torr. The irradiations were performed below 12.5 K, with 0.5, 1.0 and 1.5 MeV $^1H^+$, 1.33 MeV $^4He^+$ and 1.46 MeV $^{40}Ar^{2+}$ from 2MV Van de Graaff accelerator, and with 99 MeV $^{35}Cl^{8+}$, 140 MeV $^{35}Cl^{9+}$, 160 MeV $^{81}Br^{10+}$ and 195 MeV $^{127}I^{12+}$ from

the JAERI tandem accelerator. The thicknesses of the specimens are much smaller than the ranges of the incident ions, thus we did not implant ions in the specimens.

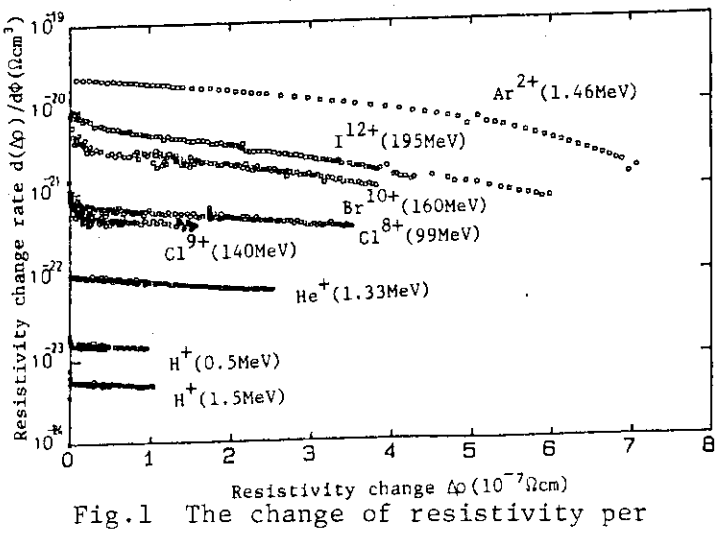

Fig.1 The change of resistivity per ion/cm^2 as a function of $\Delta\rho$.

Fig.1 shows the results of our measurements on $d(\Delta\rho)/d\Phi$ against $\Delta\rho$. The changes of electrical resistivity have been corrected for the electrical size effect.[7)8)] The figure shows that $d(\Delta\rho)/d\Phi$ decrease with increasing $\Delta\rho$. These behaviors are attributed to the irradiation annealing effect. In order to eliminate this effect, we adopted the values of $d(\Delta\rho)/d\Phi$, which were extrapolated from the linear portions of the curves to zero resistivity increments, for the determinations of the defect production cross sections.

Fig.2 shows the damage efficiency, the ratio of the experimental defect cross section to the calculated one as a function of the median primary knock on atom(PKA) energy $T_{1/2}$, where half of the displaced atoms result from PKA with energies higher than $T_{1/2}$. Here the calculated defect production cross section was evaluated by the following equation.

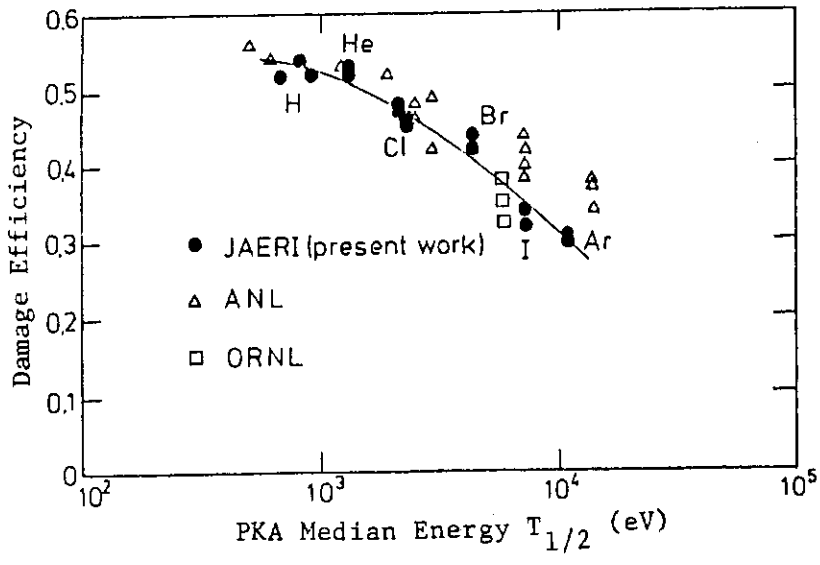

Fig. 2 Damage efficiency in Al as a function of PKA median energy $T_{1/2}$.

$$\sigma_d = \int_{E_d}^{T_{max}} \nu(T)\,(d\sigma/dT)\,dT, \quad (2)$$

where E_d is the average threshold energy, T_{max} the maximum transfer energy to PKA, $d\sigma/dT$ is the differential scattering cross section and $\nu(T)$ is the number of atoms displaced by PKA with energy T. In the numerical evaluation, we used Lucasson's recommended value 27 eV for E_d,[9)] Winterbon's formula for $d\sigma/dT$[10)] and

modified Kinchin-Pease expression for $\nu(T)$.[1] In Fig.2, the results of ANL[2] and ORNL[11] are plotted for comparison. The figure shows that the damage efficiency decreases monotonously with the median PKA energy $T_{1/2}$. This fact suggests that the recombinations of Frenkel defects in the cascade damage region, which are not considered in the calculations, occur more frequently for the cascade damage produced by PKA of higher energy. Fig.2 also shows that the present results are in good agreement with those of other experiments although the energy ranges of ions used in the three experiments are very different. The agreement of the damage efficiency as a function of $T_{1/2}$ indicates that, for the defect production cross section, the median PKA energy $T_{1/2}$ is a good parameter that characterizes the PKA energy spectrum.

References

1) M. T. Robinson and I. M. Torrens: Phys. Rev. B9 (1974) 5008.
2) R. S. Averback, R. Benedek, K. L. Merkle, J. Sprinkle and L. J. Thompson: J. Nucl. Mater. 113 (1983) 211.
3) R. S. Averback, R. Benedek and K. L. Merkle: Phys. Rev. B18 (1978) 4156.
4) C. E. Klabunde and R. R. Coltman,Jr: J. Nucl. Mater. 108&109 (1982) 183.
5) H. J. Wollenberger: in Vacancies and Interstitials in Metals, A. Seeger, D. Schumacher, W. Schilling and J. Diels eds.,(North-Holland, Amsterdam, 1970) p.215.
6) P. Ehrhart and W.Schilling: Phys. Rev. B8 (1978) 2604.
7) E. H. Sondheimer: Advan. Phys. 1 (1952) 1.
8) F. Dworschak, W. Sassin, J. Wick, and J. Wurm: KFA-Report Jül-575-FN (1969).
9) P. Lucasson: in Fundamental Aspects of Radiation Damage in Metals, M.T. Robinson and F. W. Young eds., USERDA CONF-751006-p1,vol.1(1975) 42.
10) K. B. Winterbon, P. Sigmund and J. B. Sanders: Kgl. Danske. Vidensk. Selsk. mat.-fys.Medd. 37 (1970) No. 14.
11) T. S. Noggle, B. R. Appleton, J. M. Williams, O. S. Oen, T. Iwata and G. W. Vogl: ORNL-Report July(1983).

III RADIATION EFFECTS IN MATERIALS

3.1 Irradiation Damages in Oxygen Ion Irradiated Li_2O

Kenji Noda*, Yoshinobu Ishii*, Hisayuki Matsui**,
Mikio Horiki**, Tomoo Kirihara** and Hitoshi Watanabe*

*Department of Fuels and Materials Research, Japan Atomic Energy Research Institute, ** Faculty of Engineering, Nagoya University.

Lithium oxide (Li_2O) is a prime candidate of the tritium breeding blanket materials of a fusion experimental reactor designed at Japan Atomic Energy Research Institute (JAERI). A severe irradiation damage will be introduced in the blanket material by neutrons with energies up to 14 MeV, tritons (2.7 MeV) and helium ions (2.1 MeV) produced by $^6Li(n,\alpha)^3H$ reaction. Since highly energetic oxygen ion irradiation produces enormous irradiation defects for a short period in comparison with thermal neutron reactor irradiation, paramagnetic defects in Li_2O single crystals irradiated with oxygen ions generated by a tandem accelerator at JAERI were studied using an electron spin resonance (ESR) method[1]. In the present study, an optical absorption study has been done for oxygen ion irradiated Li_2O single crystals, in order to investigate the behavior of non-paramagnetic defects as well as paramagnetic defects.

Specimens used were thin disks (about 6 mmϕ×0.5 mm) cleaved from Li_2O single crystals[2] and they were irradiated to 4×10^{18} to 6×10^{19} ions/m^2 at an ambient temperature in the high temperature irradiation chamber or the swelling test chamber attached to the tandem accelerator by oxygen ions with an energy of 100 MeV. The temperature of the specimens during the irradiation is considered to rise to about 450 K. After the irradiation, optical absorption spectra of the specimens were measured at room temperature.

A typical example of optical absorption spectra of Li_2O single crystals irradiated to 3×10^{19} ions/m^2 is shown in Fig. 1. A remarkable absorption band is observed at about 310 nm in wave length and the intensity increases with the ion fluence. In addition to this band, relatively weak bands are observed at about 375 and 570 nm. The 375 and 570 nm bands become to be observable at high fluence. These bands were also observed for Li_2O single crystals and the sintered pellets irradiated in JRR-2 or 4 by thermal neutrons and the 310 nm band was found to be predominant in the neutron irradiated Li_2O[3]. In the study of neutron irradiated Li_2O, the 310 nm band was determined to be due to the F^+-center (an oxygen ion vacancy trapping an electron) from the experimental

result that the isochronal annealing behavior of the band was in good agreement with that of the F^+-center in an ESR study of neutron irradiated Li_2O[4]. In addition, the 375 and 570 nm bands were conjectured to be associated with F aggregate centers, since the bands were observable in the specimens containing the F^+-centers in high concentration. Thus, in oxygen ion irradiated Li_2O as well as in neutron irradiated Li_2O, the F^+-centers are dominant irradiation defects and increase with the fluence. At the high fluence, formation of F aggregate centers is considered to occur.

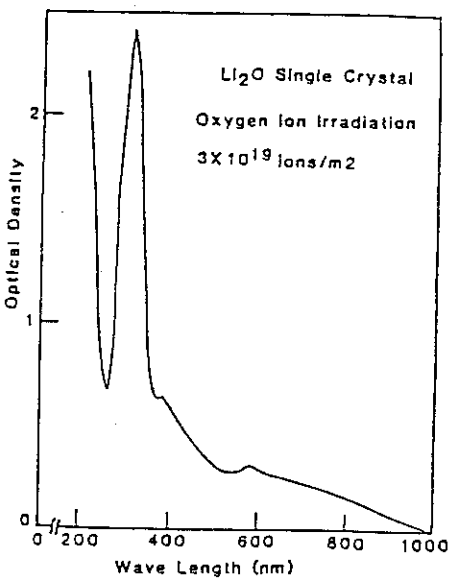

Fig. 1 A typical absorption spectrum of oxygen ion irradiated Li_2O.

Fig. 2 shows that concentration of defects corresponding to the 310, 375 and 570 nm bands as a function of the ion fluence. The concentration of the defects corresponding to the 310 nm band (the F^+-center) was calculated using Smakula's equation of which parameters were adequately determined to make the calculated results consistent with those obtained in an ESR study of oxygen ion irradiated Li_2O [1]. The concentration of the defects corresponding to the 375 and 570 nm bands was relatively calculated with Smakula's equation on the assumption that the values of the parameters were equal to those in case of the 310 nm band. In Fig. 2 the gradient of relationship between the concentration of the defects considered to be F aggregate centers and the ion fluence is larger than that of the F^+-centers. This suggests that some parts of the F^+-centers are annihilated by migration of the interstitial oxygen atoms and the some parts combine to form the F aggregate centers. The formation rate of F aggregate centers increases with the ion fluence, since the probability for coalescence of the F^+-centers becomes large with the concentration of the F^+-centers. As a result, fraction of the F aggregate centers in

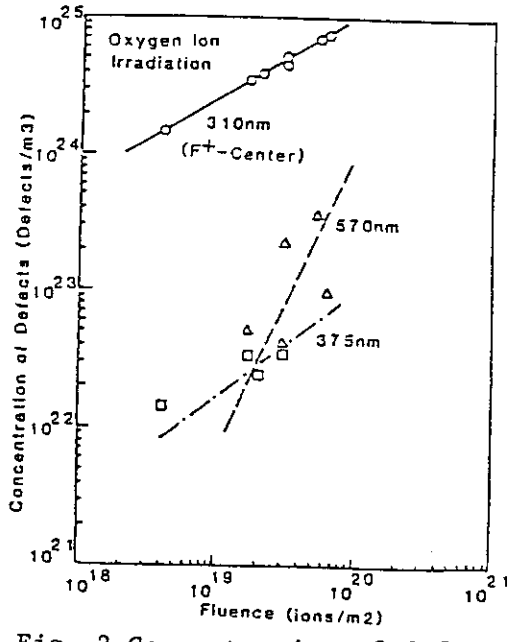

Fig. 2 Concentration of defects corresponding to the 310, 375 and 570 nm bands.

irradiation defects is considered to increase gradually with the ion fluence.

The recovery behavior of the 310 and 570 nm bands in the oxygen ion irradiated Li_2O was investigated by isochronal annealing experiments. The specimens were maintained for 30 min. at each annealing temperature and the temperature was increased stepwise up to 670 K at intervals of about 50 K. Fig. 3 shows the intensity of the 310 or 570 nm band normalized to that before annealing as a function of the annealing temperature. The 310 nm band begins to decrease at about 520 K and almost disappears at about 670 K. On the other hand, the 570 nm band increases once around 420 K and vanished at 670 K. Comparing the above results with those in case of the thermal neutron irradiation, the temperature at which the recovery occurs shifts to high temperature side in case of oxygen ion irradiated Li_2O. This shows that the high temperature is required to recover the highly concentrated F^+-centers and F aggregate centers. From this result, the recovery of these defects is conjectured to be caused not by vacancy clustering but by migration of oxygen interstitial atoms from the surrounding of the defects.

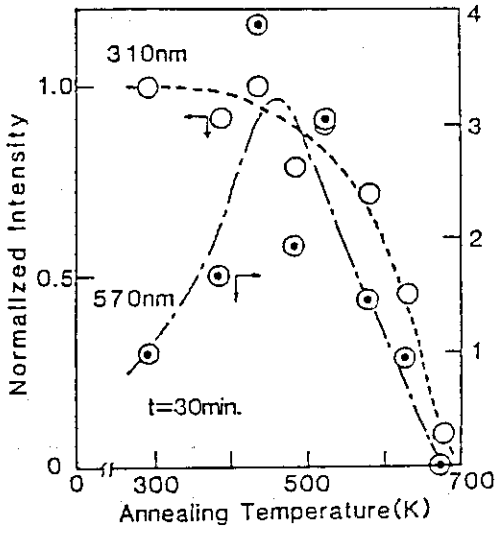

Fig. 3 Annealing behavior of the 310 and 570 nm bands.

The authors wish to express their thanks to Dr. K. Ozawa for making the optical absorption spectrometer available.

References

1) K. Noda, T. Tanifuji, Y. Ishii, H. Matsui, N. Masaki, S. Nasu and H. Watanabe, J. Nucl. Mater., in press.

2) I. Shindo, S. Kimura, K. Noda, T. Kurasawa and S. Nasu, J. Nucl. Mater., 79, 418 (1979).

3) K. Uchida, K. Noda, T. Tanifuji, S. Nasu, T. Kirihara and A. Kikuchi, phys. stat. sol. (a), 58, 557 (1980).

4) K. Noda, K. Uchida, T. Tanifuji and S. Nasu, Phys. Rev. B, 24, 3736 (1981).

3.2 Measurement of Mean Projected Ranges for Carbon-Ion in Stainless Steel

Shozo Hamada, Tomotsugu Sawai and Kensuke Shiraishi

Department of Fuels and Materials Research, Japan Atomic Energy Research Institute.

The heavy-ion irradiation experiment is useful to evaluate the radiation damage of the materials in a short period. The radiation damage produced by ions has a strong gradient and highly damage region is limited to a zone around the mean projected range of the incident-ion. Then, fairly accurate estimation of the mean projected range is required for the observation of the heavily damaged region with transmission electron microscopy. However, the mean projected range has not yet been well evaluated for high-energy heavy-ion irradiation to the materals. In this experiment, the mean projected range for carbon-ion with energies of 40 to 90 MeV injected into stainless steel were measured and compared with the calculations.

Type 316 stainless steel plates of 2.5 mm x 12 mm with 0.2 mm in thickness were solution annealed for 1 h at 1373 K in a vacuum of 10^{-3} Pa followed by rapid cooling to ambient temperature. The plates were irradiated with 40 ~ 90 MeV carbon-ions at ambient temperature by using the swelling chamber in light-ion target room of the JAERI Tandem Accelerator. After the irradiation, the plate was electroplated with nickel on both the

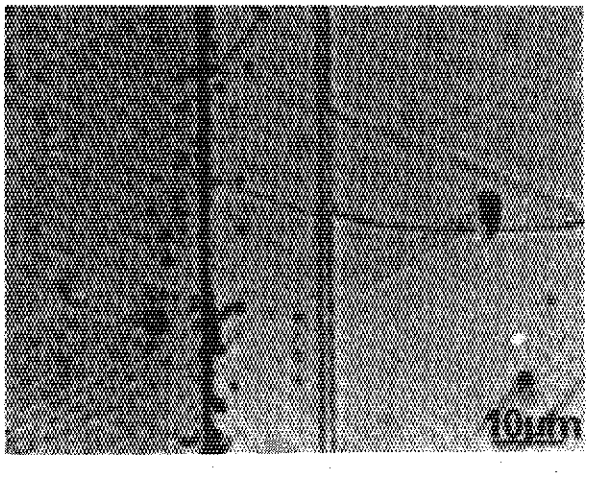

Fig.1 Microstructure on the transetion of 316 stainless ateel irradiated with 40 MeV carbon ions to 1.5 x 10^{22} ions/m^2 at ambient temperature.

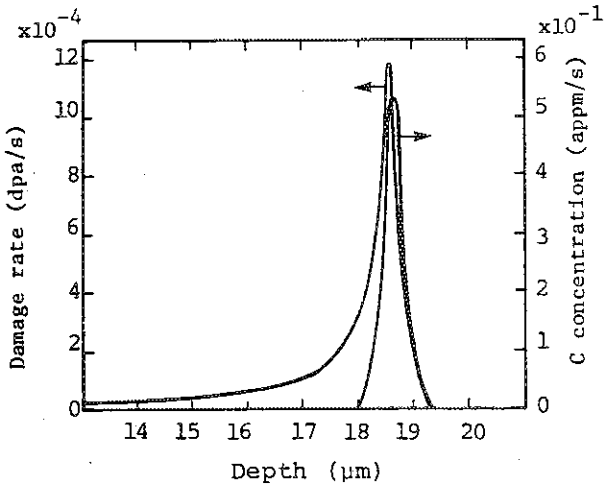

Fig.2 Depth dependance of displacement damage and injected ion distribution for 40 MeV carbon injected into amorphous iron with a current density of 10 mA/m^2.

irradiated and back surfaces to a thickness of about 1.5 mm, and then sliced in a plane normal to the original incident surface with low-speed diamond saw. The sectioned sample was mechanically polished and etched by a saturated solution of CuCl in aqua regia. The optical micrograph of the etched surface revealed a pair of parallel lines at the depths of 18 μm and 19 μm from the incident surface for 40 MeV carbon-ion irradiation(Fig.1).

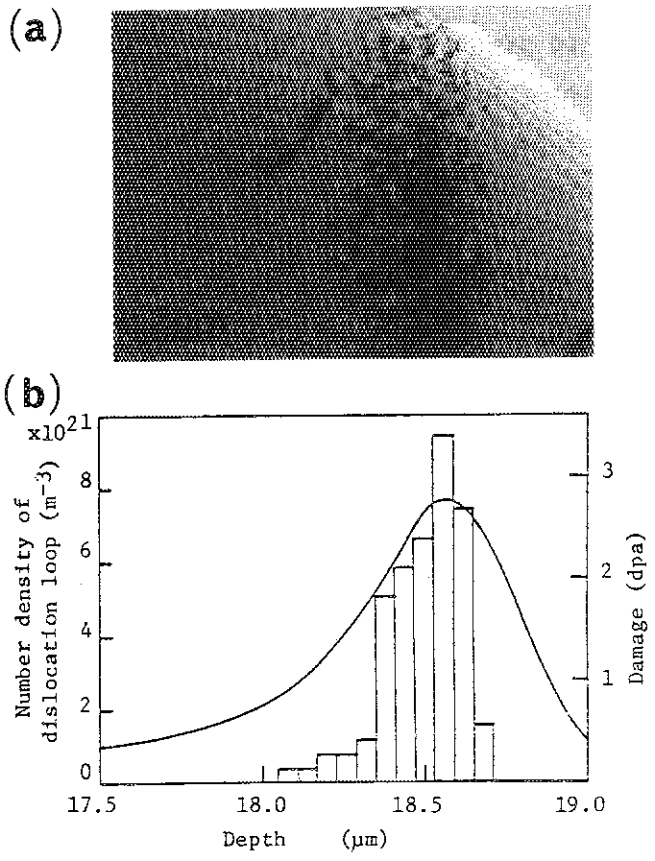

Fig.3 (a):Transmission electron micrograph of the damage region and (b):the number density of dislocation loop in the relevant region.

Figure 2 shows the displacement damage and injected ion distribution curves for 40 MeV carbon-ion irradiation into amorphous iron calculated by the expanded E-DEP-1 computer code with Ziegler's electronic stopping power[1]. The curves for the damage and carbon distributions, respectively, peak at depths of 18.6 and 18.7 μm from the ion-incident surface; The mean projected range of the carbon-ion into iron is closely approximated by the peak position of the displacement damage curve. The cross sectional micrograph given as Fig.3(a) is a typical damage structure in the region relevant to a pair of parallel lines shown in Fig.1. The damage structure observed in the micrograph consists of the dislocation loops. The average diameters of the loops were little changed throughout the damage region to be about 30 nm. The depth distribution of the number density of the dislocation loop is presented in Fig.3(b). The depth histogram for the dislocation loop is in fairly good agreenent with the calculated displacement damage profile. Moreover, the dislocation loop produced by carbon-ion irradiation is distributed in depths ranging from 18.1 to 18.7 um. Then, the center line between the etched lines seen in Fig.1 is deduced to correspond to the mean projected range and the range in Type 316 stainless

steel can be measured fairly accurately with optical microscopy. The mean projected range measured for incident-ion energies ranging from 40 to 90 MeV is presented in Table 1. and compared with the calculated values. The underestimation of the electronic stopping powers is considered to be the cause of larger mean projected range in the calculation. The stopping power was simply estimated from the difference in incident energies divided by the difference in the relevant mean projected ranges. The estimated stopping powers are tabulated in Table 2; Ziegler's stopping powers are also given in the table for comparison.

Table 1 Comparison between measured and calculated ranges.

Energy (MeV)	Range (μm)	
	Measured	Caluculated
40	18	18.7
60	31	32.7
80	47	49.5
90	57	59.2

Table 2 Estimated stopping powers and calculated values by Ziegler.

E_0 (MeV)	ΔE (MeV)	R (μm)	ΔR (μm)	$(\frac{\Delta E}{\Delta R})_{measured}$ (MeV/(mg/cm²))	$E=E_0+\frac{\Delta E}{2}$ (MeV)	$(\frac{\Delta E}{\Delta R})_{Ziegler}$ (MeV/(mg/cm²))
40	20	18	13	1.96	50	1.83
60	20	31	16	1.59	70	1.48
80	10	47	10	1.27	85	1.26
90		57				

In conclusion, the mean projected range for carbon-ion injected into Type 316 stainless steel can be measured fairly accurately with optical microscopy on cross sectional surface of the specimen. The measured mean projected range is in good agreement with the calculation by the expanded E-DEP-1 code with Ziegler's stopping powers for incident-ion energy ranging from 40 to 90 MeV.

Reference

(1) J.F.Ziegler : Handbook of Stopping Cross-Sections for Energetic Ion in All Elements (Pergamon Press, New York, 1980)

3.3 Heavy Ion Track Filter of Polyvinylidene Fluoride.

Yoshihide Komaki*, Shinichi Ohno*, Hiroshi Ito**, Tadao Seguchi**, and Matae Iwasaki***

*Department of Chemistry and **Takasaki Radiation Research Establishment, Japan Atomic Energy Research Institute, and ***Institute of Atomic Energy, Kyoto University.

Fabrication of microfilters by a heavy ion irradiation-chemical etching method has been mostly attempted for polyesters. We have examined polyvinylidene fluoride(PVDF) film using a heavy ion from the JAERI tandem accelerator, with the result that only ions heavier than the Cl ion being able to register the tracks on PVDF.[1)]

A stack of the PVDF films of 9 μm in thickness and 13 mm in diameter was bombarded with beams of the Ni^{10+} ion incident perpendicularly. The Ni^{10+} ion energies at the entrance of each film are 2.6 MeV/amu and 1.6 MeV/amu, respectively. The bombarded films, after kept in air at room temperature for a certain time, were etched in 9N NaOH solution at 85°C. The hole density in the membrane ranged from $1x10^8$ to $6x10^8$ cm^{-2}, as listed in Table 1. The enlargement of track diameters, i.e. the effective hole diameters, as function of the time of etching was verified and measured by the gas flow rate through the perforated holes. The hole density and the shapes of perforated holes were observed simultaneously with an electron microscope.

Table 1. Irradiation conditions and hole density in PVDF.

No	Ions	Energy (MeV/amu)	Current (nA)	Irrad.time (sec)	Hole density (cm^{-2})
1	Ni^{10+}	2.6, 1.6	0.1	8	1×10^8
2	Ni^{10+}	2.6, 1.6	0.1	24	3×10^8
3	Ni^{10+}	2.6, 1.6	0.1	50	6×10^8

Figure 1 shows the effective hole diameter vs. the time of etching for the hole densities of $1x10^8$ and $6x10^8$ cm^{-2}. In a series of the experiments the films were irradiated with the Ni^{10+} ions at two kinds of energies. From the figure one sees that the hole diameter increases linearly after a certain induction time of etching and that the increase in

hole diameter is only a little affected by a difference in ion energy. The induction time after which the hole diameter begins to increase may be necessary for the etching solution to flow along the heavy ion track from both sides of the film and to reach each other forming a channel. The etching rate along the tracks is then given as $V_1 = \ell/(2T)$, ℓ being the film thickness and T the induction time. The slope of the curves, S, represents the rate of increase in track width and thus the radial etching rate is given as $V_2 = S/2$. The values of V_1 and V_2 thus calculated and the ratios V_1/V_2 are presented in Table 2.

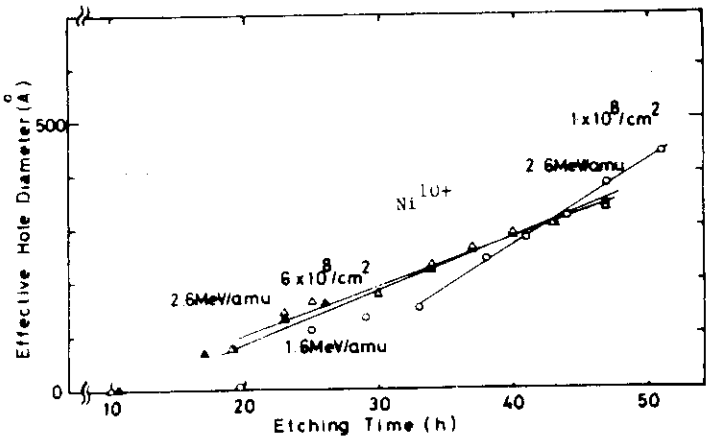

Figure 1.

Growth of hole diameter in PVDF exposed to the Ni^{10+} ions and etched in 9N NaOH solution at 85°C.

Table 2.

The etching rate along the track (V_1), the radial rate(V_2) for PVDF films etched in 9N NaOH solution at 85°C.

Ni^{10+}		V_1	V_2	V_1/V_2
$\cdot cm^{-2}$	MeV/amu	Å/h		
1×10^8	2.6	2.1×10^3	8	260
6×10^8	2.6	4.9×10^3	5 (5*, 1, 6)	940
	1.6	3.9×10^3	5	780

* From micrographs.
9N NaOH, 85C°, etching

This Table demonstrates that 1) the value of V_1 is very large in comparison with that of V_2, 2) the value of V_2 is small, that is, the dissolved layer from single surface of the film is thin, and 3) the value of V_2 which has been obtained from the measurement of gas flow rate roughly corresponds to the radial etching rate of tracks in micrographs. The ratios V_1/V_2 explain the shapes of the etched tracks observed in micrographs having a taper with a small angle. It was concluded that the hole diameters in the microfilter of PVDF fabricated by bombardment of the Ni ion were homogeneous and the diameters measured from the gas flow rate corresponded to the ones observed on micrographs.

Reference ;

1) Y. Komaki et al, "JAERI TANDEM Annual Report,1982",JAERI-M 83-095(1983) 31.

3.4 Heavy Ion Irradiation Experiments Using Low Temperature Irradiation Chamber

Eiji Sakai* and Yukio Kazumata**

*Department of Nuclear Engineering, Japan Atomic Energy Research Institute and **Department of Physics, Japan Atomic Energy Research Institute.

Various materials were irradiated at 77 K in the Low Temperature Irradiation Chamber located at the beam line L2 with 60 MeV $^{11}B^{3+}$, 143 MeV $^{58}N^{10+}$, 150 MeV $^{115}In^{10+}$, 180 MeV $^{63}Cu^{11+}$ and 100 MeV $^{12}C^{5+}$. The dates of the experiments, user's names, specimens irradiated, numbers of particles, purposes of the experiments and the species of heavy ions are listed in Table 1. The materials irradiated were brought back to individual user's laboratories to characterize their own specimens. A small hoist using an oil pressure cylinder was manufactured to provide a way of holding the lid of the chamber during opening it. The results of the experiments will be described by the individual users in the separate sections.

Table 1. Heavy ion irradiation experiments performed using Low Temperature Irradiation Chamber during the fiscal year of 1983

Experiment	User	Date	Heavy ion	Number of particles	Specimen	Characterization
1st	S.Furuno	10 May 1983	60MeV $^{11}B^{3+}$	2.19E12*	Ge,etc.	T.E.M.
	H.Naramoto			1.2 E14	MgO,etc.	Optical absorption
	E.Sakai			8.05E13	Ge	Induced radioact.
	E.Sakai			7.21E13	Si	Induced radioact.
	H.Tomimitsu			1.06E14	Si	X-ray topography
2nd	S.Furuno	8 July 1983	143MeV $^{58}Ni^{10+}$	2.24E12	SUS,Al,etc.	T.E.M.
	M.Komaki			1.16E11	PVDF	E.S.R.
	H.Maeta			2.11E13	Fe,Ni,etc.	X-ray diffraction
	E.Sakai			2.91E13	GaSe	Induced radioact.
	Y.Kazumata			1.99E13	graphite	E.S.R.
3rd	M.Komaki	2 Dec. 1983	150MeV $^{115}In^{10+}$	6.65E11	PVDF	E.S.R.
	S.Furuno			1.25E12	Ge,Si,Al	T.E.M.
	E.Sakai			5.12E13	Ge	Induced radioact.
	E.Sakai			2.88E13	Si	Induced radioact.
	H.Naramoto			6.40E13	SiC,Fe	Mössbauer effect
4th	S.Furuno	6 Feb. 1984	180MeV $^{63}Cu^{11+}$	2.27E13	Ge	T.E.M.
	H.Naramoto			2.18E12	LiF,etc.	Optical absorption
	H.Naramoto			9.81E13	MgO,SiC	Optical absorption
	E.Sakai			8.0 E13	Si	Induced radioact.
	E.Sakai			6.32E13	Ge	Induced radioact.
5th	H.Naramoto	23 Feb. 1984	100MeV $^{12}C^{5+}$	2.19E12	LiF	Optical absorption
	H.Naramoto			6.28E13	MgO	Optical absorption
	H.Tomimitsu			1.6 E15	Si	X-ray topography
	Y.Kazumata			3.13E14	graphite	E.S.R.
	E.Sakai			3.1 E15	Ge	Induced radioact.

* 2.19×10^{12}

3.5 Residual Radioactivities in Semiconductors and Other Materials for Solid-State Physics Research Irradiated with High-Energy Heavy Ions

Eiji Sakai* and Hideo Nakatani**

*Department of Nuclear Engineering, Japan Atomic Energy Research Institute and **Faculty of Engineering, Toyama University.

Measurements of the residual radioactivities induced in semiconductors (Ge, Si, GaAs) and other materials(Cu, Mo, stainless steel) irradiated with various high-energy heavy ions from JAERI tandem accelerator have been continued using a high-purity germanium gamma-ray detector. Table 1 summarizes the results obtained from the semiconductors after irradiation during the fiscal year 1983 and Table 2 those from other materials. In the Tables, the species and the numbers of particles of heavy ions, the residual gamma-ray-emitting nuclides found, their radioactivities with the corresponding numbers of atoms as well as the numbers of atoms per particle extrapolated to the end of the irradiation and the final stable daughter nuclides are listed. Some of the results from the irradiated silicon and germanium were reported at 1983 Nuclear Science Symposium[1].

---

1) E.Sakai: IEEE Trans. Nucl. Sci., NS-31(1984), No.1, 316.

Table 1 Residual gamma-ray emitting nuclides, their radioactivities, numbers of atoms, numbers of atoms per particle and final stable daughter nuclides found in germanium, silicon and GaAs irradiated with various heavy ions

Heavy ions (Range)	Number of particles	Irradiated material	Residual nuclide (Halflife)	Radioactivity (μCi)	Number of atoms	Number of atoms per particle	Final stable nuclide
50MeV $^{11}B^{3+}$ (60μm)	5.15E13* /3.14cm^2	Ge	As-71(61h)	1.45E-2	1.7E8	3.3E-6	Ga-71
			As-72(26.0h)	1.27E-2	6.3E7	1.2E-6	Ge-72
			As-73(80.3d)	1.20E-3	4.4E8	8.6E-6	Ge-73
			As-74(17.8d)	1.80E-3	1.5E8	2.9E-6	Ge-74,Se-74
			Se-75(118.5d)	7.16E-4	3.9E8	7.6E-6	As-75
			Br-76(16.1h)	2.75E-1	8.5E8	1.7E-5	Se-76
			Br-77(57.0h)	1.2 E-1	1.3E9	2.5E-5	Se-77
			Kr-79(35.0h)	1.9 E-1	1.3E9	2.5E-5	Br-79
			Rb-83(86.2d)	4.7 E-4	1.9E8	3.6E-6	Kr-83
50MeV $^{11}B^{3+}$ (95μm)	4.61E13 /3.14cm^2	Si**	Be-7(53.3d)	1.3 E-4	3.2E7	6.9E-7	Li-7
100MeV $^{12}C^{5+}$ (190μm)	4.38E14 /0.86cm^2	Si	Be-7(53.3d)	1.13E-6	2.8E9	6.4E-6	Li-7
			Na-22(2.60y)	2.40E-4	1.05E9	2.4E-6	Ne-22
			Na-24(15.0h)	3.10E-2	9.0E7	2.2E-8	Mg-24
143MeV $^{58}Ni^{10+}$	4.66E12 /0.79cm^2	GaSe	Zn-62(9.13h)	1.38	2.4E9	5.2E-4	Ni-62
180MeV $^{63}Cu^{11+}$ (29.1μm)	8.00E13 /3.14cm^2	Si	Y-87(80.3h)	1.2E-4	1.8E6	2.3E-8	Sr-87
			Y-87-Y-87m(2.8h)				Sr-87
			Zr-86(16.5h)	1.0E-3	3.2E6	4.6E-8	Sr-86
			Zr-86-Y-86(14.7h)				Sr-86
			Zr-88(83.4d)	1.24	1.99E10	2.04E-9	Sr-88
			Zr-88-Y-88(106.6d)				Sr-88
			Zr-89(78.4h)-Y-89m(16.1s)				Y-89
			Nb-90(14.6h)	1.08E-3	3.0E6	3.5E-7	Zr-90
180MeV $^{63}Cu^{11+}$ (20.4μm)	6.32E13 /3.14cm^2	Ge	None				
150MeV $^{115}In^{10+}$ (19.6μm)	1.84E13 /3.14cm^2	Si	None				
150MeV $^{115}In^{10+}$ (14.6μm)	3.28E13 /3.14cm^2	Ge	None				

* 5.15×10^{13}. ** Strong beta counting.

Table 2 Residual gamma-ray emitting nuclides, their radioactivities, numbers of atoms, numbers of atoms per particle and final stable daughter nuclides found in copper and molybdenum irradiated with various high-energy heavy ions

Heavy ions (Range)	Number of particles	Irradiated material	Residual nuclide (Halflife)	Radioactivity (μCi)	Number of atoms	Number of atoms per particle	Final atable nuclide
50MeV $^{11}B^{5+}$ (35.8μm)	2.90E13*$_2$ /1.767cm^2	Cu	Ga-67(78.28h)	1.31E-2	1.97E2	6.8E-6	Zn-67
			Ge-69(39.05h)	2.30E-2	2.30E8	7.95E-6	Ga-67
			As-71(61h)	1.05E-2	1.29E8	4.44E-6	Ga-71
			As-72(26h)	1.9 E-2	9.56E7	3.3 E-6	Ge-72
			Se-72(8.40d)	7.2 E-4	2.78E7	9.6 E-7	Ge-72
80MeV $^{12}C^{6+}$ (48μm)	1.47E16?$_2$ /1.767cm^2	Cu	Co-58(70.78d)	4.6 E-4	1.50E7		Fe-57
			Co-60(5.27y)	1.72E-4	1.52E9		Ni-60
			Zn-65(244.0d)	3.86E-4	3.01E8		Cu-65
			Ga-67(78.26h)	2.12E-3	2.21E7		Zn-67
			Ge-69(39.05h)	1.34E-2	6.97E7		Ga-69
			As-71(61h)	9.52E-3	7.74E7		Ga-71
			As-72(26.0h)	0.192	6.64E8		Ge-72
			As-73(80.30d)				Ge-73
			As-74(17.79d)	5.8 E-5	3.3 E6		Ge-74,Se-74
			Se-72(8.4d)				Ge-72
			Se-75(118.45d)	7.15E-5	2.71E7		As-75
143MeV $^{58}Ni^{10+}$ (10μm)	2.45E13$_2$ /4.12cm^2	Cu	Zn-62(9.13h)	1.79	3.15E9	1.3 E-4	Ni-62
			Zn-65(244.1d)	1.6 E-5	1.76E7	7.2 E-7	Cu-65
180MeV $^{63}Cu^{11+}$ (11.6μm)		Cu	None				
50MeV $^{11}B^{3+}$ (34.3μm)	3.34E13$_2$ /1.55cm^2	Mo	Mo-99(66.02h)	8.23E-4	1.05E7	3.13E-7	Ru-99
			Tc-95(34.97d)	2.63E-5	4.24E6	1.27E-7	Mo-95
			Tc-96(4.35d)	4.37E-4	8.76E6	2.63E-7	Mo-96
			Ru-97(2.88d)	7.11E-4	9.45E6	2.83E-7	Mo-97
			Rh-99(15.0d)	1.19E-4	8.25E6	2.47E-7	Ru-99
			Rh-100(20.8h)	3.60E-2	1.44E8	4.30E-6	Ru-100
			Rh-101m(4.34d)	6.14E-3	1.23E8	3.68E-6	Ru-101
			Pd-100(3.63d)				Ru-100
			Ag-105(41.29d)	2.98E-4	5.68E7	1.70E-6	Pd-105
			Ag-106m(8.5d)	6.67E-4	2.62E7	7.83E-7	Pd-106,Cd-106

* 2.90 x 10^{13}.

3.6 ESR of Pyro-Graphite Irradiated by Cl^{8+} Ions

Yukio Kazumata*, Shigemi Yugo** and Tadamasa Kimura**

*Department of Physics, Japan Atomic Energy Research Institute.
**University of Electro-Communications.

So far two paramagnetic centers have been observed by high energy chlorine ion bombardments.[1] The one has been assigned to localized spin centers from no change of g-value and width in its esr spectrum with annealing and measuring temperature. This center is associated with clustered-defects formed at the end, near the range, of the trajectory of the projectile. The other stems from acceptor rich region on the way of the penetration of the projectile. On the contray to the former center, this center changes its g-value and width with annealing and measuring temperature.

Further details of these two spin centers will be described in this paper; that is, antiferromagnetic interaction between spins in the localized spin centers and correlation of the latter center with hopping motion of carriers.

A high concentration of the localized spin centers, $\sim 10^{19}$ spins/cm^2, suggests the mutual interaction between themselves. The nature of the interaction is found by the change of an intensity of the esr line with measuring temperature. The results of the measurements have been followed by the formula,

$$\chi(T)= \frac{a_1}{T+\Theta_{AF}} + \frac{b_1}{T+\Theta_F} + \frac{c_1}{T} \qquad (1).$$

Here $\chi(T)$ is the static susceptibility proportional to the intensity. The characteristic temperatures of Θ_{AF} and Θ_F stand for antiferromagnetic and ferromagnetic Curie's temperature, respectively.
The first term, as is well known, repesents antiferromagnetic interaction between spins. The coefficient a_1 is proportional to the spin concentration in this interaction. Similarly, the second term is due to ferromagnetic interaction and the third no interacting spins. From the fitting of experimental values with the eq.(1), the greater part of the interactions, about 98 % of the total spin concentration, have been reduced to the first term and the rest due to the second or the third term.

Similar localized spin centers observed by the bombardments of low

energy P^+ or D^+ ions show weaker interaction between spins and less concentration of interacting spins. Clearly,the strength of the interaction and the concentration of the interacting spins depend on the masses of projectiles, which will correlate with the concentration of defects in a defect cluster.

Next, discussion will proceed to the spin center from acceptor rich region. As shown in Fig.1, the g-value and the width with measuring temperature are well fitted by exponential functions. These curves are quite different from those due to the localized spin centers mentioned above and conduction carriers. On the conduction carriers in unirradiated pyro-graphite, the g-value and width increase with a decrease of measuring temperature, just opposite tendency to the spin center. From the comparison with these two spin centers in temperature dependence, the spin centers now taken up will be in the intermediate state between conduction carriers and the localized spin centers. The intermediate state probably corresponds to the hopping motion of carriers. The exponential nature of g-value and width in Fig.1 would be derived from the medel of the hopping carriers.

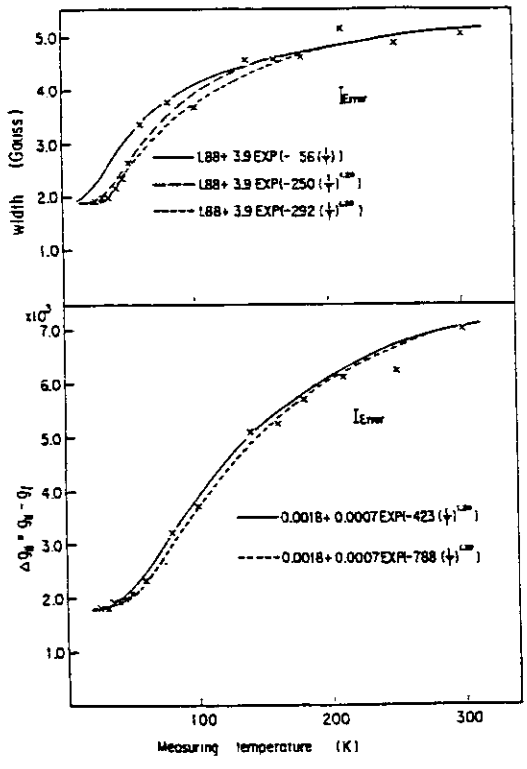

Fig.1, Change of g-value and width with measuring temperature for the spectrum stemed from acceptor rich region. These curves show exponential variation.

Reference

1) Y. Kazumata and S. Yugo; J. Phys. Soc. Jpn. 51(1982) 3753

3.7 Irradiation Effect with Heavy Ions on Alkali Halides

Hiroshi Naramoto*, Akira Kikuchi** and Kunio Ozawa**

*Department of Physics, Japan Atomic Energy Research Institute, **Faculty of Engineering, Ibaraki University.

Energetic ions interact with solids through the electronic and nuclear process, and at high energies the interaction process is characterized by the intense electronic excitation. This process can be visualized especially in insulators such as alkali halides where the lattice defects are produced through ionizing radiation. Heavy ions penetrating through alkali halides are reasonably expected to leave tracks which are locally damaged regions, and defect density within tracks varies with the depth from the incident surface.[1] In the present study, the direct measurement is made for the depth profile of color centers in order to extract the information associated with the energy dissipation process of heavy ions.

LiF and NaF single crystals were purchased from Harshaw Chemical Co. and a typical specimen had dimensions $1 \times 0.8 \times 0.1$ cm^3. Irradiation was performed at liquid nitrogen temperature(LNT) with heavy ions from JAERI tandem accelerator, and specimens were exposed to 180 MeV Cu^{11+} and 100 MeV C^{5+} ions to the dose of 7×10^{12} /cm^2. Irradiation with 1.8 MeV protons was also employed to compare the coloration with that by energetic heavy ions. The coloration limited at the near surface region was examined in the wavelength region of ultra violet and visible light using a micro-spectrophoto-meter with the spot size of 2 μm in diameter.

Fig. 1 shows the optical absorption spectra taken at the local spots 8 and 18 μm from the surface in LiF irradiated with 180 MeV Cu^{11+} ions to the dose of 7×10^{12} /cm^2. Different from a typical absorption spectrum which was obtained in LiF irradiated with 1.8 MeV protons, a broad envelope appeared around the

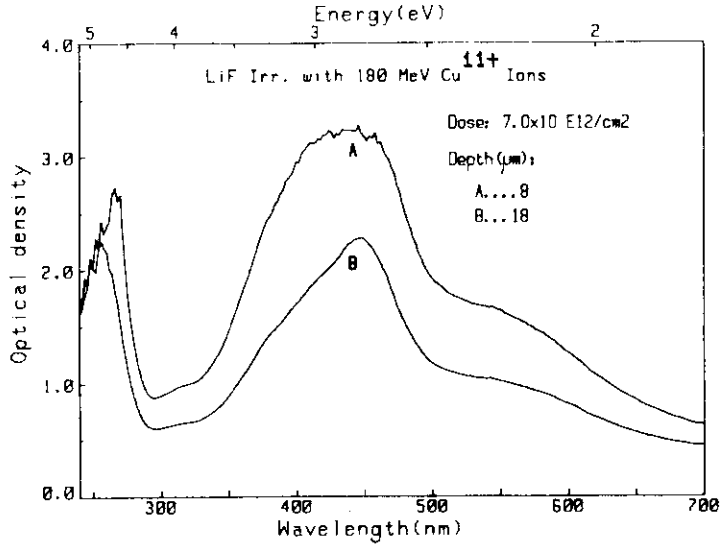

Fig. 1. Optical absorption spectra at the local spots in LiF irradiated with 180 MeV Cu^{11+} ions to 7×10^{12} /cm^2.

F_2 band region accompanying the highly aggregated F_4 centers at 528 nm. To make clear the origin of this envelope, optical absorption was measured at low temperatures. With decreasing the temperature, the F-type centers should shift the wavelength at the absorption maximum to the shorter one. However, the envelope observed held its position constant even at LNT. This implies the formation of Li colloids, and its feature can be seen in the spectrum A of fig. 1.

In fig. 2, the depth profiles are illustrated for four kinds of electron trapped color centers, A, B, C and D which correspond to F, F_3, F_2 and F_4 centers, respectively. At the near surface region, the F center concentration is saturated and conversions from F centers to F_2, F_3 and F_4 centers are recognized. At the middle region of the projected range, the F center profile is still saturated but the F_2 center profile has the maximum at the depth of ∿9 μm where the colloidal band is formed as shown in fig. 1. At the deeper region, every profile tends to decrease, and both profiles of A and C cross together at ∿22 μm. This depth coincides with R_p the calculated projected range. In the region beyond R_p, coloration is still observed and dominant defects are the F centers. Optical absorption spectrum is similar to that induced by ionizing radiation like electrons, which suggests that the secondary electrons generated during the penetration of heavy ions contribute to the coloration in this region. Thus, it is reasonable to take the cross point of A and C profiles for the limit of coloration directly induced by incident ions.

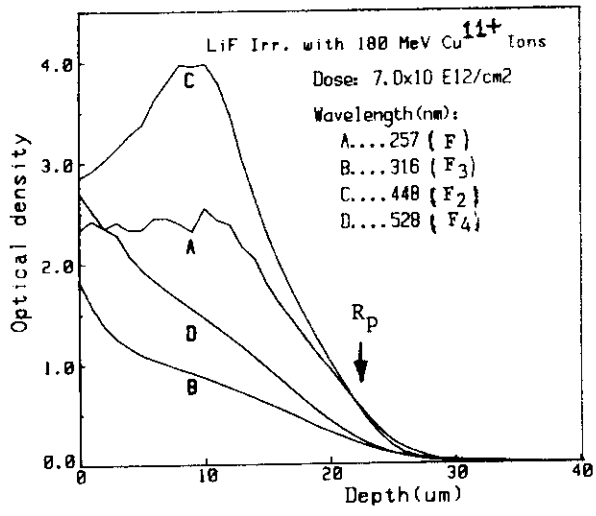

Fig. 2. Depth profiles of color centers in LiF irradiated with 180 MeV Cu^{11+} ions to 7×10^{12} /cm^2. R_p denotes the same quantity as in Fig. 1.

The depth where the profile C shows the maximum is much shallower than R_p and is rather close to that where the electronic energy loss amounts to the maximum. This result supports an idea that Li colloids are formed associating with defect generation at the fluorine lattice through the intense electronic excitation. In NaF, the colloidal band was also observed, whereas some differences are found in the details of depth profiles. C^{5+}(100 MeV) irradiation did not induce a definite colloidal band, and the main feature is just between 1.8 MeV proton and 180 Cu^{11+} irradiations.

Reference

1) J. M. Loman and R. B. Murray: Radiation Effects 52 (1980) 1.

3.8 Electron Microscope Observations of Tracks of High Energy Heavy Ions in Solids

Shigemi Furuno, Kazuhiko Izui and Hitoshi Otsu

Department of Chemistry, Japan Atomic Energy Research Institute

The observations of tracks of high energy heavy ions produced in some solid materials were made with an electron microscope in order to clarify the governing factors and mechanisms for track formation. In this report, the effect of the energy deposition of the incident ions on the track production phenomena is investigated in the deposited films of germanium, silicon and titanium.

Thin films of germanium, silicon and titanium of 50 Å in thickness were prepared by vacuum evaporation on collodion films. These specimens were set on the low temperature stage cooled at 77 K and were irradiated with Ni^{10+} and In^{10+} ions obtained from the JAERI tandem accelerator with incident angle of about 10°. In order to obtain the wide range of incident energies, some irradiations were performed with the ions which were transmitted through thin nickel or aluminium foils mounted in front of the specimens. In this case, the energies were estimated from the range-energy relations obtained from the calculated stopping powers by J. F. Ziegler[3]. After the irradiations, the observations were carried out with the electron microscope of JEM-100C type.

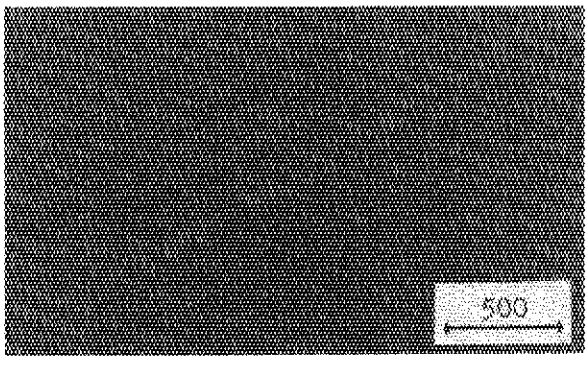

Fig. 1 Track of 143 MeV Ni ion in germanium

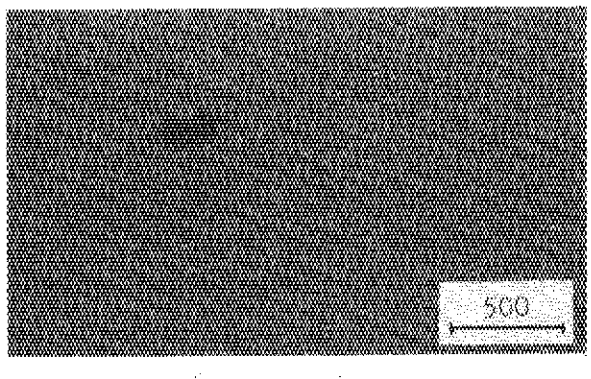

Fig. 2 Track of 12 MeV Ni ion in germanium

Figures 1 and 2 show the tracks of Ni ions with energies of 143 and 12 MeV in germanium respectively. Correspoding energy depositions are 11 and 5.3 MeV/μm[3]. The widths of the tracks were found to decrease from 100 to 80 Å with decreasing the deposited energy.

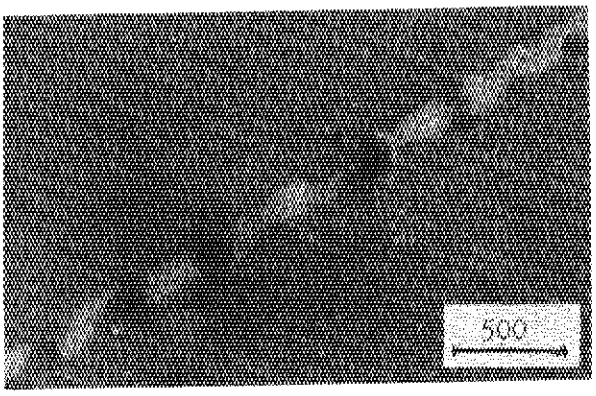

Fig. 3 Track of 150 MeV In ion in germanium

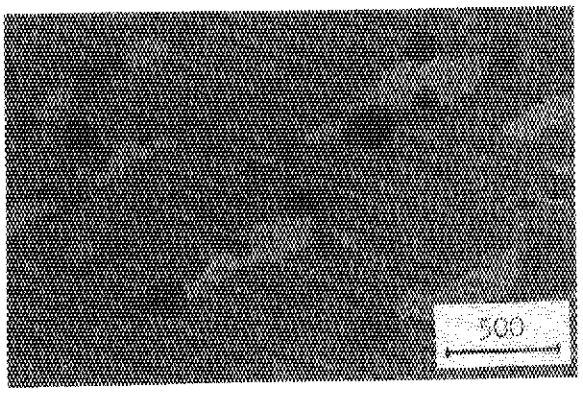

Fig. 4 Tracks of 85 MeV In ions in germanium

Figures 3 and 4 show the tracks of In ions with energies of 150 and 85 MeV in germanium respectively. Corresponding energy depositions are 18 and 15 MeV/μm^3), and the widths of the tracks were 170 and 130 Å respectively. In silicon irradiated with 150 MeV In ions no track was observed. From these observed results, the local temperature along the tracks of 150 MeV In ions is considered to be raised up to the melting point of germanium (950°C) but not to that of silicon (1400°C).

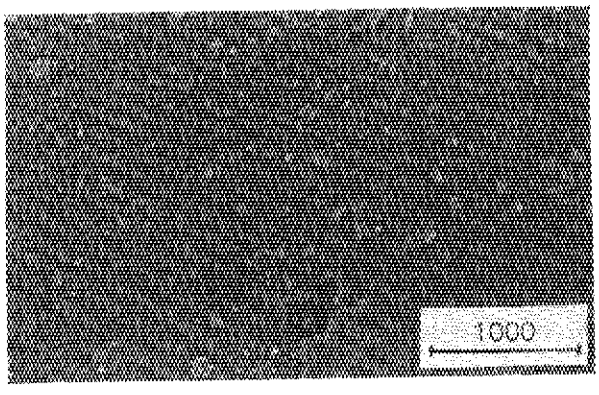

Fig. 5 No visible track in titanium film irradiated with 150 MeV In ions

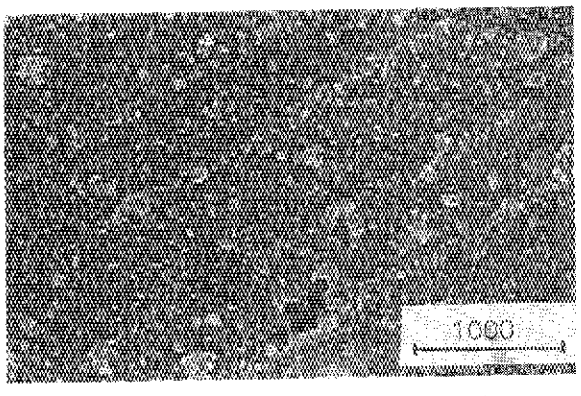

Fig. 6 Tracks visible in the same area of titanium as fig. 5 after annealing

In the case of titanium irradiated with 150 MeV In ions, no visible track appeared as shown in figure 5, but after annealing by illumination of a strong electron beam, visible tracks appeared as shown in figure 6.

The results of experiments are summarized in table 1, where some previous works are also referred[1,2].

Comparing the image contrasts of tracks in the present work with that obtained in the previous work[2], these tracks of Ni and In ions in germanium are thought to consist of both small crystallites of about 100 Å in diameter and evaporated regions. The evaporated regions become dominant and the widths of tracks increase with increasing the deposited energy.

Table 1 Ions and Specimens used in experiments, some parameters and experimental results

Ion	Specimen	Melting point of specimen (°C)	Energy deposition (MeV/μm)	Width of track (Å)
143 MeV Ni	Ge	958	11	100
12 MeV Ni	Ge	958	5.3	80
150 MeV In	Ge	958	18	170
85 MeV In	Ge	958	15	130
128 MeV Cl	Ge	958	5.3	80
150 MeV In	Si	1415	12	
150 MeV In	Ti	1820	19	
130 MeV Cl	MoO_3	795	5.5	42
130 MeV Cl	MoS_2	1185	6.4	discrete

These recrystallization and evaporation along the tracks are considered to arise from the thermal spike effect due to the energy dissipated in electron excitation. Concerning the result for titanium film, it is inferred that small invisible crystallites or nuclei for recrystallization are formed along the path of the 150 MeV In ions, and that by the annealing treatment the crystallites grow to form the visible tracks. As already reported, the tracks of Cl ions in molybdenum disulphide consist of small spots in linear array, in which the high energy knock-on process is considered to produce discrete structural changes. On the other hand, the tracks of Cl ions in molybdenum trioxide consist of the regions fully evaporated by the thermal spike effect due to the energy dissipated in electron excitation.

From these results, it is concluded that not only knock-on process but electron excitation process play important roles in the damage production in some materials mentioned above .

Reference

1) S. Furuno, H. Otsu and K. Izui: J. Electron Microsc. 30 (1981) 327.
2) S. Furuno, H. Otsu and K. Izui: "JAERI TANDEM Annual Report, 1982" JAERI-M 83-095 (1983) 43.
3) J. F. Ziegler: Handbook of Stopping Cross Sections for Energetic Ions in All Elements (Pergamon Press, New York, 1980).

3.9 X-Ray Diffraction Topographic Observation of Si Single Crystals Irradiated with 58 MeV B^{3+} and 100 MeV C^{5+} Ions

Hiroshi Tomimitsu

Department of Physics, Japan Atomic Energy Research Institute.

It has become very important to investigate the nature of ion-irradiated materials for the development of heavy-duty semiconductors, heat-resistant materials, etc[1]. The present author has also examined the Si specimens irradiated with 150 MeV Ni^{9+} and Cl^{9+} ions, the preliminary results being briefly published[2]. In this report, the Si specimens were prepared by the irradiation with B^{3+}(58 MeV) and C^{5+}(100 MeV) ions, which were expected to have much longer ranges in the Si crystal[3].

Similar to the previous examination, the Si single crystal used in this experiment was grown by the Cz.method along [001] direction, and was sliced parallel to the (001) plane, chemically etched and mechanically polished, the resultant thickness being 0.3 mm. The Si wafer thus obtained was then cut into two rectangular pieces of about 3x3 cm^2, giving the specimens for the ion-irradiation. The X-ray diffraction topographs of these original Si wafers showed no significant contrast, indicating that they were almost perfect.

One Si wafer was irradiated with 58 MeV B^{3+} ions for 4.5 hrs, with an average ion current of 30 nA receiving a total dose of about $1x10^{14}$ ions/cm^2. For the second wafer irradiated with 100 MeV C^{5+} ions, the values were 3.5 hrs, 165 nA and about $5x10^{14}$ ions/cm^2, respectively. In both cases, the Si wafers were partially covered with specially designed Mo-masks to facilitate the analysis. The Mo-masked Si wafers were mounted on a Cu-made specimen supporter cooled with liquid nitrogen during the irradiation.

The X-ray diffraction topography (XDT) was carried out with a fine focus X-ray generator, being operated at 50 kV with 1.2 mA using the targets of Cu and Mo.

Although the XDT observations are only at their preliminary stage, a significant phenomenon was observed; that is the X-ray topographs taken showed no characteristic images, except for only the black-and-white contrast observed at the boundaries between the irradiated- and non-irradiated areas, as indicated by the arrows in Fig.1, which indicates the existence of the lattice strains concentrated at the irradiation boundaries.

This is quite different from the previous observation on the specimens

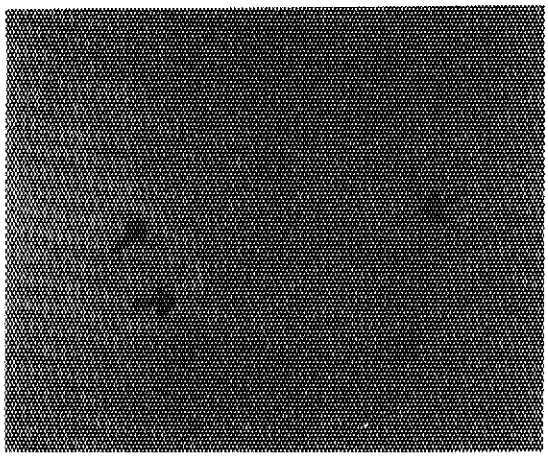

Fig.1
X-ray diffraction topograph of Si single crystal irradiated with C^{5+} ions. The black-and-white contrasts are faintly visible, as indicated by the arrows. Cu-$K_{\alpha}1$ radiation was used, and 220 reflection.

I 1 mm

irradiated with 150 MeV Ni^{9+} and Cl^{9+} ions, which gave, in addition to the above-mentioned black-and-white contrasts at the irradiation boundaries, some characteristic results[2];

--- some of the topographs taken showed systematic circular fringes within the irradiated areas, and

--- specimens after the ion-irradiation were macroscopically deformed throughout the whole crystal.

These differences of the topographic images between the specimens irradiated with Ni^{9+} and Cl^{9+} ions and with B^{3+} and C^{5+} ions, will be studied further by the present author in terms of the so-called 'ranges' and 'dpa's within the Si crystal.

References

1) For examples,
U.Bonse, M.Hart and G.H.Schwuttke: phys. Status Solidi 33 (1969) 361,
A.R.Lang and V.F.Miuscov: Appl. Phys. Lett. 7 (1968) 214,
D.Simon and A.Authier: Acta Crystallogr. A24 (1965) 527.
2) H.Tomimitsu: Japan. J. Appl. Phys. 22 (1983) L674.
3) U.Littmark and J.F.Ziegler: Handbook of Range Distributions for Energetic Ions in All Elements (Pergamon Press, N.Y., 1980).

3.10 A Study of Defect Structures in Heavy Ion Irradiated Nickel and bcc Iron by Measurements of Magnetic Anisotropy

Hiroshi Maeta, Fumihisa Ono*, Atushi Taketani** and Tomayoshi Kittaka*

Department of Physics, Japan Atomic Energy Research Institute, *College of Liberal Arts and Sciences, Okayama University and **Fauculty of Sciences, Okayama University.

We are making a study of the structures of radiation-induced defects by x-ray Huang scattering and magnetic anisotropy. In ferromagnetic metals, a measurement of magnetic anisotropy has been a useful experimental method to investigate the defect symmetry and clustering. In our group, for example, we have used this method to study the structures of the radiation-induced defects in nickel and bcc iron single crystals after fast neutron irradiation at 5 K and determined the structure of interstitial atoms to be 100- and 110-dumbbell in nickel and bcc iron, respectively[1]. The clustering of the defects have also been observed during the annealing procedures.

In the present paper, we will describe measurements of magnetic anisotropy in pure nickel and bcc iron after high energy nickel ion bombardment and discuss the structures of the defects in comparison with fast neutron irradiation at 5 K.

The specimens were circular discs of 99.99 % pure single crystals. The diameters of the specimens were 0.5 mm for nickel and 0.3 mm for iron, respectively. Those specimens were holded on a copper block by using a piece of permanent magnet from the back side of the holder. These specimens were bombarded with 145 MeV Ni^{10+} ion to 4.2×10^{12} ion/cm^2 at liquid nitrogen temperature. After irradiation, the specimens were warmed up to room temperature. To observe magnetic anisotropy, a torque magnetometer was used and measurements of torque curves were made at room temperature in a constant magnet field of 6 kOe by rotating the external field direction in the disc plane. The difference in observed torque curves of nickel and iron before and after nickel ion bombardment were show in Fig. 1, respectively. It was found that the irradiation-induced magnetic torque in bcc iron was quite small. On the other hand, the induced torque in nickel is appreciably large and consists of uniaxial component. In the case of the fast neutron irradiated nickel at 5 K, the observed torque curves before and after irra-

diation and successive isochronal annealings were shown in Fig. 2, for comparison. In this figure it is seen that induced torque by the irradiation consists of only biaxial component and the easy direction of the biaxial component is along the (100) crystallographic direction. This fact means that the configuration of the interstitial in nickel is 100-dumbbell. After annealings at 320 K, uniaxial component appears with a small biaxial component. The easy direction of this uniaxial component was along (100) crystallographic direction. This uniaxial component is quite different from that of ion bombarded nickel. The easy direction in different by $\pi/2$. From this fact, it is suggested that interstitial clusters grow up to form dislocation loop, in agreement with the results of the Huang scattering measurements in electron irradiated nickel by Bender and Ehrhart[2]. In the ion bombarded nickel, it is considered that the initial nucleation and the growth of the interstitial clusters during ion bombardment and/or being kept at the temperature of 77 K make a complicated effect to the uniaxial torque component by changing the total distribution of the interstitial clustering configuration. A detailed observation and discussion will be reported in future.

A small change in torque curve of iron can be explained as follows ; In the high damaged region around the projected ions, the surroundings of the atoms are quite different from other iron atoms at the normal

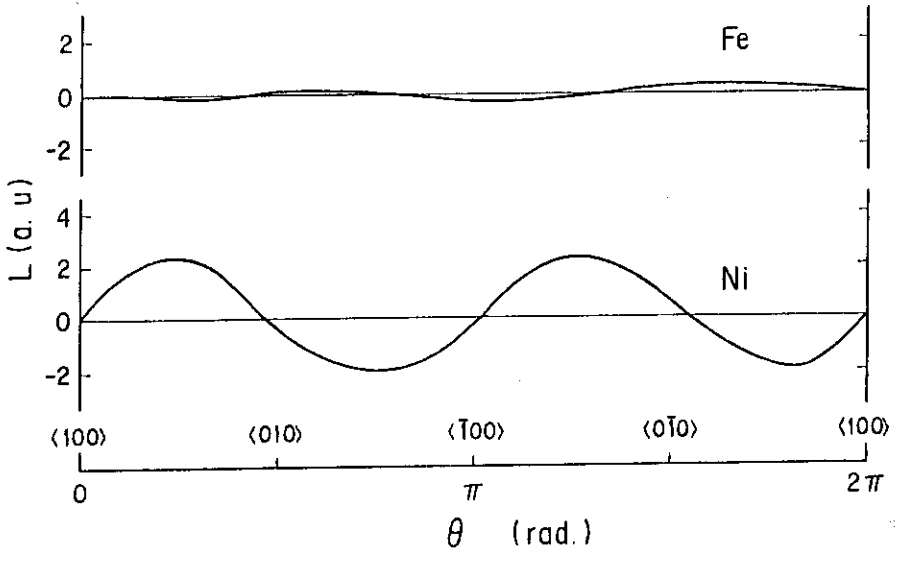

Fig. 1 Induced magnetic anisotropy in bcc iron and nickel by high energy nickel ion bombardment at NT; the difference in observed torque curves at RT before and after the irradiation. The angle θ is measured from a <100> crystallographic direction.

lattice points. The distances from those atoms to the neighbouring ones are pressed short. According to the Bethe-Slater curve, it suggests that fcc iron is weakly antiferromagnetic, while bcc iron is strongly ferromagnetic. The preferable state of those atoms can be considered to be not ferromagnetic but probably weakly antiferromagnetic. The more detailed discussion have been reported in ref.[3].

From the present experiment of bombardment of self-ion to bcc iron by tandem accelator, we can study in detail the transition from bcc iron to fcc iron. This method is very useful to investigate basic properties of strongly ferromagnetic metals.

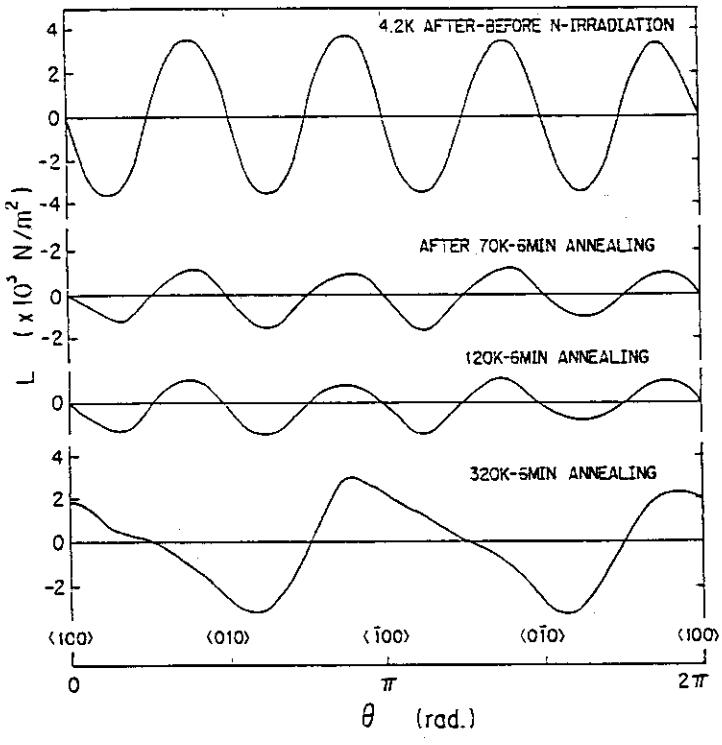

Fig. 2 Induced magnetic anisotropy in nickel by fast neutron irradiation at 5 K ; the difference in observed torque curves at 4.2 K before and after the irradiation. Changes in torque L by isochronal annealings at 70 K, 120 K and 320 K.

References

1) H. Maeta : Physics Monthly, 5 (1984) 834 (in Japaneses).
H. Maeta, F. Ono and T. Kittaka : submitted to J. Phys. Soc. Jpn.
2) O. Bender and P. Ehrhart : J. Phys. F 13 (1983) 911.
3) F. Ono, H. Maeta and T. Kittaka : J. Phys. Soc. Jpn. 53 (1984) 920.

3.11 Preliminary Testing of 17 MeV Proton Irradiation Creep in Solution Annealed 316 Stainless Steel

Akimichi Hishinuma and Takeo Aruga

Department of Fuel and Materials Research, Japan Atomic Energy Research Institute

When the stressed materials are subjected, at appropriate temperature, to a high flux of neutron which produces displacement damage, an enhancement of creep rate is in general exhibited. This paper describes preliminary proton irradiation creep data in tension, on solution annealed 316 stainless steel.

The thermal and irradiation creep measurements were made on the thin sheet specimens in a tensional creep apparatus. The specimen having form of 25 mm in length, 4 mm in width and 0.07 mm in thickness, was solution annealed for 1 hr at 1373 K and proton-irradiated under 130-260 MPa at 723 K using JAERI 20 UR Tandem accelerator with 20 particles.mA/m^2 in current density. The irradiation can get similar helium production rate per displacement damage rate as anticipated in fusion reactor first wall materials. The proton beam was focussed to about 4 mm in diameter and then,the beam was scanned up and down on 600 cycles per second to get uniform beam profile in the specimen. The projected protons having energy of 17 MeV decrease in energy and increase in displacement damage rate with increasing the penetrating depth, as shown in Fig.1. The distribution of damage in the specimen can be considered as uniform within ~1 %. The corresponding displacement damage rate was about 5×10^{-8}dpa/sec. The apparatus consists of a direct loading system for stressing the specimen and of a laser interference device for measuring the specimen length. The temperature control of the specimen is obtained by specimen resistance control and coupling between the control and measuring functions is through an infra-red pyrometer based feed-back system.

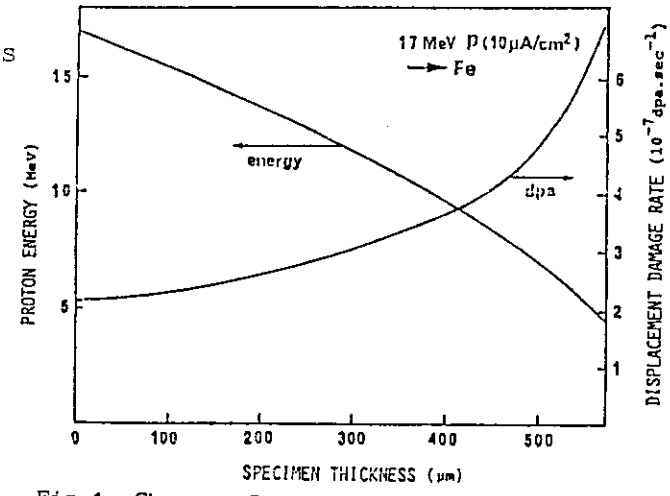

Fig.1. Change of energy and displacement damage rate of 17 MeV proton projected into iron as a function of penetration depth.

Both thermal and irradiation creep behavior are illustrated in Fig.2, which shows the specimen length as a function of time. The most striking feature of the behavior is that the negative rates of deformation were observed in irradiation creep measurement, in stead of forward creep in thermal creep. The trend was clearer when the applied stress was smaller. This may be due to the balancing of forward creep and the contraction. It is not clear, however, whether this is a real effect or a setting-in transient due to slight changes in enviroment or specimen emissivity. The specimen emissivity could increase with the experimental time elapsed and if so, real specimen temperature may decrease during the experiment. The change may result in the decrease in the specimen length and show the contraction apparently.

The phenomena of the contration has been only observed in a torsional creep apparatus[1], however, not clear in a tensional creep though the slight trend was observed[2]. The contraction may be occured due to the segregation of nickel and/or silicon during the irradiation. The segregation changes modulus of the matrix, which gives rise to the reduction of elestic strain at a constant applied stress. Another possibility of the contraction may be due to the radiation induced increase in volume either by void swelling or by precipitation. Because the torsional creep strain is inversely proportional to the specimen volume. In contrast,the tensional creep strain is proportional to the volume, then it is necessary and very important to get reliable data using a tensional creep apparatus for understanding the essential mechanism of the negative creep behavior.

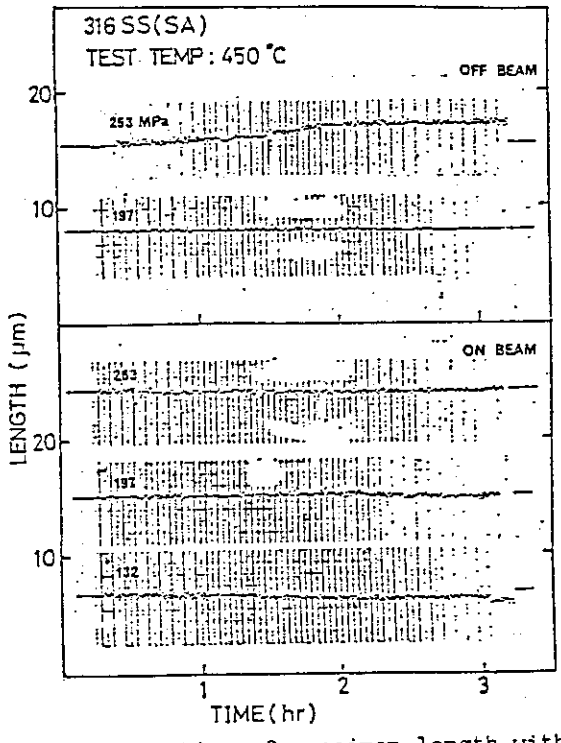

Fig.2. Variation of specimen length with time under creep tests with and without irradiation.

References:

(1) V. K. Sethi et al. :"Phase Stability During Irradiation", (Eds., J. R. Holland et al.) Met. Soc., AIME (1980) p.437.

(2) J. A. Hudson et al. : J. Nucl. Mater., 65 (1977) 279.

IV NUCLEAR CHEMISTRY

4.1 Nuclear Chemistry of Actinoids
II. Formation Cross Sections of Transuranium Nuclides from Interaction of ^{16}O with ^{238}U

Nobuo Shinohara*, Shin-ichi Ichikawa*, Shigekazu Usuda*, Toshio Suzuki*, Hiroshi Okashita*, Toshiaki Sekine**, Kentaro Hata**, Takayoshi Horiguchi***, Yasukazu Yoshizawa***, Seiichi Shibata**** and Ichiro Fujiwara*****

*Department of Chemistry, **Department of Radioisotope Production, Japan Atomic Energy Research Institute, ***Department of Physics, Hiroshima University, ****Institute for Nuclear Study, University of Tokyo and *****Institute of Atomic Energy, Kyoto University

To investigate nuclear and chemical properties of the heavy actinoids and the reaction mechanism, the interaction of ^{16}O with ^{238}U has been studied using radiochemical method. Of the seven identified actinoid nuclides, ^{250}Fm, ^{246}Cf, ^{242}Cm, ^{238}Np, ^{239}Np, ^{237}U and ^{239}U, the respective formation cross sections were determined. This paper deals with the experimental results and discussion.

EXPERIMENTAL

The preparation of uranium targets, the irradiation and the radiochemical analysis were made by the same method described in previous report[1]. By varying the energy of projectile ^{16}O, several produced actinoid nuclides were determined radiochemically and their excitation functions were acquired.

To identify short-lived actinoid nuclides ($T_{1/2} < 3$ min.), a rapid α-emitter-detection system was developed; the system consists of targets and their holder, a rotating disc for capturing the recoil nuclei, and Si-surface barrier detector in scattering chamber. Eight of thin aluminum catcher foils were attached to the disc. Immediately after irradiation, the disc was rotated automatically to transfer the aluminum catcher foil to the position of the detector, and α-activity measurement of recoil nuclei which were collected by the foil was performed. Total time from the end of irradiation to the start of measurement was about 5 seconds.

RESULTS AND DISCUSSION

According to their chemical behaviors, α- or γ-energies and measured half-lives, the nuclides of ^{250}Fm, ^{246}Cf, ^{242}Cm, ^{238}Np, ^{239}Np, ^{237}U and ^{239}U were identified. The excitation functions of these seven actinoids are shown in Fig. 1.

The excitation function of $^{238}U(^{16}O,4n)^{250}Fm$ reaction was reported by Flerov et al.[2] and the excitation functions of $^{238}U(^{16}O,4n)^{250}Fm$, $^{238}U(^{16}O,\alpha 4n)^{246}Cf$ and $^{238}U(^{16}O,2\alpha 4n)^{242}Cm$ reactions can be calculated by ALICE code[3,4]. The present experimental results of ^{250}Fm and ^{246}Cf would be formed by particle evaporation from the compound nucleus, ^{254}Fm. The formation cross section of ^{242}Cm is about a hundred times as large as that of ^{250}Fm or ^{246}Cf and differed apparently from the calculated values by the ALICE code. Sikkeland et al. also investigated the formation of ^{242}Cm in the similar ^{16}O bombardments of ^{238}U and computed the excitation function for the production of ^{242}Cm using a kinematic model[5]. The formation of ^{242}Cm is probably from the direct reaction such as incomplete fusion reaction as discussed by Sikkeland et al. The nuclides of ^{238}Np, ^{239}Np, ^{237}U and ^{239}U seem to be formed by transfer reactions.

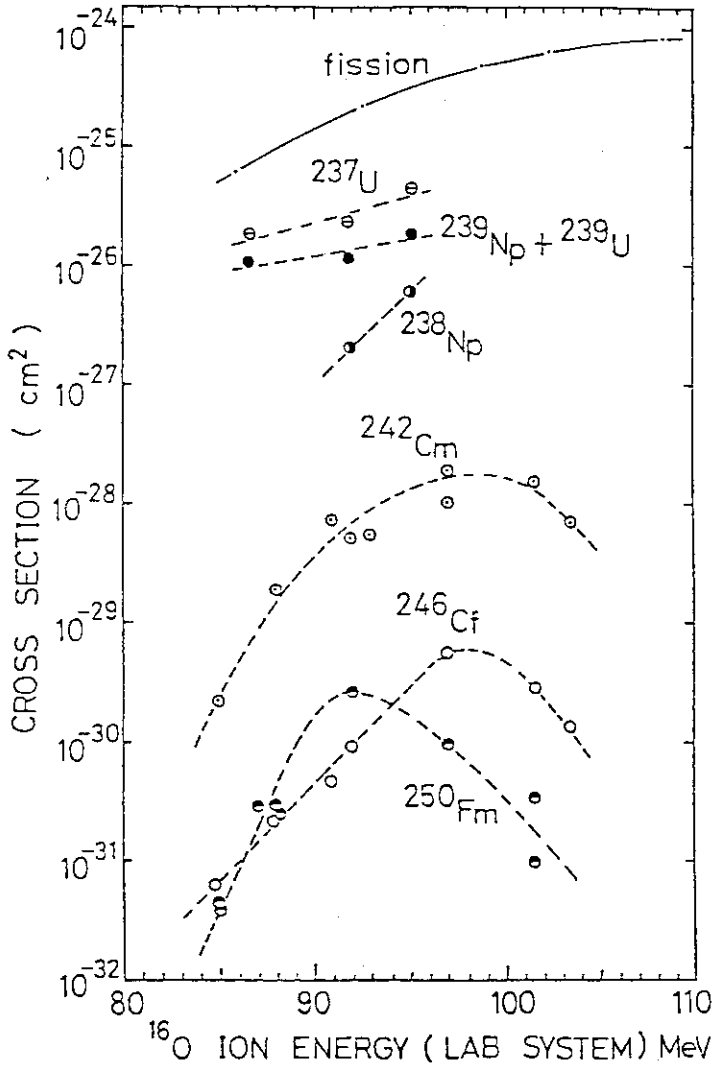

Fig. 1. Excitation functions for the reactions $^{238}U + ^{16}O$. The broken curves connect the data points. The fission data are quoted from Ref. 6.

Existence of the nuclides of ^{249}Fm ($T_{1/2}$; 2.6 min.), ^{248}Fm ($T_{1/2}$;

36 sec.) and ^{247}Fm ($T_{1/2}$; 35 sec. or 9.2 sec.), formed by $^{238}U(^{16}O,xn)^{254-x}Fm$ (x = 5, 6, 7) reactions, were examined by the rapid α-emitter-detection system. The upper limits of the formation cross sections of ^{249}Fm, ^{248}Fm and ^{247}Fm were estimated equally to be 7×10^{-32} cm^2 for 100 MeV ^{16}O (lab. system). The value is considerably small as compared with the calculated one by ALICE code.

REFERENCES

[1] N.Shinohara et al.: "JAERI TANDEM Annual Report 1982", JAERI-M 83-095 (1983)53.

[2] V.P.Perelygin, E.D.Donets and G.N.Flerov: Sov. Phys. JETP, 37(1960)1106.

[3] F.Plasil and M.Blann: Phys. Rev. C, 11(1975)508.

[4] M.Blann: Report COO-3494-29 (1976).

[5] T.Sikkeland, N.H.Shafrir and N.Trautmann: Phys. Lett., 42B(1972)201.

[6] V.E.Viola,Jr. and T.Sikkeland: Phys. Rev., 128(1962)767.

4.2 Experiments on Nuclides far from Stability by ISOL

Shin-ichi Ichikawa*, Toshiaki Sekine**, Kentaro Hata**, Tsutomu Tamura***, Eisuke Minehara****, Naruto Takahashi*****, Ichiro Fujiwara******, and Nobutsugu Imanishi******

*Department of Chemistry, **Department of Radioisotope Production, ***Nuclear Engineering School, ****Department of Physics, Japan Atomic Energy Research Institute; *****Department of Chemistry, Faculty of Science, Osaka University; ******Institute of Atomic Energy, Kyoto University.

An isotope separator on-line (ISOL) has been coupled to the JAERI tandem accelerator. As the first experiment using the ISOL, we planned a series of investigation of short-lived neutron deficient isotopes of cesium, barium and rare earths. A surface-ionization ion source, which can ionize effectively these elements, has been developed to facilitate the aiming experiments.

The present paper describes the design and performance of the ion source integrated in the ISOL as well as the decay of ^{119}Cs nuclide. With respect to the nuclide, it is known that there exists a pair of isomers. Although the level schemes in the decay of a mixture of the isomers were reported[1,2], the respective decay schemes of the individual isomers are not known. We have performed gamma-ray spectroscopic measurements of the mass-separated ^{119}Cs nuclei to obtain these decay schemes.

Design and Performance of the Ion Source

The surface-ionization ion source constructed is shown schematically in Fig.1. It is connected to the beam line from the tandem accelerator through a differential-pumping system and a thin window (2μm Haver foil), which keep a hydrocarbon "free" vacuum (10^{-5} Pa) in the accelerator side.

The ion source consists of a vaporizer, an ionizer, a couple of tungsten filaments and a heat shield. The tungsten ionizer has the form of a hollow cylinder, and its inner surface is coverd by rhenium foil. A target is usually placed at the vaporizer entrance. If the target is likely to melt due to the high temperature at this position, it is moved 5mm outward and the vaporizer entrance is sealed by a thin foil (20μm carbon or 1.5μm tantalum). The ionizer and vaporizer are heated by electron bombardment from tungsten filaments. The maximum voltage between the filament and the ionizer is equal

to 600 V and maximum electron current is 5 A. The temperature around the ionizer was measured by an optical pyrometer; it reached about 2500 K.

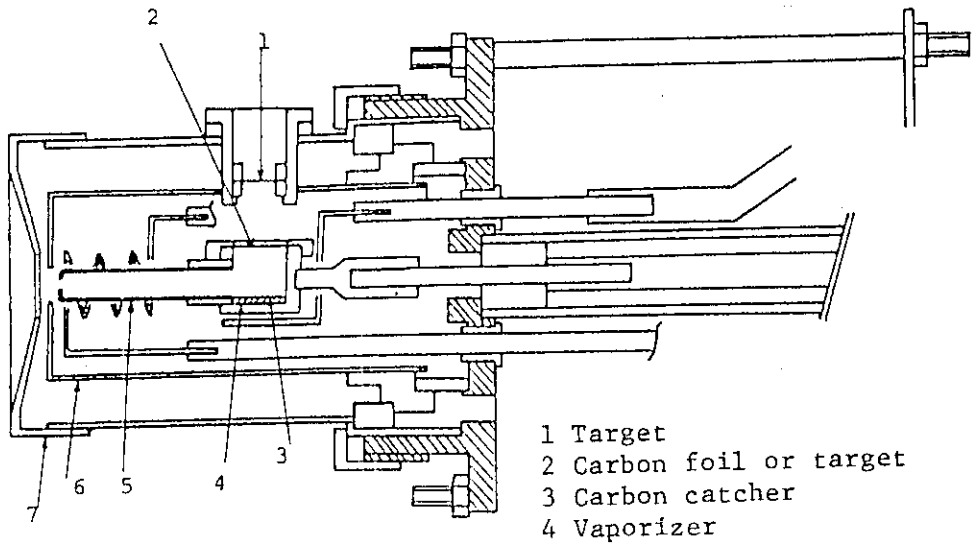

Fig.1 Ion source for the ISOL

The efficiency of the ion source was determined in off-line operation for cesium and barium isotopes by comparing the activity collected in the focal plane with that introduced into the ionizer. The cesium and barium isotopes were obtained by the $^{nat}Ag(^{16}O,X)^{125,127}Cs$ and $^{93}Nb(^{37}Cl,X)^{126}Ba$ reactions, respectively. The ion-source efficiency was estimated to be 30% for cesium and 18% for barium atoms. The transport efficiency from the focal plane to the detection point was also found to be 50%. In on-line operation the overall efficiency was measured for cesium isotopes produced by the $^{93}Nb(^{32}S,X)^{121}Cs$ reaction; it proved to be 15%.

Decay of ^{119}Cs

The ^{119}Cs nuclei were produced by $^{93}Nb(^{32}S,2p4n)^{119}Cs$ reaction with 180-MeV ^{32}S beams, separated by the ISOL, and collected on an aluminum-coated mylar tape in a tape-transport system. The mass-separated ^{119}Cs nuclei were moved in a second to a measuring port and measured by Ge(Li) detectors. Single gamma and gamma-gamma coincidence measurements were performed.

The decay of gamma rays emitted from the ^{119}Cs nuclei was traced and shown in Fig.2. One can note that these gamma rays are classified in three groups. The gamma rays of 179, 197, 225.1, 459.5 and 667 keV have a half-life of 43.2±2.1 sec and are assigned to the ^{119g}Cs. Those of 245.5, 257.9 and 315.2 keV with a half-life of 30.6±3.2 sec are assigned to the ^{119m}Cs. The 169 keV gamma ray, however, decays with a half-life 37.9±1.3 sec, which is inbetween the half-lives of these isomers, and cannot be assigned definitely to one of the isomers. This gamma ray is considered to be emitted from a level fed by both the isomers.

Further analysis is still in progress.

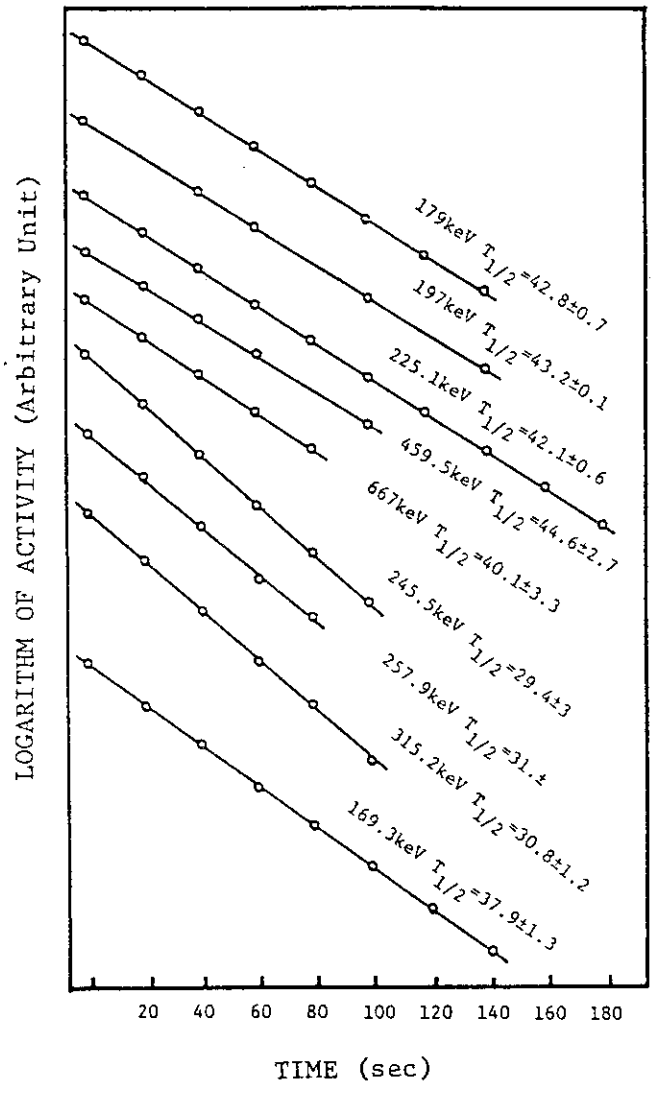

Fig.2 Decay curves of the gamma rays from ^{119}Cs nuclei.

Reference

1) R. F. Parry; LBL-15875 (1983)

2) L. Westgaad, K. Alekiett, G. Nyman and E. Roeckl: Z. Phys. A 275 (1975) 127.

4.3 An Experiment of Irradiated ^{197}Au with ^{16}O and ^{12}C Ions

Sumiko Baba*, Kentaro Hata*, Toshiaki Sekine*, Shin-ichi Ichikawa**, Toshio Suzuki**, Nobuo Shinohara**, Hiroshi Baba***, Tadashi Saito***, Akihiko Yokoyama***, Ichiro Fujiwara****, Nobutsugu Imanishi****

*Department of Radioisotope Production, **Department of Chemistry, Japan Atomic Energy Research Institute, ***Osaka University, ****Kyoto University

The radiochemical study of nuclear reactions of ^{197}Au with ^{16}O and ^{12}C particles has been continued. In the past experiments[1], product nuclides of complete fusion reaction, incomplete fusion reaction, deep inelastic transfer and quasi-elastic transfer had been detected by measuring their excitation functions and projected mean recoil ranges. In this work, experiments were performed to obtain further results of complete fusion and quasi-elastic transfer products for discussing the decay of the heavy-ion induced compound nucleus and the mechanism of the transfer reaction.

Complete fusion reaction products

The evaporation residues from the compound nucleus ^{213}Fr in the reaction system of $^{16}O + ^{197}Au$, such as Rn, At and Po isotopes, were already studied[1]. As to the Fr isotopes induced by the $(^{16}O,xn)$ reactions, formation cross sections were reported by Valli et al.[2] and Griffion et al.[3]. These experimental cross sections were, however, given only in relative values; the excitation functions of Fr isotopes with almost the same half-lives and alpha-ray energies[4] were not resolved. We intended to obtain more accurate cross sections than previous works, using a rapid alpha-emitter-detection system and an ISOL.

The Au target of 2 mg/cm^2 thick was mounted on the rapid alpha-emitter-detection system in the vacuum chamber at the R-2 beam line, and bombarded for 1 minute by the ^{16}O particles with the energy of 5-7 MeV/amu. After the bombardment, the catcher foil mounted on a rotating wheel was moved to the position in front of the surface barrier detector, and the alpha-ray measurement started at once. From the decay analysis of thus obtained alpha-counts, the excitation functions of Fr isotopes were deduced as shown in Fig. 1. With ISOL the yields of ^{208}Fr and ^{209}Fr were resolved at the beam energies of 90 MeV and 105 MeV. The resulted cross sections are also plotted in Fig. 1.

Quasi-elastic collision products

The stacked targets of Au foil and Al catcher foil were bombarded with ^{16}O- and ^{12}C-beams. Then the yields of Au isotopes in Au target and catcher foil were determined by the Ge(Li) gamma-ray spectrometry. The cross sections and the recoil ranges were deduced (Fig. 2). In-beam measurements of angular and kinetic energy distributions of projectile-like particles were performed using a solid state ΔE-E counter telescope for the ^{197}Au + 112-MeV ^{16}O reaction.

Energy depencence of the recoil range reveals a typical feature of the quasi-elastic scattering especially in the case of one-neutron transfer reactions which enables us to calculate the closest approach in the scattering.

References

1. S.Baba et al., JAERI-M 83-095(1983)56.
2. K.Valli et al., J. Inorg. Nucl. Chem., 29(1967)2503.
3. R.D.Griffion et al., Phys. Rev., 133(1964)B1373.
4. C.M.Lederer et al., "Table of Isotopes, 7th edition" Wiley,1978.

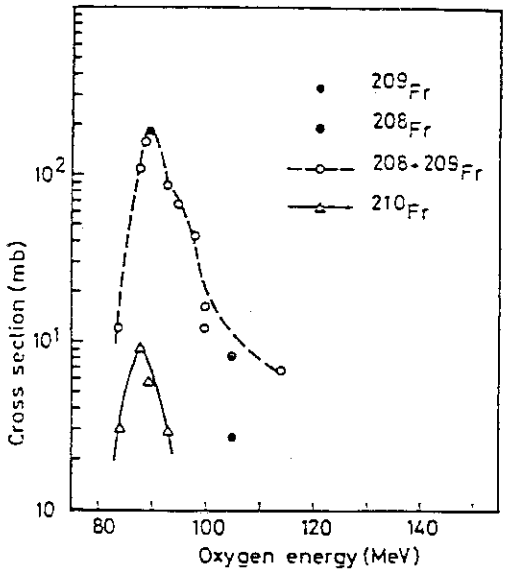

Fig.1 Excitation functions of $^{197}Au(^{16}O,xn)^{213-x}Fr$ reactions.

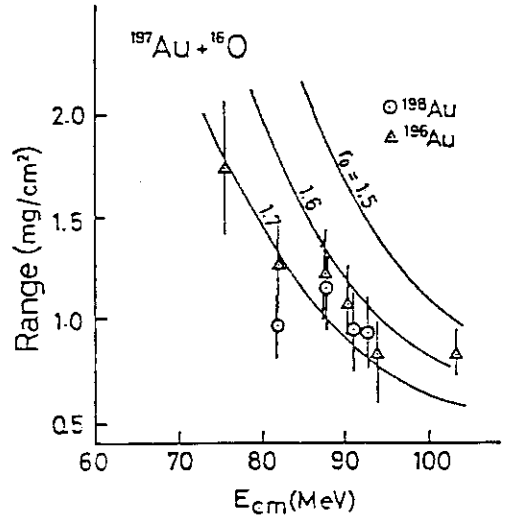

Fig.2. The recoil ranges of ^{196}Au and ^{198}Au in the reaction of $^{197}Au+^{16}O$. The solid curves represent the calculated ranges by elastic scattering where the closest approach is expressed by $r_0(A_1^{1/3}+A_2^{1/3})$.

4.4 A Radiochemical Study on the Existence of the Low-ℓ Cutoff in Complete Fusion

Toshiaki Sekine*, Sumiko Baba*, Kentaro Hata*, Shin-ich Ichikawa** and Nobuo Shinohara**

*Production Development Division, Department of Radioisotope Production and **Nuclear Chemistry Laboratory, Department of Chemistry, Japan Atomic Energy Research Institute.

The existence of the low-ℓ cutoff in complete fusion was suggested by Orsay group[1] from the observation of threshold shifts of excitation functions to higher energies in some (HI,xn) reactions of near-symmetric projectile and target systems. The experimental results, however, are not very persuasive.[2]

In order to test this possibility, isomer ratios offer some hope since they are expected to reflect the initial angular momentum distribution of compound nuclei.[3] For this aim, it is necessary to compare the isomer ratios between two initial channels leading to the same compound nucleus; the lowest ℓ waves in the formation of the compound nucleus are assumed to be cut off in one channel and not in the other. On this principle, we intended to investigate the possibility of the existence of the low-ℓ cutoff.[§] We have chosen as the initial channels $^{12}C + ^{93}Nb$ and $^{37}Cl + ^{68}Zn$ systems, and as the isomer pair $^{99m}Rh(9/2+, 4.7h)$ and $^{99g}Rh(1/2-, 15d)$ induced by (HI,α2n) or (HI,2p4n) reaction. Here, it is assumed that the low-ℓ cutoff comes into being in the $^{37}Cl + ^{68}Zn$ reaction if it exists.

The isomer ratios, however, should not be compared in a direct manner, since incomplete fusion[5] may occur intensively besides the complete fusion by α-particle emission, which would be a significant part in various incomplete fusion channels, followed by two-neutron evaporation. The incomplete fusion is anticipated to contribute to the $^{12}C + ^{93}Nb$ system consisting of considerably asymmetric combination of projectile and target. Therefore, we must be well-informed as to the contribution of the incomplete fusion to the

[§]Nomura reported a possible evidence for the low-ℓ cutoff on almost the same principle as written here, independently with us.[4]

$^{12}C + ^{93}Nb$ reaction prior to studying the isomer ratios.

The experiment is still on its way. The present paper describes mean recoil ranges of products in both the reaction systems, since the recoil range reflects the momentum transferred from the projectile to the target; they will be observed to be shorter than those expected from the complete fusion if the incomplete fusion occurs.

With a ^{12}C beam, we irradiated foil stacks consisting of "thick" niobium targets (3.4 mg/cm^2) separated by aluminum catcher foils to obtain average recoil ranges by means of thick target and thick catcher method.[6] This method, however, is not applicable to the $^{37}Cl + ^{68}Zn$ reaction. With a ^{37}Cl beam, we irradiated a foil stack consisting of a thin ^{68}Zn target ($\sim$0.5mg/cm^2) and several thin aluminum catcher foils. The isotopically enriched ^{68}Zn targets were prepared by evaporation onto Au backings or by electrodeposition onto Al backings. The targets were bombarded for 15 m or 1.5 h with the beams obtained from the JAERI tandem accelerator. The integrated beam current was monitored with a Faraday cup. The products were identified and measured with Ge(Li) detectors.

We have calculated the recoil ranges with the formalism given by Delagrange et al.[7] on the assumption of the complete momentum transfer. This calculation gives the mean recoil ranges projected on the beam direction, which is directly obtainable by experiment, taking into account the multiple scattering of heavy ions in the target. However, it neglects influence of particle evaporations; the values obtained may be underestimated by a few percent.

Most of the nuclides, except for target-like nuclides, show recoil ranges in agreement with the values calculated above. Figure 1 displays an activity distribution in the catcher foils for ^{99m}Rh produced in the $^{37}Cl + ^{68}Zn$ reaction at beam energy of 131 MeV. The mean recoil range and the activity distribution agree well with the

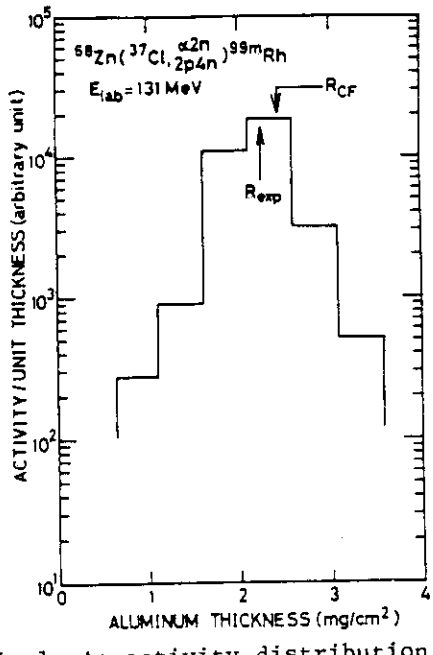

Fig.1 An activity distribution in catcher foils. R_{exp} is a mean recoil range determined experimentally and R_{CF} that calculated for complete fusion reaction.

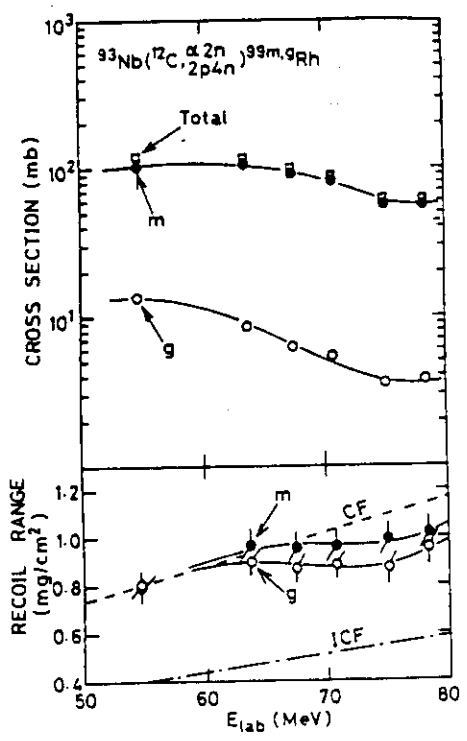

Fig.2 Excitation functions and mean recoil ranges. Calculated mean recoil ranges for complete (CF) and incomplete (ICF) fusion reacions are also shown.

predictions by the complete fusion mechanism.

The recoil ranges and formation cross sections of ^{99m}Rh and ^{99g}Rh in the ^{12}C + ^{93}Nb reaction are plotted against beam energy in Fig.2. Note that the recoil ranges of both ^{99m}Rh and ^{99g}Rh almost stop increasing at 65 MeV and restart increasing around 75 MeV. This means that the complete fusion is predominant at energies less than 65 MeV, while above 65 MeV another reaction process takes place besides the complete fusion to reduce the mean recoil range. We consider this process to be the incomplete fusion expected before.

It is also interesting that in Fig.2 the recoil range differs appreciably from one isomer to the other at energies in which the incomplete fusion occurs. This phenomenon, which probably has been noticed for the first time, can be interpreted as a consequence of the coexistence of two fusion mechanisms.

References

1) H. Gaubin, Y. Le Beyec, M. Lefort and R.L. Hahn: Phys. Rev. C10 (1974) 722.
2) H.C. Britt et al.: Phys. Rev. Lett. 39 (1977) 1458.
3) G. Rudstam: Phys. Scripta 20 (1979) 165.
4) T. Nomura: JAERI-M 84-085 (1984) 104.
5) K. Siwek-Wilczynska, E.H. du Marchie van Voorthuysen, J. van Popta, R.H. Siemssen and J. Wilczynski: Nucl. Phys. A330 (1979) 150.
6) A. Ewart, C. Valentine and M. Blann: Nucl. Phys. 69 (1965) 625.
7) H. Delagrange, F. Hubert and A. Fleury: Nucl. Phys. A228 (1974) 397.

4.5 Preparation of ^{237}Pu from ^{237}Np Irradiated with Deuterons

Sumiko Baba*, Kentaro Hata*, Toshiaki Sekine*, Mishiroku Izumo*, Ryozo Motoki*, and Shin-ichi Ichikawa**

*Department of Radioisotope Production, and **Department of Chemistry, Japan Atomic Energy Research Institute

The gamma-ray emitting plutonium isotope ^{237}Pu is known to be a useful tracer in the experiments of environmental or metabolic distribution of plutonium. It is generally prepared with the reactions induced by ^{4}He and ^{3}He particles on ^{235}U and ^{238}U targets, respectively.[1,2] The excitation functions and thick target yields for ^{237}Pu in those reactions have been reported.[3] As to the $^{237}Np(d,2n)^{237}Pu$ reaction, the cross section was found by Vandenbosch[4] to be relatively large. Its excitation function around the Coulomb barrier, however, has not been measured. In this work, the excitation function of $^{237}Np(d,2n)^{237}Pu$ reaction in a wider energy range was measured to estimate the thick target yield of ^{237}Pu, and to discuss the possibility of using this reaction for production of ^{237}Pu.

The oxide of ^{237}Np was dissolved in hydrochloric acid solution and separated from Pu impurity by the anion exchange method[5] repeated two times. The thin Np targets were then made by electrodeposition from the hydrochloric acid solution contained in isopropyl alcohol as solvent.[6] The thickness of deposits obtained was about 700 $\mu g/cm^2$. Uniformity of thickness was tested for each target by measuring the distribution of alpha-ray intensity. The stacked targets constructed with Np targets and Al foils were bombarded by deuterons from the tandem accelerator in JAERI. The incident energy of deuterons to the Np targets ranged from 10 MeV to 25 MeV. After about 30-days cooling Pu was separated from each Np target and its gamma-ray and alpha-ray measurements were carried out to obtain the yields of ^{236}Pu, ^{237}Pu and ^{238}Pu.

The excitation functions for the formation reactions of Pu isotopes were obtained as shown in Fig.1. Their shape without any distinct peak is characteristic of direct reaction mechanism. The reaction of ^{237}Pu formation starts near the Coulomb-barrier energy. Its cross section reaches about 10 mb, which is a little lower than given in ref.[4], at deuteron energy of 15 MeV and then slowly decreases with the energy. The thick target yield of ^{237}Pu by the reaction, therefore, increases

rapidly with the increase of projectile energy, in contrast with the cases of $^{235}U + ^{4}He$ and $^{238}U + ^{3}He$. Table 1 shows the thick target yields of ^{237}Pu with the ratio of the yield of ^{237}Pu to that of $^{236}Pu + ^{238}Pu$ obtained in this work and others[2,3]. The long range of deuterons in the Np target as compared with the ranges of ^{4}He and ^{3}He in the U target results in the large yield of ^{237}Pu in the relevant reaction. The radiochemical purity of ^{237}Pu is, however, the worst of all.

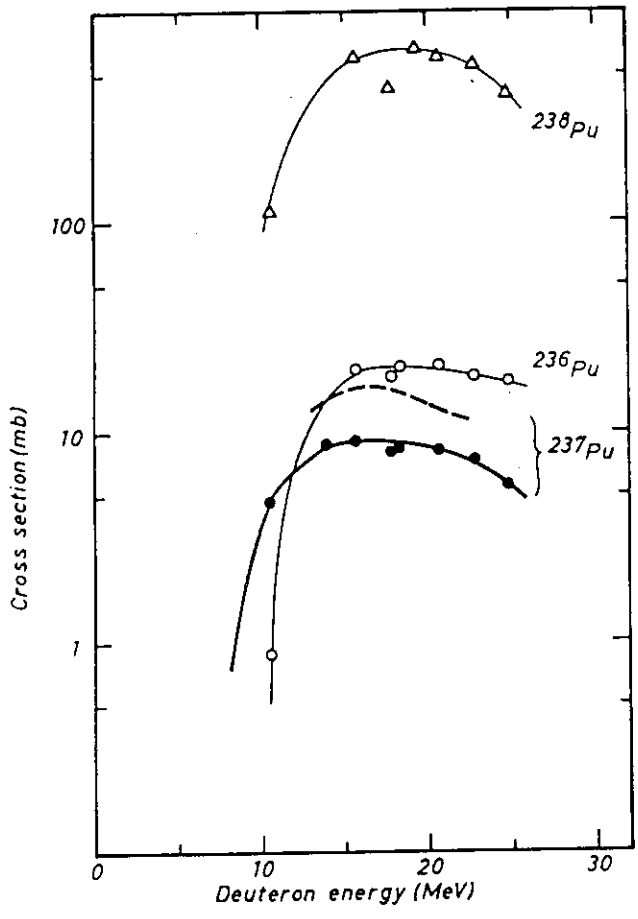

Fig.1 Measured formation cross sections of the Pu isotopes in $^{237}Np + d$ reactions. Solid lines are the smooth curve connecting the experimental points in this work. A dotted line shows the experimental excitation function for $^{237}Np(d,2n)^{237}Pu$ reaction by R.Vandenbosch[4].

Table 1 Yields and radiochemical purity of ^{237}Pu in various reactions

Reaction	Projectile energy(MeV)	^{237}Pu yield (μCi/μA-h)	$\frac{^{236}Pu + ^{238}Pu}{^{237}Pu}$
$^{235}U + ^{4}He$	30	5.4	0.002
$^{238}U + ^{3}He$	38	5.4	0.039
$^{237}Np + d$	15	39.	0.100
$^{237}Np + d$	25	131.	0.184

References

1. K.Hata et al., Int. J. Appl. Radiat. Isotop., 27 (1976) 713.
2. K. Komura et al., J. Nucl. Sci. Tech., 17 (1980) 75; J. Aaltonen et al., J. Radioanal. Chem., 64 (1981) 73.
3. I. L. Jenkins et al., Int. J. Appl. Radiat. Isotop., 22 (1971) 429.
4. R. Vandenbosch, UCRL 3858 (1957), cited in K. -H. Hellwege, "Landolt-Börnstein, Numerical Data and Functional Relationships in Science and Technology, Vol.5, Part b" (Springer-Verlag, 1973).
5. H. Natsume et al., J. Nucl. Sci. Tech., 9 (1972) 737.
6. G. Müller et al., Nucl. Instr. Meth., 128 (1975) 425.

V NUCLEAR PHYSICS

5.1 In-Beam Gamma-Ray Spectroscopy through Heavy-Ion Induced Fusion

Mitsuhiko Ishii, Akiyasu Makishima *, Toshiyuki Kohno *, Minoru Adachi *, Hiroshi Taketani *, Kuniaki Yamazaki ** and Masao Ogawa **

Department of Physics, Japan Atomic Energy Research Institute, Tokai-mura, Ibaraki-ken, * Department of Applied Physics, Tokyo Institute of Technology, Meguro-ku, Tokyo, ** Energy Science, the Graduate School at Nagatsuda, Tokyo Institute of Technology, Midori-ku, Yokohama

Fusion reactions induced by heavy ions provide us with many neutron-defficient nuclei. In order to study the high spin states of those nuclei, we have fabricated a 4π type of charged particle multiplicity filter (CPM filter) which permits us to identify fusion residues by counting protons and alpha-particles emitted from them. It consists of ten Si detectors without the insensitive margin; two of them are of annular type with a size of 35 mm x 35 mm x 0.5 mm and eight side detectors rectangular of 30 mm x 35 mm x 0.5 mm. They surround the target as shown in fig. 1 so that 90 % or more of the emitted charged particles can be detected. Each of them is covered with a copper foil of 20 mg/cm^2 so that scattered projectiles and low energy delta-rays can be stopped therein.

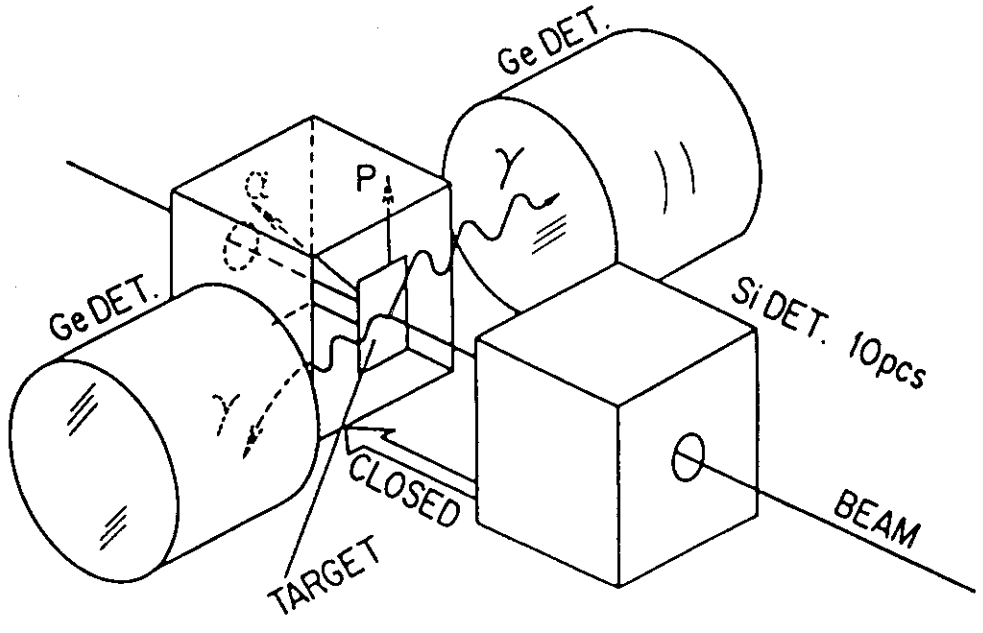

Fig. 1. Schematic drawing of the charged particle multiplicity filter.

We have employed the CPM filter to study high spin states of samarium-138 by bombarding Ag-107 with a Cl-35 beam of 155 MeV. Gamma-gamma coincidence, gamma-ray angular distribution and Doppler shift measurements have been performed with a gate set on the reaction channel emitting two protons.

A level scheme of samarium-138 is shown in fig. 2. Excited stats up to the spin 12^+, members of the ground band up to the 8^+ state and two members of another band crossing the ground band, have been established. The 10^+ state de-excites with a half lifetime of 0.5 ns, which is of the same order of magnitude as for the single particle transition. On the other hand, the transitions from the 2^+ to the ground states and from the 12^+ to the 10^+ states are enhanced by a factor of hundreds in Weisskopf units; so they can be interpreted as collective ones.

A study on high spin states of samarium-136 is in progress. A preliminary lifetime measurement has shown that the 2^+ state of the ground band possesses a half lifetime of about 60 ps and no isomeric states with longer lifetimes have been found.

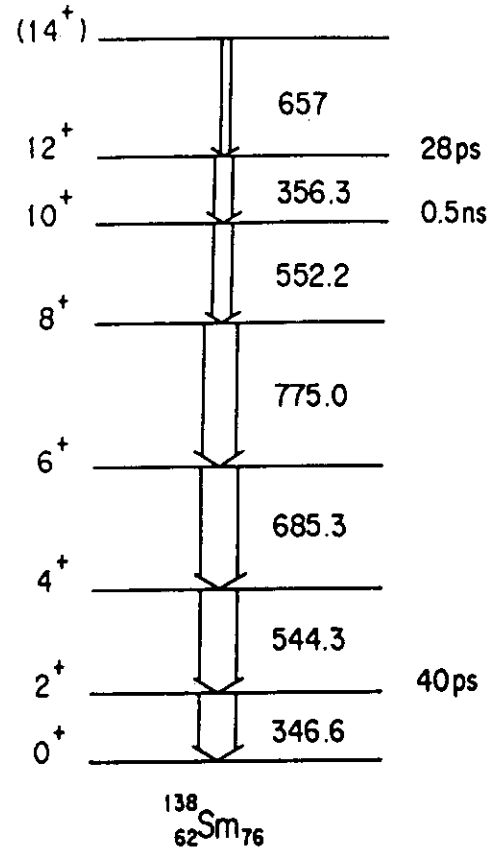

Fig. 2. A level scheme of Sm-138.

5.2 Fusion and Deep Inelastic Reactions for the Systems of $^{37}Cl + ^{27}Al$ and $^{37}Cl + ^{48}Ti$ with ^{37}Cl beams of 100 - 200 MeV

K. Ideno*, Y. Tomita*, H. Ikezoe*, S. Hanashima*, S. Takeuchi*, W. Yokota**, S. M. Lee**, Y. Nagashima**, T. Nakagawa**, Y. Fukuchi**, S. Kinouchi**, T. Komatsubara**, M. Ogihara**, T. Mikumo**, and W. Galster***

*Department of Physics, Japan Atomic Energy Research Institute,
**Tandem Accelerator Center, University of Tsukuba, and
***Hahn-Meitner Institute

In the energy region below 200 MeV of ^{37}Cl beams fusion reaction occupies a dominant part for the systems A = 60 - 90. Above 160 MeV other reactions such as deep inelastic collision begin to be important. Using the tandem accelerators of JAERI and University of Tsukuba, we measured fusion evaporation residues and deep inelastic fragments for the systems of $^{37}Cl + ^{27}Al$ and $^{37}Cl + ^{48}Ti$. Fig. 1 shows the plots of $\sigma_{E.R.}$ vs $1/E_{c.m.}$ for the two systems. At higher energies than $E_{c.m.} \approx$ 60 MeV fusion cross section takes a constant value of ~1000 mb. In this energy region observed cross sections were compared with the predictions of Lee et al.[1] and Civitareze et al.[2] In the fusion process the energy ΔQ transferred to the internal excitation of the compound nucleus is constant in Ref. 1 while it is proportional to the mass A_c of the compound nucleus in Ref. 2. The difference between the two predictions is small for the system of $^{37}Cl + ^{27}Al$. For the system of $^{37}Cl + ^{48}Ti$ the variable ΔQ model seems to fit better with the experimental data.

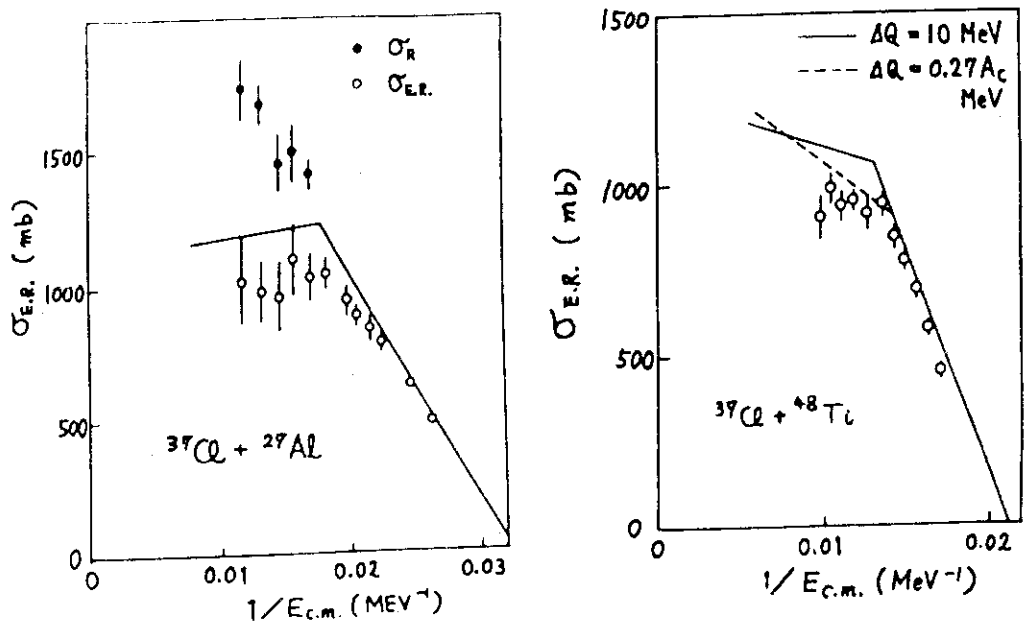

Fig. 1

Charges and kinetic energies of deep inelastic fragments were measured at 160 - 200 MeV. For the system of $^{37}Cl + ^{48}Ti$ we made coincidence measurements of two fragments in order to obtain more accurate information on the distribution of excitation energies over the fragments. Fig. 2 shows the examples of the observed charge spectrum for the coincident fragments with the 196 MeV beams. Here the coincidence angles restrict the kinematical effect for the fragments, depending on the Q-values. Further measurements are planned.

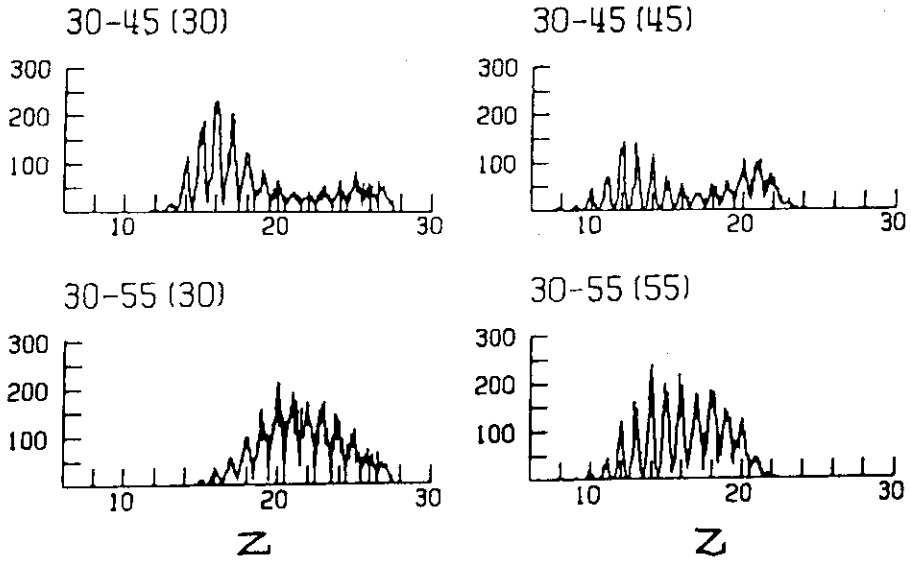

Fig. 2 Charge spectrum at coincidence angles of 30° - 55° and 30° - 45° with ^{37}Cl beams of 196 MeV

References

1) S. M. Lee et al., Phys. Rev. Lett. 45 (1980) 165.

2) O. Civitareze et al., Phys. Lett. B125 (1983) 22.

5.3 Characteristics of the ENMA Focal-Plane Detector with CF_4 Gas

Eiko Takekoshi*, Yasuharu Sugiyama*, Hiroshi Ikezoe*, Yoshiaki Tomita*, Naomoto Shikazono* and Kenzo Nagano**

*Department of Physics, Tokai Research Establishment, JAERI, **Institute of Physics, The University of Tsukuba

A large hybrid gas counter for use with the JAERI magnetic spectrograph (ENMA)[1], the focal-plane detector[2], is now used routinely in the precise measurements of the nuclear reactions with heavy ions. The counter gas was replaced isobutane, C_4H_{10}, of being flammable by tetrafluoromethane, CF_4, of being nonflammable since march 1983, according to experiences of the use of CF_4 in the focal-plane detector for the ANL linac magnetic spectrograph[3].

In CF_4, it is known that negative ions are formed by electron impact, and it is considered that this property may have some disadvantages on the characteristics of ion chamber and proportional counter constituting a hybrid counter as the ENMA focal-plane detector, as compared with the case of C_4H_{10}. Thus characteristics of the focal-plane detector with CF_4 were examined[4].

Some results present in Figs.1 - 3. Fig.1 shows the ΔE pulse height obtained from the front anode of the ion chamber as a function of E(ANODE-FRISCH.GRID) / P under the condition of E(CATHODE-FRISCH.GRID) / P = 1 - 6, where E(VOLT/CM) and P(TORR) were the electric field strength and fill gas pressure, respectively. It is seen that the values of $(\alpha - \eta)/P$ (CM^{-1}. $TORR^{-1}$) are negative in the region of E/P = (12 - 45)[4], where α and η are the Townsend's primary ionization coefficient and the electron attachment frequency, respectively. The plateau for each gas pressure is the region to use as the ion chamber. Fig.2 shows the reduced distribution width(KEV), which has been derived semi-empirically by Schmidt-Bocking and Hornung[5],

$$\alpha^{red.}\ \Delta E.\ Z_P = \alpha.\{S(E_0) / S(E_0 - \overline{\Delta E})\} \cdot \{(Z_p^{1/3} + Z_T^{1/3})/Z_P\}^{1/2} = K(\overline{\Delta E})^{0.53}$$

for different projectiles at different incident energies E_0 in CF_4 and C_4H_{10} of the ion chamber, as a function of $\overline{\Delta E}$ (MEV). The width α (FWHM) of the energy loss $\overline{\Delta E}$ is the experimental value corrected for an electronic width, S(E) the stopping power for the fill gas, Z_P the projectile nuclear charge and Z_T the nuclear charge of fill gas. The solid line (X) with K = 80 represents fit to the C, CL and NI data denoted by X, which were corrected by the path-length differences of ions projected on the ΔE electrode and the multiple scattering at the 45^0 incidence. The dashed line (Y) with K = 67

represents the fit to data in C_4H_{10} of the Daresbury ion chamber[6]. The value of $Z_T = 6$ for C_4H_{10} and CF_4 is assumed. There is a little difference between the lines (X) and (Y). This may require a little more corrections with the vertical path length differences in the focal-plane detector[1]. Fig.3 shows DIETHORN'S plots[7] for the front proportional counter(position counter) in C_4H_{10} and CF_4. In the equation of

$$\ln M.\ \ln(B/A)/V = (\ln 2 / \Delta V).\{\ln(V/(P.A.\ln(B/A))) - \ln\overline{K}\} ,$$

M is the gas amplification factor, V the anode bias voltage(VOLT), B the cathode radius(CM), A the anode wire radius(CM), P the fill gas pressure(BAR). ΔV is the potential difference through which an electron has moved in covering the distance between successive ionizing events, and $\overline{K}$ is the critical value of E/P below which ionization does not occur. Both values are constants determined only by the properties of the fill gas. It is seen that the values of ΔV are almost same in both fill gases and the $\overline{K}$ value of CF_4 is larger than one of C_4H_{10}.

In conclusion, the disadvantages caused by $(\alpha - \eta) / P < 0$ in the region of E/P = (12 - 45) in CF_4 and $\overline{K}(CF_4) > \overline{K}(C_4H_{10})$ are not important in measurements for the heavy ions. The detailed discussion will be presented in another report[4]. The gas of CF_4 has another advantage of large electron drift velocity[8], in addition to advantage of being nonflammable.

References

1). Y. Sugiyama, N. Shikazono, H. Ikezoe and H. Ikegami; Nucl. Instr. and Meth. 187(1981)25, Y. Sugiyama, N. Shikazono, T. Sato and H. Ikegami; Nucl. Instr. and Meth. 215(1983)17

2). M. Sawada, Y. Sugiyama, E. Takekoshi; JAERI-M83-014 (1983), E. Takekoshi, Y. Sugiyama, H. Ikezoe, Y. Tomita, N, Shikazono, M. Sawada, S. Kubono, M. Tanaka, M. Sugitani, S. Kato and T. Suehiro; "JAERI TANDEM Annual Report 1982" JAERI-M 83-095, (1983) 67

3). K.E. Rehm, W. Kutschera and D.G. Kovar; ANL Annual Report (1982/83) p.119

4). K. Nagano, Y. Sugiyama, E. Takekoshi, H. Ikezoe, Y. Tomita and N. Shikazono; Meetings of Japan Physical Society in Kobe and Fukuoka, Oct.6,1983 and Apr.1, 1984 and submitted to JAERI-M Report (1984)

5). H. Schmidt-Bocking and Hornung; Z. Physik A286(1978)253

6). A.N. James, P.A. Butler, T.P. Morrison, J. Simpson and K.A. Connell; DL/NUC/P168E Daresbury Report (1982)

7). W. Diethorn; NTO-6628(1956)

8). L. Cristophorou, D.L. McCorkle, D.V. Maxey and J.G. Carter; Nucl. Instr. and Meth. 163(1979)141

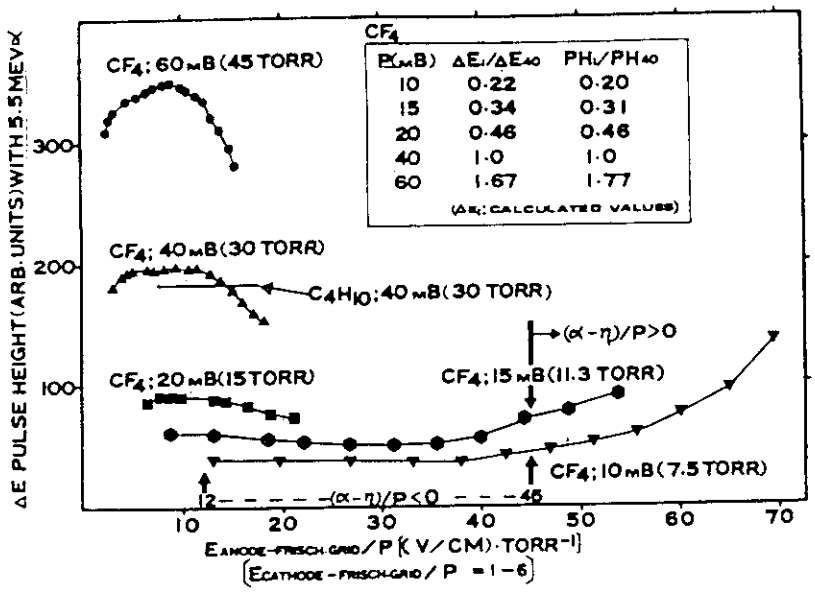

Fig.1.
The ΔE puise height obtained from the front anode of the ion chamber as a function of E(ANODE-FRISCH.GRID)/P under the condition of E(CATHODE-FRISCH.GRID)/P = 1 - 6.

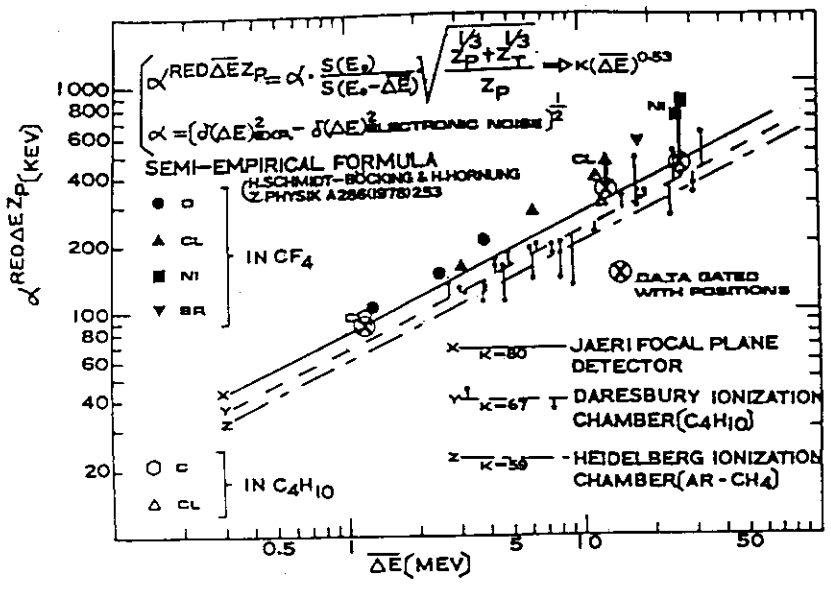

Fig.2.
The reduced distribution width as a function of ΔE.

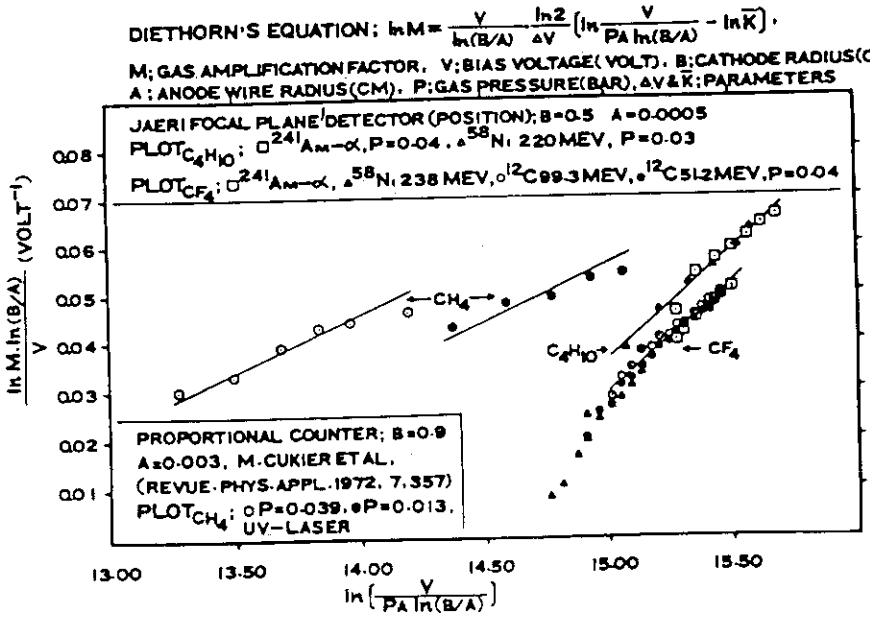

Fig.3.
DIETHORN'S plots for the front proportional counter.

5.4 Measurements of the spin alignment in the $^{12}C+^{12}C$ inelastic scattering via γ recoil

Yasuharu Sugiyama*, Naomoto Shikazono*, Yoshiaki Tomita*, Hiroshi Ikezoe*, Kenzo Nagano*, Eiko Takekoshi*, Shigeru Kubono**, Masahiko Tanaka** and Michiro Sugitani**

*Department of Physics, Tokai Research Establishment, JAERI, **Institute for Nuclear Study, University of Tokyo

In experiments with heavy ions it is known that γ-decay in flight of an excited nucleus broadens a line width in the momentum spectrum of the outgoing nucleus, reflecting the Doppler shift of the emitted rays[1]. The shape of the line is determined by angular distributions of the γ-rays, which have characteristic patterns for different m substates. Characteristic line shapes were observed in the momentum spectrum and the m substate population was deduced by unfolding the line shapes, when a high momentum resolution was achieved for the particle spectrum like as ^{12}C or ^{16}O[1,2]. The orientation of the nucleus produced in the reaction was specified by the components $\rho_{mm'}$ of the nuclear density matrix, where substate m or m′ was quantized with respect to a z axis. We introduced a new z axis which was chosen to point into the direction of $\theta_b+\tan^{-1}k$ in the reaction plane ,where θ_b was a scattering angle of laboratory system and k was a kinematic factor of $dp/p/d\theta$[2]. By taking this z axis , the line shapes are definded only by the diagonal density matrix elements and the substate population can be extracted precisely from the line shapes. This analysis was applied to the single and mutual excitations of the 2^+ state of ^{12}C in the $^{12}C+^{12}C$ inelastic scattering which was carried out at JAERI tandem Van de Graaf by using a newly constructed heavy ion magnetic spectrograph[3]. The spectrograph, named ENMA, has a characteristic feature that a kinematic momentum shift k is compensated from k=-0.7 to 2.0, so that a high momentum resolution is achieved for a wide range of k[3]. So far prominent gross structures have been observed in the angle-integrated single 2^+ and mutual 2^+ cross sections in $^{12}C+^{12}C$ inelastic

scattering and appreciable theoretical and experimental efforts have been paid in order to clarify the origin of these structures. However, the angular momenta dominating the gross structures and the mechanism responsible for these have not yet been sufficiently clarified. In order to get new informations of the gross structures, the angular distributions of the spin alignment for the single and the mutual excitations were measured in the laboratory angle range $6.6^\circ \leq \theta_{lab} \leq 34.6^\circ$ in a step of 1°. The CM energies were chosen to be 19.0, 21.5, 24.25, 25.6, 27.3, 30.0, 33.0 35.0 45.0 and 55.0 MeV, respectively. Some results are shown in Fig.1 and Fig.2. It is clearly seen that the substate populations of the single excitation are characterized by angular oscillations which increase in frequency with bombarding energy, while such oscillations are not observed for the substate populations of the mutual excitation. The simple DWBA calculations were carried out for the single excitation. We present here the results calculated by the optical potential parameters Tanimura et. al.[4] : V_{e-}=18MeV, V_{inel}=20MeV, W=0.24E_{cm} MeV, $r_0=r_I$=1.35fm, a_0=0.49fm, a_I=0.2fm. The results are shown by solid lines in Fig.1. The DWBA with the present potential parameters are seemed to reproduce the experimental results.

References

1) H.G.Bohlen et al.,Phys. Rev. Lett. 37 (1976) 195 ; H.G.Bohlen and W.von Oertzen, Z.Physik A285 (1978) 371

2) Y.Sugiyama et al.,Report of the joint seminar on heavy-ion nuclear physics and nuclear chemistry in the energy region on tandem accelerators, JAERI-M 84-085 (1984) p20.

3) Y.Sugiyama, N.Shikazono H.Ikezoe and H.Ikegami, Nucl. Instr. and Meth. 187 (1981) 25 ; Y.Sugiyama, N.Shikazono, T.Sato and H.Ikegami, Nucl.Instr. and Meth.215(1983) 17 ;Y.Sugiyama, N.Shikazono, T.Sato, T.Takayama and H.Ikegami, JAERI-M 9358 (1981) ; M.Sawada, Y.Sugiyama and E.Takekoshi, JAERI-M 83-014 (1983)

4) O.Tanimura, R.Wolf and U.Mosel, Phys. Lett. 120B (1983) 275

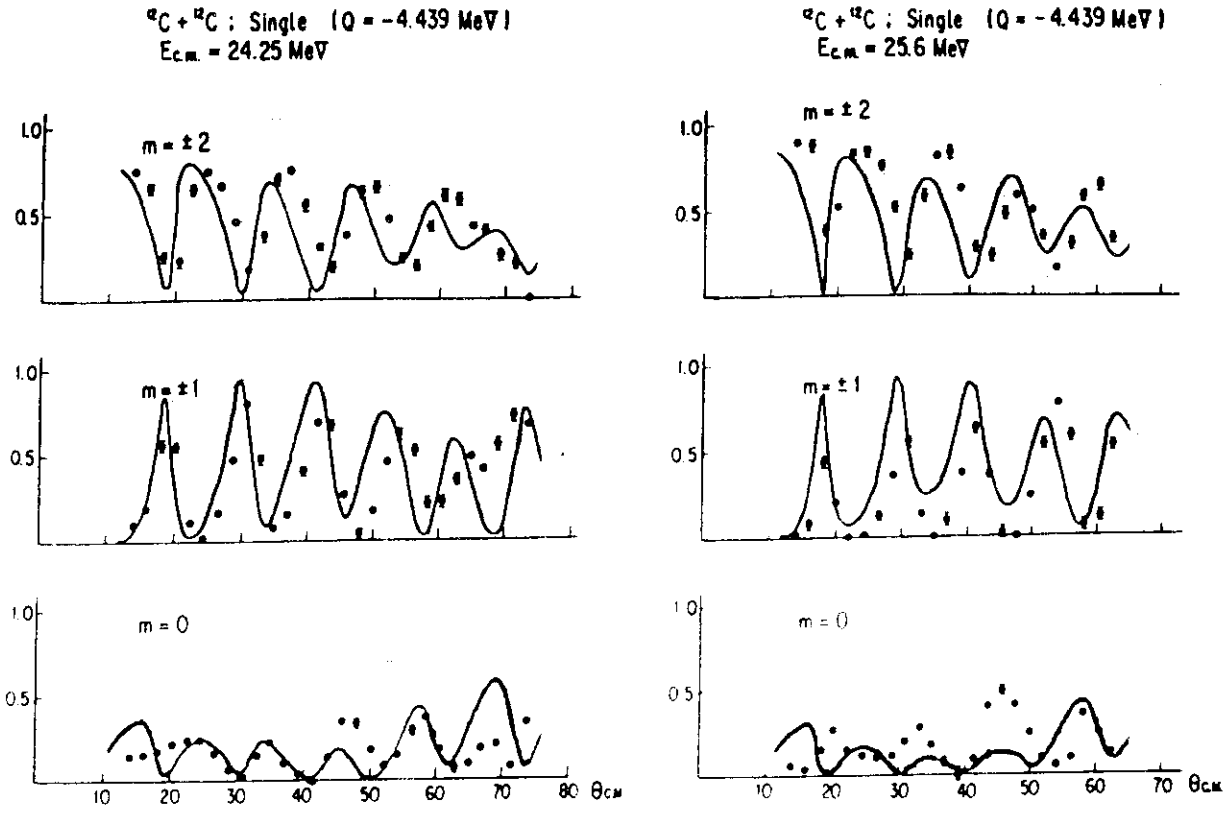

Fig.1 Angular distributions of the spin alignment for the single 2^+ excitation. Solid lines show the results of DWBA calculations.

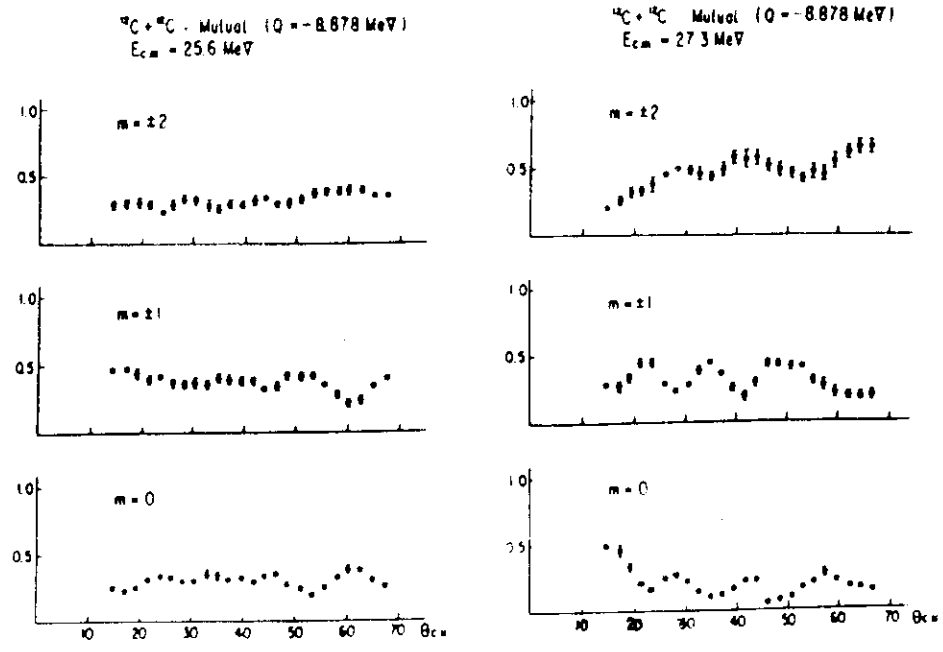

Fig.2 Angular distributions of the spin alignment for the mutual 2^+ excitation.

5.5 Measurements of Evaporation Residues Produced in $^{16}O + ^{27}Al$

Hiroshi Ikezoe, Naomoto Shikazono, Yoshiaki Tomita, Kazumi Ideno, Yasuharu Sugiyama, and Eiko Takekoshi

Department of Physics, Japan Atomic Energy Research Institute.

The complete identification (mass, atomic number and energy) of fusion evaporation residues gives us informations about a role of angular momentum in the mechanism of the incomplete fusion reaction[1]. In general, the partial fusion cross sections with lower angular momenta in the entrance channel are concerned in the productions of heavier isotopes. On the other hand, lighter isotopes are mainly produced from the entry states with higher angular momenta. This is due to the preference of α emissions from the entry states with high angular momenta and these result in productions of lighter elements. For instance, the Ar and Cl isotopes for the $^{16}O + ^{27}Al$ reaction are produced from the entry states with lower angular momenta and the Si and Al isotopes are produced from those with higher angular momenta. It is an aim of this experiment to investigate influences of the incomplete momentum transfer in the velocity cross section of each evaporation residue.

Fusion evaporation residues for the $^{16}O + ^{27}Al$ reaction were measured at $E_{lab}(^{16}O)$ = 150 MeV using time-of-flight telescope. The mass and atomic numbers of evaporation residues were identified using two channel plate detectors (start, stop) and ionization chamber (ΔE, E). The angular distribution were also measured from 4° to 26° with respect to the beam. The analysis of the data and a comparison with statistical model calculation are underway.

References

1) H.Morgenstern, W.Bohne, W.Galster, K.Grabish, and A.Kyanowski, Phys. Rew. Lett. 52 (1984) 1104.

5.6 Calculation of Sub-barrier Fusion Cross Section

Akira Iwamoto and Kichinosuke Harada

Department of Physics, Japan Atomic Energy Research Institute

Experimental value of the heavy-ion fusion cross section for the energy below the Coulomb barrier shows an enhancement over the prediction based on one dimensional barrier penetration calculations. An example is the Ni+Ni excitation function measured by Beckerman et al.[1]. To improve the fitting, it is necessary to take into account the intrinsic structure of the colliding nuclei. Coupled channel type calculations have been done extensively along this line and it was found that the couplings to inelastic channels and transfer channels are responsible to the enhancement of the fusion cross section[2]. Although some of the data are fitted well with this , the model is very complicated and the reason for the large enhancement of the cross section is not clear. We investigate this problem by the use of more simplified model which is related to the machanism of the neck formation proposed by Krappe et al.[3].

For the Hamiltonian H of the system, we assume

$$H = \frac{1}{2}\mu\dot{q}^2 + V(q,x) + H_{int} \quad , \tag{1}$$

where q is the relative distance of two heavy ions and x stands for an intrinsic variable. We introduce two intrinsic states, $|\alpha\rangle$ and $|\beta\rangle$ where the former stands for the ground state and the latter, an excited state. We calculate the tunneling process accompanied by the excitation of the intrinsic state from the initial $|\alpha\rangle$ state to $|\beta\rangle$ state. In order to get the S matrix, we calculate the matrix element of the propagator

$$\begin{aligned} P &= \langle \beta, q_f \mid \exp(-\frac{i}{\hbar} Ht) \mid \alpha, q_i \rangle \\ &= \langle q_f \mid K_{\beta\alpha} \exp(-\frac{i}{2\hbar}\mu\dot{q}^2) \mid q_i \rangle \quad , \end{aligned} \tag{2}$$

where the reduced propagator $K_{\beta\alpha}$ is calculated by the first order perturbation theory. We split it into two parts, $K^{(1)}$ and $K^{(2)}$, the former is the process where the intrinsic excitation occurs outside the Coulomb barrier and the latter, inside the barrier. In order to calculate Eq.(2), we use the path integral representation of P and

approximate it by the stationary phase method. For the barrier penetration, we use the method of the imaginary time [4]. By this way, we get the semiclassical paths $q^{(1)}(t)$ for $K^{(1)}$ and $q^{(2)}(t)$ for $K^{(2)}$.

We can now calculate the quantity P. As an zero-th order approximation, we assume the inverse parabola potentials for both intrinsic states and solve the equation of motion for $q^{(1)}(t)$ and $q^{(2)}(t)$. After some calculations, we get two S matrices for two processes, $K^{(1)}$ and $K^{(2)}$ and we will show the one for the former.

$$| S^{(1)} |^2 \propto A \exp \left[\frac{2}{\hbar} \{ (E-W_\alpha-\varepsilon_\alpha) + (W_\alpha-W_\beta-\hbar\omega) \} \tau \right] . \qquad (3)$$

Here W_α and W_β are the potential heights corresponding to the intrinsic states $|\alpha\rangle$ and $|\beta\rangle$ whose energies are ε_α and ε_β. The effective time needed to penetrate the barrier is written as τ. The overall normalization A is essentially proportional to $|V_{\beta\alpha}|^2$ where $V_{\beta\alpha}$ is the transition matrix element from $|\alpha\rangle$ to $|\beta\rangle$ and $\hbar\omega=\varepsilon_\beta-\varepsilon_\alpha$.

The S matrix for the penetration process without intrinsic excitation is given as

$$| S^{(0)} |^2 \propto \exp \left[\frac{2}{\hbar} \{ (E-W_\alpha-\varepsilon_\alpha) \tau \} \right] . \qquad (4)$$

Thus for $W_\alpha-W_\beta-\hbar\omega>0$, the cross section will be enhanced. The calculation of the potential energy surface for medium and heavy mass system shows that the adiabatic potential barrier is typically several to 10 MeV lower than the cold density barrier. The adiabatic potential barrier corresponds to the large prolate deformation of the nuclei (neck formation). We identify our intrinsic state $|\beta\rangle$ to such state and then we get the following interpretation of the enhancement: As two nuclei approaches each other, the residual interaction brings about the deformation of the two nuclei. The neck is formed and the potential barrier is lowered as a result. Numerical calculation for such process is under way.

References

1) M. Beckerman et al., Phys.Rev.Lett. 45 (1980) 1472.
M. Beckerman et al., Phys.Rev. C23 (1981) 1581.

2) see for example, R.A. Broglia, Nucl.Phys. A409 (1983) 163.

3) H.J. Krappe et al., Z.Phys. A314 (1983) 23.

4) W.H. Miller, Adv.in Chem.Phys. XXV (1974) 69.

VI FAST NEUTRON PHYSICS

6.1 Fast Neutron t-o-f Spectrometer for the scattering measurements

Masayoshi Sugimoto*, Yoshimaro Yamanouti*, Shigeya Tanaka*,
Yutaka Furuta*, Motoharu Mizumoto* and Mikio Hyakutake**

* Department of Physics, Japan Atomic Energy Research Institute and
**Department of Nuclear Engineering, Fuculty of Engineering,
Kyushu University

A fast neutron t-o-f spectrometer was installed at the JAERI Tandem accelerator, and its performances were investigated by using the $^{27}Al(d,n)^{28}Si$ reaction at the deuteron energy 10 MeV and the $^{28}Si+n$ reaction at the incident energy 13 MeV.

The spectrometer consists of the neutron target system (D_2 gas target and ^{7}Li metal target) and the goniometer, on which the massive detector shields for two distinct types of the neutron detectors were put, with 8 meter flight paths. One type of the neutron detector (A) is an array (2x2) of the voluminous liquid scintillator, 35 cm x 22 cmø NE213, coupled to the two RCA8854 photomultipliers. The method of the time-compensation is same as the one developed at Ohio University[1]. Another type of the detector (B) is also a liquid scintillator, 80 cm x 10 cmø NE213, coupled to the two RCA8854 photomultipliers and the conventional mean-timing method is used as the time-compensation method.

The checked perfomances are 1) the monochromaticity of the D(d,n) neutron source at En=13 MeV: the effect of the deuteron breakup and the (d,n) reactions at the beam stop, 2) the time resolution of the spectrometer, 3) the effectiveness of the pulse shape discrimination of the large detectors and 4) the effectiveness of the detector shields.

The results are as follows: 1) Fig. 1 is the typical source spectrum at the beam direction using a 5 cm x 12.5cmø NE213 detector. The breakup component was modest compared to the main peak from the $D(d,n)^{3}He$ reaction, however it will interfere the observation of the scattering to the higher excited levels at the angles up to 60 deg or more. The applicability of the $^{3}He(d,np)^{3}He$ reaction for evaluating the breakup component[2] was examined, but the several difficulties were found on the yield, the precise shape and so on. Some components between the main peak and the breakup are attributed to the (d,n) neutrons from the target cell.

2) Fig.2 is the result of the time resolution measurement for the detectors (A) using the $^{27}Al(d,n)^{28}Si$ reaction to the lower excited levels. The overall time resolution was 2 nsec FWHM for the fastest 17.5 MeV neutrons, and the beam pulse width was 1.5 nsec FWHM. The similar result of the time resolution for the detector (B) was obtained. 3) The pulse shape spectrum was obtained at the above measurements with the bias level 1-2 Co LU. The figure of merit is satisfactory one for measuring the scattered neutrons.

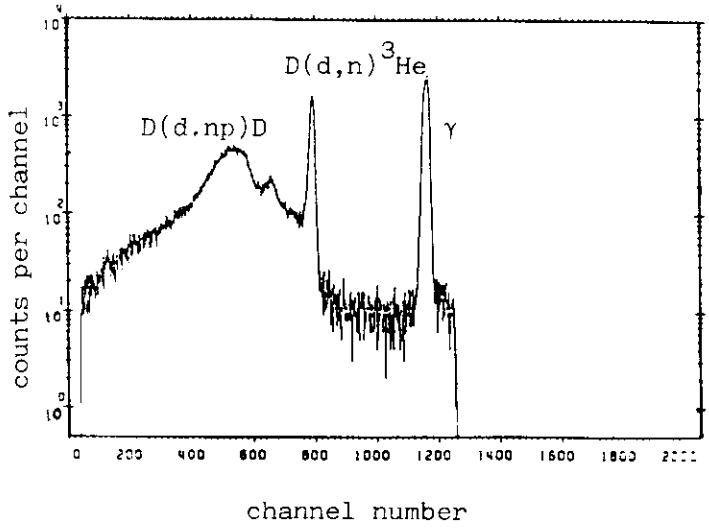

Fig.1. The neutron t-o-f spectrum from the D_2 gas target at 10 MeV incident energy. A peak of the 13 MeV neutrons from the $D(d,n)^3He$ reaction and the deuteron breakup are seen and the component between them is due to the (d,n) reactions of the C,N,O and the target cell materials.

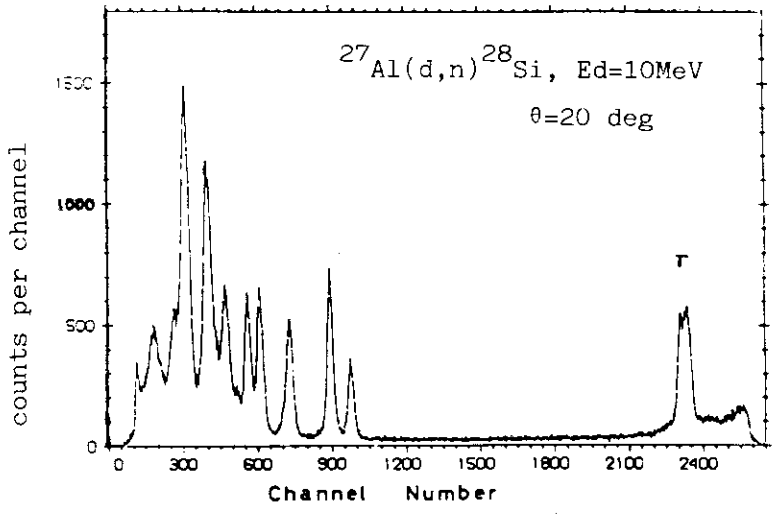

Fig.2 The time resolution measurement of the large detector system by using the $^{27}Al(d,n)^{28}Si$ reaction. The time resolution is 2 nsec FWHM at best with the time-compensation.

4) The detector shields completely shut the direct source neutrons at the scattering angles larger than 30 deg. At the scattering angle of 15 deg, a part of the detector was exposed to the direct neutrons, so the measurements must be done by the use of a half of the array of detectors (A). Fig. 3(a)-(c) are the examples of the spectra obtained from the reaction ^{28}Si(n,n) and (n,n') at En=13 MeV. The sample-out runs were plotted in the same figures.

As a consequence the perfomances of the neutron t-o-f spectrometer are satisfactory, and the problems to be solved in the near future are also revealed, i.e. the contaminations in the neutron source, the high random background level in the t-o-f spectra, and the stability of the pulsed beam and the detector response.

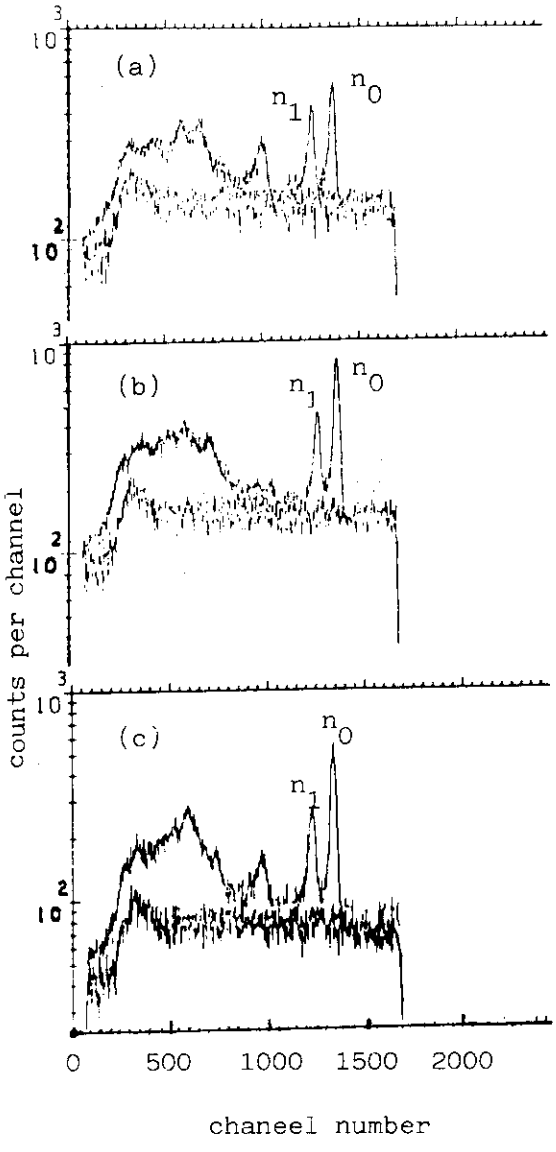

Fig.3 The scattered neutron spectra of the ^{28}Si+n reaction at En=13 MeV and the sample out background spectra at the scattered angle (a) 60 deg, (b) 90 deg and (c) 120 deg, respectively.

references

1) J.D.Carlson,R.W.Finlay and D.E.Bainum, Nucl. Instr. Methods 147(1977)353.

2) S.M.Grimes,P.Grabmayr,R.W.Finlay,S.L.Graham,G.Randers-Pehrson and J.Rapaport, Nucl. Instr. Methods 203(1982),269.

6.2 Scattering of 12.8 MeV Neutrons from ^{28}Si

Yoshimaro Yamanouti*, Masayoshi Sugimoto*, Shigeya Tanaka*
Mikio Hyakutake**, Yutaka Furuta* and Motoharu Mizumoto*

*Department of Physics, Japan Atomic Energy Research Institute
and **Department of Nuclear Engineering, Kyushu University

Differential cross sections for the scattering of 12.8 MeV neutrons from ^{28}Si were measured in order to investigate the reaction mechanism of neutron-nucleus interaction and collective properties of the low-lying states of ^{28}Si. Scattered neutrons were observed by a newly constructed time-of-flight spectrometer with an array of four 20 cmϕ x 35 cm NE213 liquid scintillator detectors. Monoenergetic neutrons were generated in a gas cell filled with deuterium gas up to 2×10^5 Pa by the D(d,n)^{3}He reaction as a neutron source reaction.

Neutron time-of-flight spectra were taken every 5° for scattering angles from 15° to 130°. Inelastic cross sections leading to the first 2^+ state at 1.779 MeV and the 4^+ state at 4.618 MeV were measured simultaneously with the elastic scattering. Fig.1 shows the background subtracted time-of-flight spectrum taken at Θ_{lab} = 60°. The time-of-flight spectra were analyzed using a least square curve-fitting program. The relative efficiencies for the neutron detector were determined by measuring the known angular distribution of neutrons from the D(d,n)^{3}He reaction.

The optical potential parameters to give the best fit to the elastic cross sections were obtained by the optical potential search code ELIESE3. The initial set of the parameter searches was the set obtained by Haouat et al.[1] The compound elastic and inelastic cross sections were estimated by using the Hauser-Feshbach formalism.

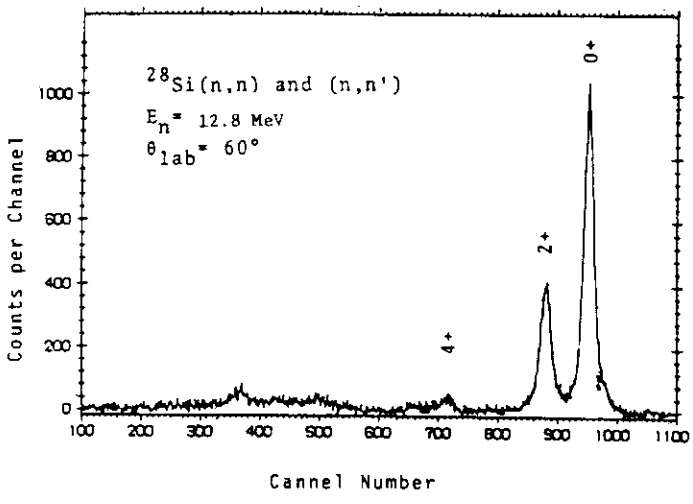

Fig.1 The neutron time-of-flight spectrum taken at Θ_{lab} = 60°.

The experimental cross sections were analyzed in terms of the DWBA theory and the coupled-channels formalism. The coupled-channels calculations based on the rotational model and the vibrational model were carried out with the 0^+-2^+-4^+ coupling scheme.
In the rotational model calculations the negative β_2 value gives a better fit to the experimental cross sections than the positive β_2 value. The DWBA predictions and the results of the coupled-channels calculations are shown in Fig.2 together with the experimental cross sections. The results of the rotational model calculations in the figure were obtained with the quadrupole deformation only.

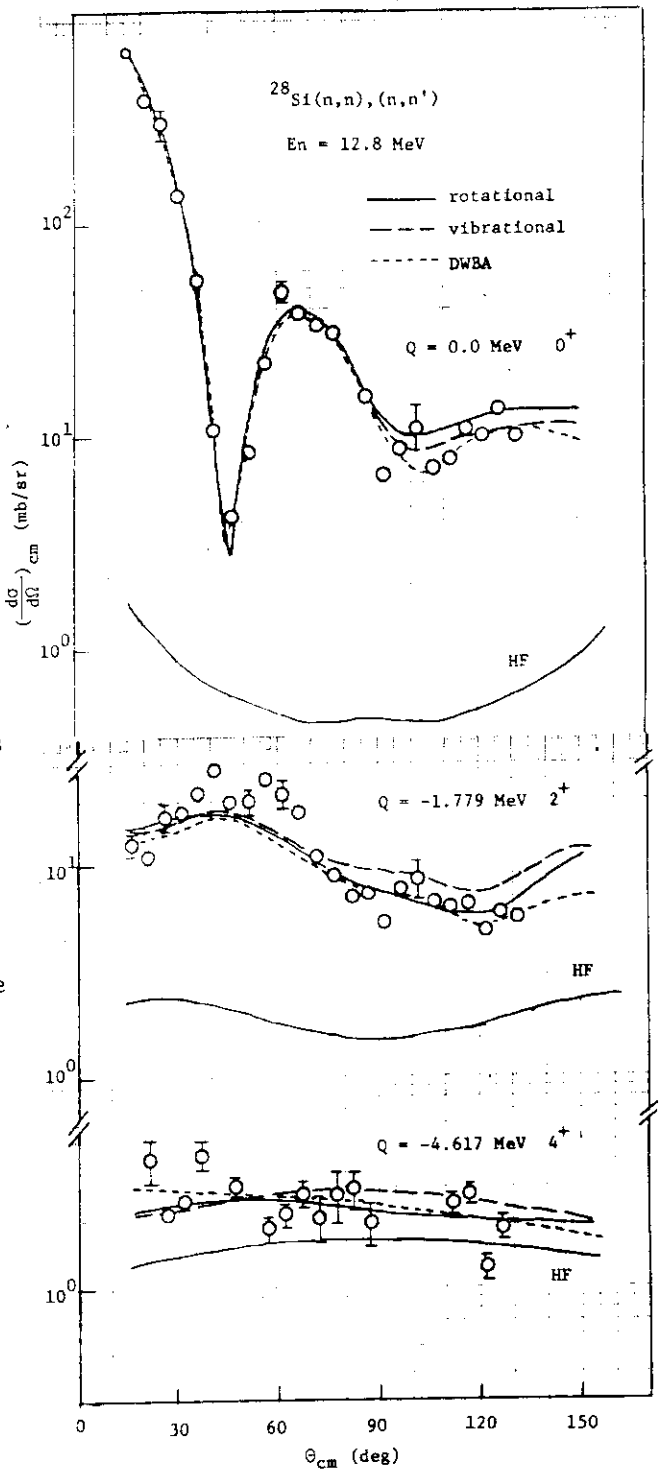

Fig.2 The DWBA and coupled-channels fits to the scattering of 12.8 MeV neutrons from ^{28}Si.

Reference

1) G.Haouat et al, Proc. Int. Conf. Sept. 1982 (Antwerp)

VII PUBLICATIONS

7.1 Publications in Journals and Proceedings Articles

1. Baba, Y. and Sasaki, T.
Application of X-ray-induced Auger Electron Spectroscopy to State Analyses of Hydrogen Implanted in Y, Zr and Nb Metals.
Accepted for Publication in Surface and Interface Analysis.

2. Baba, Y. and Sasaki, T.
X-ray Excited Auger Electron Spectra of Hydrogen Implanted 4d Transition Metals and Related Compounds , 1983, unpublished.

3. Baba, Y. and Sasaki, T.
X-ray Photoelectron and X-ray-induced Auger Electron Spectroscopic Data I. 3d Transition Metals and Related Oxides.
JAERI-M 84-005.

4. Baba, Y. and Sasaki, T.
X-ray Photoelectron and X-ray-induced Auger Electron Spectroscopic Data II. 4d Transition Metals and Related Oxides.
JAERI-M 84-071.

5. Fujiwara, I., Ichikawa, S., Shinohara, N., Usuda, S., Suzuki, T., Okashita, H., Sekine, T., Horiguchi, T., Yoshizawa, Y. and Shibata, S.
Heavy Elements and Superheavy Elements.
JAERI-M 84-085 (1984) 57.

6. Furuno, S., Otsu, H. and Izui, K.
Electron Microscope Observations of Tracks of 130 MeV Cl^{9+} Ions in Solids.
J. Electron Microsc. 30 (1981) 327.

7. Hamada, S., Sawai, T. and Shiraishi, K.
Measurement of Mean Projected Range for Carbon-Ion Irradiated into Stainless Steel.
J. Atomic Energy Soc. Japan (to be published).

8. Ideno, K., Tomita, Y., Takeuchi, S., Hanashima, S., Yokota, W., Lee, S.M., Nagashima, Y., Nakagawa, T., Fukuchi, Y., Mikumo, T. and Galster, W.
Scission of the Composite System ^{64}Zn from $^{37}Cl + ^{27}Al$ and $^{16}O + ^{48}Ti$.
Proc. Int. Conf. on Nuclear Physics, Florence (1983) Vol.I, p.549.

9. Ikezoe, H.
Coincidence Measurement between Evaporation Residues and Light Particles Produced in $^{16}O + ^{40}Ca$ Reaction.
JAERI-M 84-085 (1984) 32.

10. Ishii, M. and Makishima, A.
In-Beam Gamma-Ray Spectroscopy through Heavy-Ion-Induced Fusion Reaction.
JAERI-M 84-085 (1984) 75.

11. Iwamoto, A. and Harada, K.
Extension of Generalized Exciton Model and Calculation of (p,α) Angular Distribution.
Proc. Int. Conf. on Nuclear Physics, Florence (1983) Vol.I, p.440.

12. Iwamoto, A. and Harada, K.
Extension of Generalized Exciton Model and Calculation of (p,p') Angular Distrubition.
Proceedings of the 1983 International Symposium on Light Ion Reaction Mechanism, RCNP, Osaka (1983) 727.

13. Iwamoto, A. and Harada, K.
Extension of Generalized Exciton Model and Calculation of (p,p') and (p,α) Angular Distribution ,1983, unpublished,
to be published in Nucl. Phys. A.

14. Iwase, A., Sasaki, S., Iwata, T. and Nihira, T.
Calorimetric Measurements of Stopping Power for ^{35}Cl and ^{12}C Ions in Al and Ni , 1984, unpublished

15. Minehara, E., Tajima, S. and Arakawa, K.
Impurities in a SF_6 Insulating Gas Medium of the JAERI Tandem Accelerator.
JAERI-M 84-004.

16. Noda, K., Tanifuji, T., Ishii, Y., Matsui, H., Masaki, N., Nasu, S. and Watanabe, H.
Irradiation Effects of Lithium Oxide.
J. Nucl. Mater., in press.

17. Noda, K., Ishii, Y. and Watanabe, H.
Irradiation Damages in Oxygen Ion Irradiated Lithium Oxide.
Progress Report on Fusion Reactor Materials Research and Development in Japan 1982.

18. Sakai, E.
Induced Radioactivities in Silicon and Germanium Irradiated with High-energy Heavy Ions.
IEEE Trans. Nucl. Sci., NS-31 (1984) 316.

19. Sakurai, T., Hinatsu, Y., Takahashi, A. and Fujisawa, G.
Adsorption of Ruthenium Tetroxide on Metal Surfaces.
J. Phys. Chem. (to be published).

20. Sato, K., Iwamoto, A. and Harada, K.
Pre-equilibrium Emission of Light Composite Particles in the Framework of the Exciton Model.
Phys. Rev. C28 (1983) 1527.

21. Sekine, T., Baba, S., Hata, K. and Ichikawa, S.
Incomplete Fusion in the $^{12}C + ^{93}Nb$ Reaction.
JAERI-M 84-085 (1984) 65.

22. Sugimoto, M. and Yamanouti, Y.
Proceedings of the 1983 Seminar on Nuclear Data, Tokai, JAERI-M 84-010, NEANDC(J)97/AU.
INDC(JPN)84/G (1984) 312.

23. Sugiyama, Y.
JAERI Magnetic Spectrograph 'ENMA' for Heavy Ion Research.
Report on Work Shop of Magnetic Spectrograph in Sendai, Jan. (1983).

24. Sugiyama, Y., Shikazono, N., Tomita, Y., Ikezoe, H., Takekoshi, E., Kubono, S., Tanaka, M. and Sugitani, M.
Measurement of the Spin Alignment in the $^{12}C + ^{12}C$ Inelastic Scattering via γ-recoil.
JAERI-M 84-085 (1984) 20.

25. Sugiyama, Y., Shikazono, N., Sato, T. and Ikegami, H.
Magnetic Field Measurement of the JAERI Heavy-Ion Spectrograph "ENMA".
Nucl. Instr. and Meth. 215 (1983) 17.

26. Tamura, T.
Nuclear Spectroscopy of Radioisotope Produced by Heavy-Ion Reactions.
JAERI-M 84-085 (1984) 79.

27. Tomimitsu, H.
XDT-Observation of Si Single Crystals Irradiated with 150 MeV Ni^{+9} and Cl^{+9} Ions, 1983, unpublished

28. Tomimitsu, H.
X-ray Diffraction Topographic Observation of Si Single Crystals Irradiated with 150 MeV Ni^{+9} and Cl^{+9} Ions.
Japan. J. Appl. Phys. 22 (1983) L674.

29. Yamaji, S. and Iwamoto, A.
Friction Coefficients for Deep Inelastic Heavy-Ion Collisions.
Z. Phys. A-Atoms and Nuclei 313 (1983) 161.

7.2 Contributions to Scientific and Technical Meetings

1. Baba, H., Baba, S., Fujiwara, I., Hata, K., Ichikawa, S., Saito, S., Sekine, T., Suzuki, T. and Yokoyama, A.
   Heavy-ion Fusion Reaction of ^{197}Au.
   The 27th Symposium on Radiochemistry in Nagoya, (1983).

2. Baba, Y. and Sasaki, T.
   XPS Observations of Materials Exposed to Hydrogen Ions(I) Surface of Zr.
   1984th Annual Meeting of the Atomic Energy Society of Japan in Osaka, Mar. 29-31, (1984).

3. Furuno, S., Izui, K. and Otsu, H.
   Electron Microscope Observations of Tracks of High Energy Heavy Ions in Evaporated films of Germanium.
   Autumn Meeting of Japan Physical Society in Okayama, Oct. 9-12, (1983).

4. Hamada, S., Sawai, T. and Shiraishi, K.
   Measurement of Stopping Power by Carbon-irradiated into Stainless Steel.
   Spring Meeting of Japan Institute of Metals in Narashino, Apr. 1-3, (1984).

5. Hata, K., Sekine, T., Baba, S., Nagame, M., Ichikawa, S., Baba, H., Saito, S., Yokoyama, A. and Imanishi, N.
   Release of Light Fragments in 112 MeV ^{16}O + Au Reaction.
   The 27th Symposium on Radiochemistry in Nagoya, (1983).

6. Hamada, S., Sawai, T. and Shiraishi, K.
   Study of 80 MeV Carbon Ion Irradiated Austenitic Stainless Steel.
   Autumn Meeting of Japan Institute of Metals in Akita, Oct. 4-6, (1984).

7. Hishinuma, A. and Aruga, T.
Preliminary Testing of Irradiation Creep and Damage Structure Using In-beam Creep Apparatus.
Spring Meeting of Japan Institute of Metals in Narashino, Apr. 1-3, (1984).

8. Horiguchi, T. et al.
A Study of $^{238}U + ^{16}O$ Reaction
Spring Meeting of Physical Society of Japan in Fukuoka, Apr. (1984).

9. Ikezoe, H.
Bragg-Curve Counter and Time-of-Fleght System for Heavy Ion Reaction.
IPCR Symposium on "Detectors for Heavy Ion Reaction and Application", March 16-17, (1983).

10. Ikezoe, H.
Time-of-Flight Measurements in Heavy Ion Reaction.
IPCR Symposium on "Nuclear Research in the Energy Region of 10-100 MeV/u", Nov. 24-26, (1983).

11. Ichikawa, S. et al.
A Surface Ionization Source for an On-line Mass Separator.
The 27th Symposium on Radiochemistry in Nagoya, Oct. 21-23, (1983).

12. Ikezoe, H., Kovar, D.G., Rosner, G., Stephans, G., Ungricht, E. and Wilkins, B., Argonne Natl. Lab., and Awes, T. and Young, G., Oak Ridge Natl. Lab., and Maguire, C., Kui, Z., Ma, W.C., Robinson, S., Watson, D. and Ward, G., Vanderbilt Univ.
Coincidence Measurements between Evaporation Residues and Light Particles Produced in $^{16}O + ^{40}Ca$ at Ecab (^{16}O) = 160 MeV.
Bull. of the Am. Phys. Soc. 28 (1983) 974.

13. Iwase, A., Sasaki, S., Iwata, T. and Nihira, T.
Calorimetric Measurements of Stopping Power for ^{35}Cl and ^{12}C Ions in Ni.
Autumn Meeting of Japan Physical Society in Okayama, Oct. 11-14, (1983).

14. Iwase, A., Sasaki, S., Iwata, T. and Nihira, T.
Electrical Resistivity Changes and Defect Production Cross Sections of Al for Energetic Heavy Ion Irradiations.
Spring Meeting of Japan Physical Society in Fukuoka, Apr. 1-4, (1984).

15. Kolata, J.J. and Vojtech, R.J., Univ. of Notre Dame, Stephans, G.S.F., Kovar, D.G., Rehm, K.E., Rosner, G. and Ikezoe, H., Argonne Natl. Lab.
Quasielastic Processes in the $^{28}Si + ^{40}Ca$ and $^{28}Si + ^{208}Pb$ Reactions at 8 MeV/A.
Bull. of the Am. Phys. Soc. 28 (1983) 995.

16. Makishima, A. and Ishii, M.
A Charged Particle Multiplicity Filter.
Autumn Meeting of Japan Physical Society in Kobe, Oct. (1983).

17. Maruyama, M.
Status of the JAERI Tandem Accelerator.
The Second China-Japan Joint Symposium on Accelerators for Nuclear Science and Their Applications.

18. Mateja, J.F., Tennessee Technological U., Frawly, A.D., Florida State U., Kovar, D.G., Henderson, D., Ikezoe, H., Janssens, R., Rosner, G., Stephans, G. and Wilkins, B., Argonne Natl. Lab.
A Recent Study of Particles Emitted in the $^{11}B + ^{12}C$ Reaction.
Bull. of the Am. Phys. Soc. 29 (1984) 624.

19. Mateja, J.F., Garman, J. and Fields, D.E., Tennessee Technological U., Frawley, A.D., Florida State U., Kovar, D.G., Henderson, D., Ikezoe, H., Janssens, R., Rosner, G., Stephans, G. and Wilkins, B., Argonne Natl. Lab.
Mass Spectra of Evaporation Residues in $^{11}B + ^{12}C$ and $^{10}B + ^{13}C$ for Boron Energies from 50- to 100-MeV.
Bull. of the Am. Phys. Soc. 28 (1983) 994.

20. Minehara, E.
Production and Acceleration of Negative Heavy Ions from the Group V_B, VI_B and VII_B Elements at the JAERI Tandem Accelerator.
Autumn Meeting of Japan Physical Society in Kobe, Oct. 9-12, (1984).

21. Minehara, E.
Negative Ion Sputter Source Developments.
Spring Meeting of Japan Physical Society in Fukuoka, Apr. 1-4, (1984).

22. Nagano, K., Sugiyama, Y., Takekoshi, E., Ikezoe, H., Tomita, Y. and Shikazono, N.
Characteristics of the ENMA Focal-Plane Detector with CF_4 Gas.
Meetings of Japan Physical Society in Kobe and Fukuoka, Oct. 6, (1983) and Apr. 1, (1984).

23. Noda, K., Tanifuji, T., Ishii, Y., Matsui, H., Masaki, N., Nasu, S. and Watanabe, H.
Irradiation Effects of Lithium Oxide.
3rd Topical Meeting on Fusion Reactor Materials in Albuquerque, Sept. 19-22, (1983).

24. Sakai, E.
Residual Radioactivities in Various Materials for Solid-State Physics Research Irradiated with High-Energy Heavy ions(II).
The 20th Annual Meeting on Radioisotopes in the Physical Sciences and Industry in Tokyo, July 6, (1983).

25. Sasaki, T. and Baba, Y.
XPS Observations of Materials Exposed to Hydrogen Ions(II) Surface of Nb.
1984th Annual Meeting of the Atomic Energy Society of Japan in Osaka, Mar. 29-31, (1984).

26. Sasaki, T. and Baba, Y.
XPS Spectra of Zirconium Hydride and Niobium Hydride.
Spring Meeting of Chemical Society of Japan in Kyoto, Apr. 1-4, (1983).

27. Sasaki, T.
Electronic Structure and XPS Spectra of ScH_2 and NiH_2.
Spring Meeting of Chemical Society of Japan in Kyoto, Apr. 1-4, (1983).

28. Sekine, T., Hata, K., Baba, S. and Ichikawa, S.
Heavy-Ion Reaction between ^{12}C and ^{93}Nb.
The 27th Symposium on Radiochemistry in Nagoya, Oct. 21-23, (1983).

29. Sugimoto, M., Yamanouti, Y., Tanaka, S., Furuta, Y. and Hyakutake, M.
Neutron Response of the Large Volume Detector with an Incidence- time Compensation.
Fall Meeting of Japan Physical Society in Kobe, Oct. 9-12, (1983).

30. Shinohara, N. et al.
Synthesis of Transuranium Nuclides from Interaction of ^{16}O with ^{238}U.
The 27th Symposium on Radiochemistry in Nagoya, Oct. 21-23, (1983).

31. Sugiyama, Y., Shikazono, N., Tomita, Y., Ikezoe, H., Takekoshi, E., Nagano, K., Kubono, S., Tanaka, M. and Sugitani, M.
Spin Alignment in the $^{12}C + ^{12}C$ Inelastic Scattering by γ Recoil Method(I).
Autumn Meeting of Japan Physical Society in Kobe, Oct. 9-12, (1983).

32. Sugiyama, Y., Shikazono, N., Ikezoe, H., Tomita, Y., Takekoshi, E., Nagano, K., Kubono, S., Tanaka, M. and Sugitani, M.
Spin Alignment in the $^{12}C + ^{12}C$ Inelastic Scattering by γ Recoil Method(II).
Spring Meeting of Japan Physical Society in Fukuoka, (1984).

33. Yamanouti, Y., Sugimoto, M., Tanaka, S., Hyakutake, M. and Furuta, Y.
JAERI Fast Neutron TOF Spectrometer.
Fall Meeting of Japan Physical Society in Kobe, Oct. 9-12, (1983).

34. Yamanouti, Y., Sugimoto, M., Tanaka, S., Hyakutake, M. and Furuya, Y.
JAERI Neutron Time-Of-Flight Facility.
Fall Meeting of the Atomic Energy Society of Japan in Sapporo, Sep. 28-30, (1983).

35. Yokota, W., Ideno, K., Ogihara, M., Komatsubara, T., Fukuchi, Y., Nagashima, Y., Furuno, K., Lee, S.M., Mikumo, T., Tomita, Y., Hanashima, S.
Fusion and Fission-like Reactions in the System of $^{37}Cl + ^{48}Ti$.
Autumn Meeting of Japan Physical Society in Kobe, Oct. 9, (1983).

36. Yokoyama, A., Saito, S., Shoji, M., Shinohara, A., Baba, H., Baba, S., Hata, K., Sekine, T., Ichikawa, S., Suzuki, T.
Projectile Dependence of ^{197}Au Reactions.
The 27th Symposium on Radiochemistry, in Nagoya, (1983).

VIII PERSONNEL AND COMMITTEES

8.1 Personnel

Department of Physics

	Kichinosuke	Harada	Director
	Nobuyoshi	Tsuda	Administrative Manager

Accelerators Division

Scientific Staff	Michio	Maruyama*
	Yuki	Kawarasaki
	Shiro	Kikuchi
	Suehiro	Takeuchi
	Eisuke	Minehara
	Susumu	Hanashima
Technical Staff	Chiaki	Kobayashi**
	Isao	Ohuchi
	Yutaka	Sato
	Tadashi	Yoshida
	Susumu	Kanda
	Katsuzo	Horie
	Satoshi	Tajima
	Yoshihiro	Tsukihashi
	Shinichi	Abe
	Shuhei	Kanazawa

Nuclear Physics Laboratory

Scientific Staff	Naomoto	Shikazono***
	Eiko	Takekoshi
	Tsutomu	Tamura (∿ May, 1983)
	Mitsuhiko	Ishii
	Yoshiaki	Tomita
	Yasuharu	Sugiyama
	Akira	Iwamoto

* Chief, Accelerators Division

** Chief, Technical Staff

*** Deputy Director, Department of Physics and Chief of Nuclear Physics Laboratory

Nuclear Physics Laboratory (continued)

Scientific Staff	Kazumi	Ideno	
	Hiroshi	Ikezoe	
	Masumi	Ohshima	
	Takaharu	Ohtsuka	
Scholarship Fellow	Kenzo	Nagano	(University of Tsukuba)
	Akiyasu	Makishima	(Tokyo Institute of Technology)

Linac Laboratory

Scientific Staff	Shigeya	Tanaka*	
	Yutaka	Furuta	
	Motoharu	Mizumoto	
	Yoshimaro	Yamanouchi	
	Masayoshi	Sugimoto	

Solid State Physics Laboratory I

Scientific Staff	Kazuo	Geshi**	
	Kunio	Ozawa	
	Yukio	Kazumata	
	Kiyoshi	Kawatsura	
	Hiroshi	Naramoto	
	Hiroshi	Tomimitsu	
	Masao	Sataka	
Scholarship Fellow	Hidenori	Yamaguchi	(University of Tsukuba)

Solid State Physics Laboratory II

Scientific Staff	Tadao	Iwata***	
	Akihiro	Iwase	
	Shigemi	Sasaki	

* Chief, Linac Laboratory

** Chief, Solid State Physics Laboratory I

*** Chief, Solid State Physics Laboratory II

Department of Chemistry

Nuclear Chemistry Laboratory

Scientific Staff	Hiroshi	Okashita*
	Toshio	Suzuki
	Shigekazu	Usuda
	Nobuaki	Kono
	Shin-ichi	Ichikawa
	Nobuo	Shinohara

Analytical Chemistry Laboratory

Scientific Staff	Yuji	Baba

Physical Chemistry Laboratory

Scientific Staff	Mutsuhide	Komaki

Solid State Chemistry Laboratory

Scientific Staff	Kazuhiko	Izui**
	Shin-ichi	Ohno
	Teikichi	Sasaki
	Shigemi	Furuno
	Hitoshi	Ohtsu

Department of Radioisotope Production

Production Development Division

Scientific Staff	Sumiko	Baba
	Kentaro	Hata
	Toshiaki	Sekine

* Chief, Nuclear Chemistry Laboratory

** Chief, Solid State Chemistry Laboratory

Department of Fuels and Materials Research
Physical Metallurgy Laboratory

Scientific Staff	Kensuke	Shiraishi*
	Akimichi	Hishinuma
	Takeo	Aruga
	Shozo	Hamada
	Tomotsugu	Sawai

Fuel Property Laboratory

Scientific Staff	Hitoshi	Watanabe**
	Kenji	Noda
	Yoshinobu	Ishii

Department of Reactor Engineering
Reactor Instrumentation Laboratory

Scientific Staff	Eiji	Sakai

Department of Health Physics

Technical Staff	Syoji	Izawa
	Toshihiro	Miyamoto
	Takeo	Seki

* Chief, Physical Metallurgy Laboratory
** Chief, Fuel Property Laboratory

8.2 Steering Committee

(Chairman)	Tetsuo	Aochi	(Deputy Director General, Tokai Research Establishment)
	Takumi	Asaoka	(Director, Department of Reactor Engineering)
	Kaxumi	Iwamoto	(Director, Department of Fuels and Materials Research)
	Kichinosuke	Harada	(Director, Department of Physics)
	Haruo	Natsume	(Director, Department of Chemistry)
	Yukio	Obata	(Director, Department of Thermonuclear Fusion Research)
	Toshihiko	Abe	(Director, Department of Radioisotope Production)
(Secretary)	Naomoto	Shikazono	(Deputy Director, Department of Physics)
(Secretary)	Michio	Maruyama	(Chief, Accelerators Division)
(Secretary)	Nobuyoshi	Tsuda	(Administrative Manager, Department of Physics)

8.3 Consultative Committee

(Chairman)	Hiroshi	Ishikawa	(Executive Director)
(Vice Chairman)	Tetsuo	Aochi	(Deputy Director General, Tokai Research Establishment)
(Vice Chairman)	Kichinosuke	Harada	(Director, Department of Physics)
	Hiromichi	Kamitsubo	(Principal Scientist, Institute of Physical and Chemical Research)
	Kozi	Nakai	(Associate Professor, University of Tokyo)
	Hiroyasu	Ejiri	(Professor, Osaka University)
	Shiori	Ishino	(Professor, University of Tokyo)
	Nobuo	Oda	(Professor, Tokyo Institute of Technology)
	Kohzoh	Masuda	(Professor, University of Tsukuba)
	Shiro	Iwata	(Professor, Kyoto University)
	Ichiro	Fujiwara	(Associate Professor, Kyoto University)
	Kenji	Sumita	(Professor, Osaka University)
	Itsuro	Kimura	(Professor, Kyoto University)
(Secretary)	Naomoto	Shikazono	(Deputy Director, Department of Physics)
(Secretary)	Michio	Maruyama	(Chief, Accelerators Division)
(Secretary)	Nobuyoshi	Tsuda	(Administrative Manager, Department of Physics)

8.4 Program odvisory Committee

(Chairman)	Kichinosuke	Harada	(Director, Department of Physics)
	Shoji	Izawa	(Chief, Radiation Control Group, Department of Health Physics)
	Kensuke	Shiraishi	(Chief, Physical Metallurgy Laboratory, Department of Fuels and Materials Research)
	Hiroshi	Okashita	(Chief, Nuclear Chemistry Laboratory, Department of Chemistry)
	Kunio	Ozawa	(Principal Scientist, Department of Physics)
	Naomoto	Shikazono	(Deputy Director, Department of Physics)
	Shigeya	Tanaka	(Chief, Linac Laboratory, Department of Physics)
	Michio	Maruyama	(Chief, Accelerators Division, Department of Physics)
	Chiaki	Kobayashi	(Chief, Tandem Operation Group, Department of Physics)

IX CO-OPERATIVE RESEARCHES

	Title	Co-operating Institution
2.2	Beam-Foil Interaction of Highly Ionized Chlorine ion in High Energy Region	Faculty of Engineering, Ibaraki University* College of General Education, University of Tokyo*
2.3	Beam-Foil Spectra of Chlorine Ions in High Energy Region	College of General Education, University of Tokyo* Department of Engineering Science, Kyoto University Faculty of Engineering, Ibaraki University*
2.4	Defect Production Cross Sections of Aluminum for Energetic Heavy Ion Irradiations	Faculty of Engineering, Ibaraki University*
3.1	Irradiation Damages in Oxygen Ion Irradiated Li_2O	Faculty of Engineering, Nagoya University*
3.3	Heavy Ion Track Filter of Polyvinylidene Fluoride	Institute of Atomic Energy, Kyoto University
3.5	Residual Radioactities in Semiconductors and Other Materials for Solid-State Physics Research Irradiated with High-Energy Heavy Ions	Faculty of Engineering, Toyama University*
3.6	ESR of Pyro-Graphite Irradiated by CI^{8+} Ions	University of Electro-Communications
3.7	Irradiation Effect with Heavy Ions on Alkali Halides	Faculty of Engineering, Ibaraki University*

3.10	A Study of Defect Structures in Heavy Ion Irradiated Nickel and bcc Iron by Measurements of Magnetic Anisotropy	College of Liberal Arts and Sciences, Okayama University
4.1	Nuclear Chemistry of Actinoids II. Formation Cross Sections of Transuranium Nuclides from Interaction of ^{16}O with ^{238}U	Department of Physics, Hiroshima University* Institute of Atomic Energy, Kyoto University* Institute for Nuclear Study, University of Tokyo
4.2	Experiments on Nuclides for from Stability by ISOL	Institute of Atomic Energy, Kyoto University* Faculty of Science, Osaka University*
4.3	An Experiment of Irradiated ^{197}Au with ^{16}O and ^{12}C Ions	Institute of Atomic Energy, Kyoto University* Osaka University*
5.1	In-Beam Gamma-Ray Spectroscopy through Heavy-Ion Induced Fusion	Department of Applied Physics, Tokyo Institute of Technology*
5.2	Fusion and Deep Inelastic Reactions for the Systems of $^{37}Cl+^{27}Al$ and $^{37}Cl+^{48}Ti$ with ^{37}Cl beams of 100-200 MeV	Tandem Accelerator Center University of Tsukuba*
5.4	Measurements of the spin alignment in the $^{12}C + ^{12}C$ inelastic scattering via γ recoil	Institute for Nuclear Study University of Tokyo*
6.1	Fast Neutron t-o-f Spectrometer for the Scattering Measurements	Faculty of Engineering, Kyushu University*
6.2	Scattering 12.8 MeV Neutrons from ^{28}Si	Faculty of Engineering, Kyushu University*

* Travel expense is supplied by JAERI